Effect of calcination conditions of P25-TiO$_2$ on photocatalytic selective hydrogenation of 3-nitrostyrene

Mr. Saknarin Chaitaworn

จุฬาลงกรณ์มหาวิทยาลัย
CHULALONGKORN UNIVERSITY

A Thesis Submitted in Partial Fulfillment of the Requirements

for the Degree of Master of Engineering in Chemical Engineering

Department of Chemical Engineering

Faculty of Engineering

Chulalongkorn University

Academic Year 2018

ผลของการแคลไซน์ตัวเร่งปฏิกิริยาไทเทเนียมไดออกไซด์ P25 ที่มีต่อปฏิกิริยาไฮโดรจีเนชั่นแบบเลือก
เกิดการใช้แสงของ3-ไนโตรสไตรีน

นายสักนรินทร์ ไชยถาวร

Thesis Title	Effect of calcination conditions of P25-TiO$_2$ on photocatalytic selective hydrogenation of 3-nitrostyrene
By	Mr. Saknarin Chaitaworn
Field of Study	Chemical Engineering
Thesis Advisor	Professor PIYASAN PRASERTHDAM, Dr.Ing.

Accepted by the Faculty of Engineering, Chulalongkorn University in Partial Fulfillment of the Requirement for the Master of Engineering

.... Dean of the Faculty of Engineering

(Professor SUPOT TEACHAVORASINSKUN, D.Eng.)

THESIS COMMITTEE

.... Chairman

(Akawat Sirisuk, Ph.D.)

.... Thesis Advisor

(Professor PIYASAN PRASERTHDAM, Dr.Ing.)

.... Examiner

(Assistant Professor Pattaraporn Kim, Ph.D.)

.... External Examiner

(Assistant Professor Okorn Mekasuwandumrong, D.Eng.)

สักนรินทร์ ไชยถาวร : ผลของการแคลไซน์ตัวเร่งปฏิกิริยาไทเทเนียมไดออกไซด์ P25 ที่มี
ต่อปฏิกิริยาไฮโดรจีเนชั่นแบบเลือกเกิดการใช้แสงของ3-ไนโตรสไตรีน. (
Effect of calcination conditions of P25-TiO$_2$ on photocatalytic selective
hydrogenation of 3-nitrostyrene) อ.ที่ปรึกษาหลัก : ศ. ดร.ปิยะสาร ประเสริฐธรรม

ในงานวิจัยนี้ศึกษาผลของการแคลไซน์ของตัวเร่งปฏิกิริยาทางการค้าขนาดนาโนของ
ไทเทเนียมไดออกไซด์ที่มีผลต่อปฏิกิริยาไฮโดรจีเนชั่นแบบเลือกเกิดการใช้แสงของ ๓-ไนโตรสไตรีน
ตัวเร่งปฏิกิริยาไทเทเนียมไดออกไซด์ทำการแคลไซน์ภายใต้บรรยากาศอากาศ ไฮโดรเจน และ
ไนโตรเจนที่อุณหภูมิ ๖๐๐ ถึง ๙๐๐ องศาเซลเซียสเป็นเวลา ๕ ชั่วโมง การวิเคราะห์คุณลักษณะ
ของตัวเร่งปฏิกิริยาไทเทเนียมไดออกไซด์หลังจากการแคลไซน์ โดยใช้เทคนิคการเลี้ยวเบนของรังสี
เอ็กซ์ การดูดซับทางกายภาพด้วยแก๊สไนโตรเจน การวัดค่าของอิเล็กตรอนที่ปลดปล่อยด้วยรังสี
เอ็กซ์ การวัดค่าการดูดกลืนแสงในช่วงอัลตร้าไวโอเลตและวิสิเบิ้ล การวัดค่าการเปล่งแสงของสาร
ด้วยวิธีกระตุ้นพลังงานโดยใช้แสง การวิเคราะห์การเปลี่ยนแปลงน้ำหนักของสารโดยใช้สมบัติทาง
ความร้อน และการวิเคราะห์โดยใช้กล้องจุลทรรศน์อิเล็กตรอนแบบส่องกราด ในการทดสอบ
ปฏิกิริยาไฮโดรจีเนชั่นแบบเลือกเกิดการใช้แสงของ ๓-ไนโตรสไตรีนกับไทเทเนียมไดออกไซด์ในไอ
โซโพรพานอล พบว่าอัตราการลดลงของ ๓-ไนโตรสไตรีนกับผลความเข้มข้นของค่าเปล่งแสงของ
สารด้วยวิธีกระตุ้นพลังงานโดยใช้แสงซึ่งมีความสัมพันธ์เป็นเส้นตรง นอกจากนี้พบว่าตัวเร่งปฏิกิริยา
ไทเทเนียมไดออกไซด์ที่แคลไซน์ภายใต้บรรยากาศอากาศที่อุณหภูมิ ๗๐๐ องศาเซลเซียสให้การ
ลดลงของ๓ไนโตรสไตรีน ๗๐ เปอร์เซนต์ โดยการเลือกเกิดเป็น ๓-ไวนิลอนิลีน ๑๐๐ เปอร์เซนต์
ความเป็นไปได้นี้เกิดจากผลของการทำงานร่วมกันของความเป็นผลึกที่สูงและความเหมาะสมของ
เฟสอนาเทสและรูไทล์ จึงนำไปสู่การลดลงของกระบวนการรวมตัวกันระหว่างอิเล็กตรอนกับโฮลซึ่ง
ได้จากผลของความเข้มข้นของค่าเปล่งแสงของสารด้วยวิธีกระตุ้นพลังงานโดยใช้แสง

สาขาวิชา	วิศวกรรมเคมี	ลายมือชื่อนิสิต ....
ปีการศึกษา	2561	ลายมือชื่อ อ.ที่ปรึกษาหลัก ....

5970336621 : MAJOR CHEMICAL ENGINEERING

KEYWORD: Photocatalytic selective hydrogenation / Calcination of titanium dioxide

Saknarin Chaitaworn : Effect of calcination conditions of P25-TiO$_2$ on photocatalytic selective hydrogenation of 3-nitrostyrene. Advisor: Prof. PIYASAN PRASERTHDAM, Dr.Ing.

In this work, we investigated the effect of calcination of nanocrystalline commercial titanium dioxide catalyst (P25) on photocatalytic selective hydrogenation of 3-nitrostyrene. TiO$_2$ supports were calcined under air, hydrogen and nitrogen atmosphere at various temperatures around 600 to 900°C for 5 hours. In order to investigate characteristic and catalytic properties of TiO$_2$ after treatment, treated-TiO$_2$ were analyzed by using X-ray diffraction (XRD), N$_2$-physisorption, X-ray photoelectron spectroscopy (XPS), UV-Vis spectroscopy (UV-Vis), photoluminescence spectroscopy (PL), thermogravimetric analysis (TGA), scanning electron microscope (SEM). Photocatalytic hydrogenation performance of treated-TiO$_2$ were tested under UV light irradiation. The 3-nitrostyrene consumption was linearly related to the photoluminescence intensity (PL intensity). TiO$_2$ calcined in air at 700°C exhibited 70% conversion of 3-nitrostyrene along with 100% selectivity to 3-vinylaniline. This probably due to the synergistic effect of high crystallinity along with optimal of anatase and rutile contents, which led to the reduction of electron-hole recombination process as observed from PL results.

Field of Study: Chemical Engineering   Student's Signature ....

Academic Year: 2018   Advisor's Signature ....

ACKNOWLEDGEMENTS

TABLE OF CONTENTS

LIST OF TABLES

LIST OF FIGURES

LIST OF SCHEMES

CHAPTER 1

INTRODUCTION

1.1   Introduction

Selecluve hydrogenation of organic molecule with the desired catalyst is one of the most important processes in the value chemical industry [1]. Functionalized anilines, which manufactured by the abatement of proportional nitroaromatic are intermediates in the production of many agrochemicals, pharmaceuticals, dyes, and pigment [2]. Ciba-Geigy has developed an effective catalyst for herbicide intermediated production, which had >99% selective product in the event of the aspired aniline, whereas the escalation of modifiers [3]. Furthermore, the additives within small intensity could affect product purity. Therefore, the additive was alternative to introduce modifier into the catalyst in order to improve selective formulation [3].

Functionalized anilines, in case of 3-vinylaniline (3-VA) is a significant compound for production supernal chemicals and functionalized polymers. 3-VA is produced by hydrogenation reaction of 3-nitrostyrene (3-NS) [3, 4]. However, 3-VA consists of both vinyl group ($-CH=CH_2$) and carbonyl group (C=C) which could be reduced. Therefore, the chemoselective reaction is a significant issue in this process [3, 4]. The reaction mechanism reaction of 3-NS hydrogenation has been represented by Haber et al. The reaction mechanism has been two different reaction routes including direct and condensation pathway [3]. Hydrogenation of 3-NS could produce 3-ethylnitrobenzene (3-ENB) and 3-ethylaniline (3-EA), which resulted from over hydrogenation of 3-NS and 3-ENB [3]. Generally, 3-NS hydrogenation has proceeded in an organic solvent such as toluene and tetrahydrofuran in order to obtain the high selective product (3-VA) up to 99% whereas low activity in the event of nitro group liquid-phase hydrogenation that was reported over Au/TiO$_2$ catalyst and operated P_{H2} = 3bar and T = 393K [1]. The obtaining higher activity for hydrogenation of 3-NS, which suspension over Pt/TiO$_2$ resulted in high activity, but a ratable formation of byproducts was detected [1, 4]. Furthermore, alloy catalyst such as Pt-Zn alloy prevented the adsorption of the vinyl group (C=C) double bond hydrogenation,

which was reported by Crespo-Quesada et al. Semiconductor (MgO, CeO$_2$, TiO$_2$, and Fe$_2$O$_3$) has been used for support and doping metal such as Pt nanoparticle or activated carbon (Pt/C) [3].

The photocatalytic hydrogenation reaction has been one of the alternative processes to produce 3-VA from 3-NS [5-7]. It has facilitated selective nitroaromatic hydrogenation under gentle reaction conditions, which are imperative for secure and clean in order to synthesize functionalized anilines. Photoexcitation ($\lambda > 300$nm) of semiconductor TiO$_2$ with alcohol has acted as a hydrogen source that promotes chemoselective hydrogenation of nitroaromatic. Normally, TiO$_2$ has a three type of polymorphic forms including anatase, rutile, and brookite. Mostly anatase and rutile forms have often applied for photocatalytic reaction. In part of, anatase form has exhibited higher activity than rutile. Furthermore, Degussa P25-TiO$_2$, which was a mixture between 80% of anatase and 20% of rutile further improved the photoactivity due to the effect of antenna their structural especially based from the synthesis method and which is synthesized by the dry process (flame pyrolysis of gaseous TiCl$_4$). In addition, this reaction has operated at room temperature and atmospheric pressure because of safe and serious significance in terms of environmental less impact. Mechanism of photocatalytic 3-NS hydrogenation is activated by irradiation of ultraviolet (UV light), that occurred oxidation and reduction reactions at valence band and conduction band respectively. Moreover, source of energy equal to and higher than band gap, the electron is excited and migrated to conduction band and hole is generated at valence band. The band gap energy is the distance between conduction band to valence band, which depend on morphology, particle size and phase content [8]. In the application of photocatalytic by TiO$_2$ semiconductor, using UV light is activated by non-metal dopant on semiconductor, which has promoted in this reaction. However, non-selective and selective transformations of reactants to aimed products are tough to attain. In this reaction using TiO$_2$ suspended in isopropanol and mixed with nitroaromatics under inert gas atmosphere, photoexcited TiO$_2$ generate the electron then excited electron transfer to the conduction band and produce positive hole pair at valence band. The isopropanol acted as hole scavenger and produces ketone group and protons. The

reduction of nitroaromatics on active sites due to receive electron thus produces the consistent aniline at conduction band. However, these reaction correlation with surface states results in recombination electron-hole pairs leading to low photoactivity.

In this work reported with the effect of calcination temperature of $P25-TiO_2$ on photocatalytic hydrogenation selective 3-NS in isopropanol. After treated $P25-TiO_2$ which obtained from calcination exhibited the characteristic of BET surface area, phase transformation, crystallinity, morphology after that treated $P25-TiO_2$ were tested by photocatalytic under UV light irradiation at atmospheric atmosphere and room temperature. After that, the substrate and product were analyzed by GC-FID for determining conversion of 3-NS and selectivity to 3-VA.

1.2 Research objectives

To investigate the effect of calcination conditions of $P25-TiO_2$ on photocatalytic selective hydrogenation of 3-nitrostyrene.

1.3 Scope of research

1.3.1. To investigate the effect of calcination conditions of $P25-TiO_2$ on photocatalytic selective hydrogenation of 3-nitrostyrene.

1.3.2. $P25-TiO_2$ catalysts were calcined under air at 600, 700, 800 and 900 ℃ for 5h.

1.3.3. Select the optimum condition of calcination in air. Then, the catalysts was calcined under H_2 and N_2 gas flow for 5h.

1.3.4. Photocatalytic selective hydrogenation of 3-NS were tested under UV-light irradiation for 6h. After the reaction, the all products were analyzed by using GC-FID.

1.3.5. Treated $P25-TiO_2$ were analyzed by using X-ray diffraction (XRD), BET surface area, X-ray photoelectron spectroscopy (XPS), UV-Vis spectroscopy (UV-Vis), Photoluminescence spectroscopy (PL), SEM-EDX, Thermogravimetric analysis (TGA).

1.4 Research of methodology

```
┌─────────────────────────────┐
│       Calcination P25        │
└─────────────────────────────┘
              │
              ▼
┌─────────────────────────────┐
│  Calcination with atmosphere │
└─────────────────────────────┘
              │
              ▼
┌─────────────────────────────┐
│  Temperature ranges 600-900°C, 5h │
└─────────────────────────────┘
```

Photocatalytic test hydrogenation of 3-nitrostyrene with $h\nu > 300$ nm, 6 h

Catalysts Characteristics
XRD
XPS
BET Surface area
UV-Vis
Photoluminescence spectroscopy
SEM-EDX
TGA

Analysis product by GC-FID

Select the optimum condition of calcination in air. Then, the catalyst was calcined under H_2 and N_2 gas flow for 5h

Discussion

Conclusion

CHAPTER 2

BACKGROUND AND LITERATURE REVIEWS

2.1 Titanium dioxide

2.1.1 Titanium dioxide structure

Titanium dioxide (TiO_2) has wide for using the application in industrial catalyst because of its stability, good ability, and non-toxic for environmental and human [9]. First-time Fujishima and Honda used TiO_2 as a semiconductor in photocatalytic decomposition of water splitting [10]. In recently year using TiO_2 in many application including foods, mixing cement, cosmetic, electronic, pigment, self-cleaning, stability of cement. The photocatalytic mechanism within semiconductor includes redox (reduction and oxidation) reaction, which simultaneously generate electron at conduction band and hole at valence band. The main point in the semiconductor of photocatalysis is band gap energy. Therefore, band gap is implicated energy between CB and VB level within the semiconductor. Some photocatalytic reaction has a different distance of band gap, so modification of the efficiently of band gap promote activity [11].

Normally, TiO_2 has three major crystalline phases, which include rutile, anatase, and brookite. In case of rutile phase has a stable phase more than another phase at high calcination temperature, which applies in application of cosmetic and sunblock due to narrow band gap (3.0eV) [12]. However, the anatase phase has a small particle size range 6-30nm, which has been exhibited the surface energy lower than rutile and brookite (0.3-1um) [13]. In addition, P25-TiO_2 (Degussa) is commercial TiO_2, which is synthesized from pyrolysis then it has anatase 80% rutile 20%. Moreover, P25-TiO_2 could transform into another phase via the process of calcination at high temperature more than 600℃ [14, 15]. The morphology structure of lattice parameter and number of atoms per cell for TiO_2 polymorphs shown in Table 2. Moreover, the structure and properties of TiO_2 on the different phase are shown in Figure 1, 2 and Table 1. In order that preparation of TiO_2 catalysts, using a titanium (IV) isopropoxide in alcohol and DI water result in amorphous, which could treat by the hydrothermal method to different phase anatase, rutile and brookite [13]. In

addition, we can classify the crystal system, density, band gap, refractive index, which are shown in Table 1.

Rutile phase is the most stable polymorph under surrounding condition. Moreover, anatase and brookite could transform to rutile by heat treatment due to dependent particle size and temperature [1 4 , 1 5]. The synthesis of TiO_2 from amorphous to nanocrystalline by sol-gel method then nanocrystalline is transformed to rutile also achieved certain particle size. This supposition was relative with particle size and anatase phase, which is the more stable form at the quality of nanoparticle. [13, 16, 17].
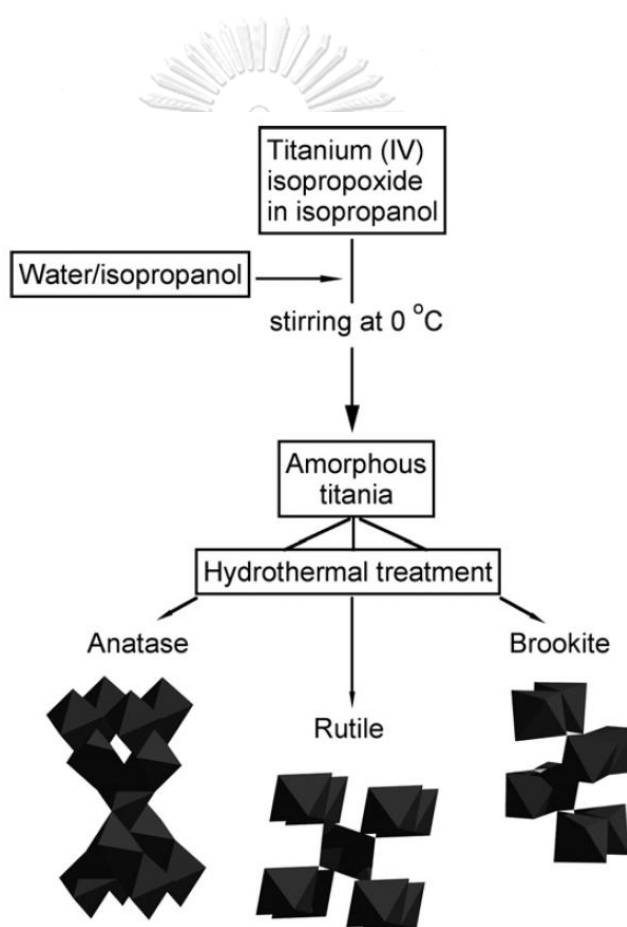
Figure 1 Hydrothermal method and structure of different phase of TiO_2 [13].
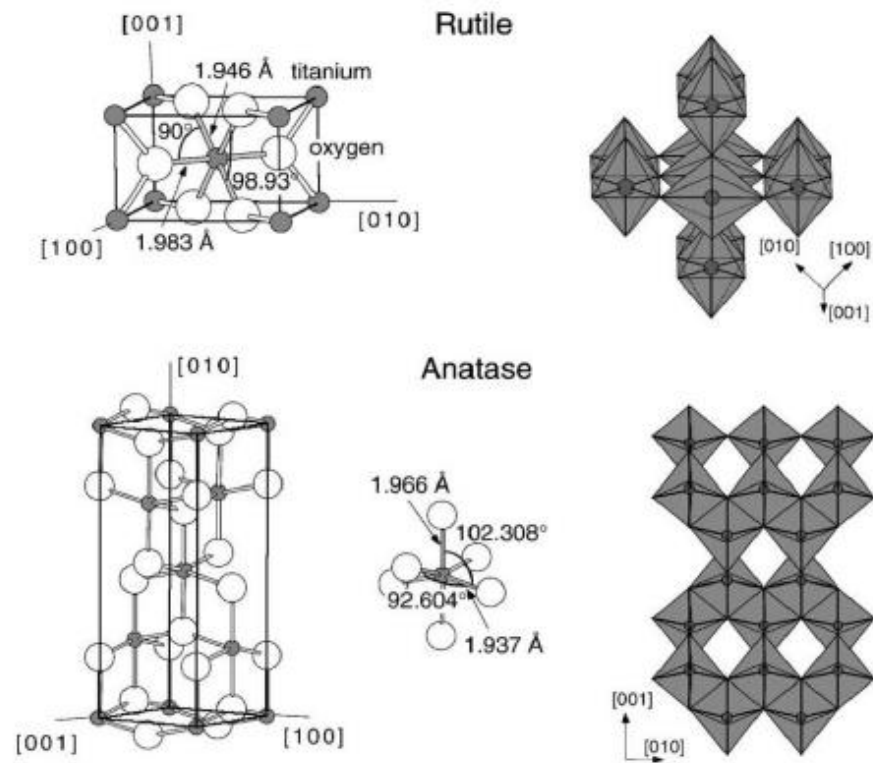
Figure 2 Crystal structure of different phase of TiO$_2$ [13, 17].

Table 1 Properties of a different phase of TiO_2 [17].

TiO_2	Molecular weight: 79.866 g/mol
	Melting point: 1844 °C
	Boiling point: 2973 °C
	Appearance: white particle
	Odorless
	Insoluble in water
Phase of TiO_2	**Properties**
Anatase	Crystal system: Tetragonal
	Density: 3.79-3.84 g/cm^3
	Refractive index: 2.52
	Band-gap: 3.19 eV
Rutile	Crystal system: Tetragonal
	Density: 4.13-4.26 g/cm^3
	Refractive index: 2.72
	Band-gap: 3.11
Brookite	Crystal system: Orthorhombic
	Density: 3.99-4.11 g/cm^3
	Refractive index: 2.63
	Band-gap: 3.00

Table 2 Crystalline properties such as lattice parameters (A, B and C (Å)) and number of atoms per cell (Z) for a different phase of TiO_2 [16].

Crystalline component	Space group	A (Å)	B (Å)	C (Å)	Z
Anatase	I41/amd	3.785	3.785	9.514	4
Rutile	P42/mnm	4.593	4.593	2.959	2
Brookite	e Pbca	9.182	5.456	5.143	8

2.1.2 Degussa P25

Degussa P25 is commercial TiO_2, which contains a mixture of anatase and rutile components in ratio 3:1. $P25\text{-}TiO_2$ is synthesized by dry technique with flame pyrolysis of gas phase $TiCl_4$. The average particle sizes of $P25\text{-}TiO_2$ is 25nm, moreover which has been a BET surface area ($\approx 50 \ m^2 \ g^{-1}$). The microstructure of $P25\text{-}TiO_2$ show in Table 3 [5, 18]. $P25\text{-}TiO_2$ suits in an application for photocatalytic fields because it shows high activity and improves the photocatalytic reaction system [5]. First time who used $P25\text{-}TiO_2$ for photocatalytic activity is Bickley et al., they reported images and diffuse reflectance spectra by transmission electron microscopic (TEM) of anatase and rutile surface structure [15, 18]. The performance of $P25\text{-}TiO_2$ has mixed phase and induce the high photocatalytic activity more than pure phase due to interface anatase and rutile. However, $P25\text{-}TiO_2$ could transform from anatase to rutile by HF treatment or heat treatment [14, 19, 20].

Table 3 Microstructure of commercial P25-TiO$_2$ [5, 20, 21].

Parameter (test method)	Commercial TiO$_2$
Anatase component (%)	83
Rutile component (%)	17
Anatase crystallite size (nm)	20.8
Rutile crystallite size (nm)	30.5
BET surface area (m^{2}g^{-1})	51.46
Total pore volume (cm^{3}g^{-1})	0.17

2.1.3 Applications of titanium dioxide

TiO$_2$ is applied in photocatalytic and photovoltaic fields. In addition, TiO$_2$ are hydrophobic or non-dissolve with water. Molecular dynamics has been demonstrated to be an essential technique in form as slurry or colloid for the investigation of basic adsorption [22]. The main patents of photocatalytic reaction could classify three categories, which include air treatment, water treatment and self-clean. The distribution of patents show in Figure 3.

Distribution of patents
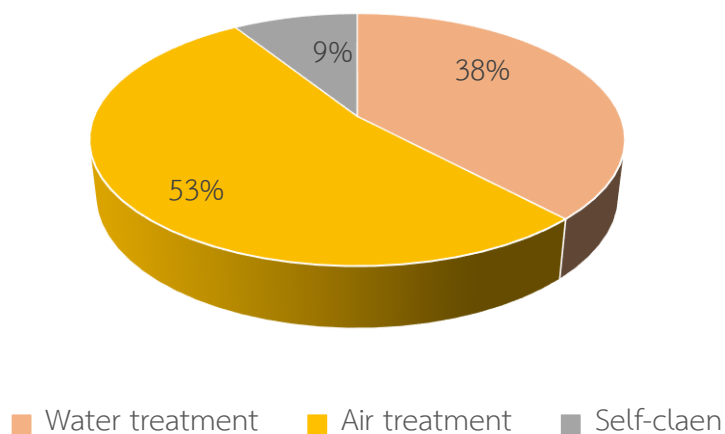
Figure 3 Distribution of patents of TiO$_2$ on a cumulative basis [10].

2.2 Effect thermal treatment of titanium dioxide on the photocatalytic

P25-TiO$_2$ used as photocatalytic activity due to improvement activity, which has a particle size in range 21-30nm [14]. Treated P25-TiO$_2$ by calcination at high temperature results in changing of properties such as the specific surface area, pore volume and micropores area, which would reduce. However, rutile component, particle size, crystalline size, and pore size, which would increase [14]. Nitrogen adsorption-desorption isotherms of treated P25-TiO$_2$, which calcined above 200°C represented type IV nitrogen isotherm and mesopores, which led to reduce calcination higher 500°C. The external surface area, pore volume of P25-TiO$_2$ would decrease when P25-TiO$_2$ was calcined at high temperature. This reasoning was suggested because pore diameter in temperature range for calcination affected to sintering and phase transformation [14].

Nadia R.C. et al [14] reported the effect of heat treatment of P25-TiO$_2$ under process reaction of alcohol decomposition on the surface particle. Therefore, this effect resulted in dehydration and dehydrogenation. Dehydration was normally catalyzed by acidic sites, while dehydrogenation had both basic sites and acidic sites. Isopropanol decomposition was investigated in dehydrogenation properties of the catalyst. However, the acidity was used in process of dehydration, which resulted in propene formation, whereas basicity involved to process dehydrogenation, which resulted in acetone formation, in addition, these process has corresponded with ratio dehydration [23]. Furthermore, the surface on TiO$_2$ has properties both acidic and basic sites [23]. The acidic sites related to unsaturated surface metal ions, whereas basic sites related to surface oxygen anions or anion oxygen vacancies [23]. In addition, thermal treatment influenced to properties on the surface, which included the acidity and basicity along with increasing calcination temperature at above 500°C, which exhibited decreasing acidity. This reasoning was suggested due to polymorphic transformation [14, 23]. The concentration of pH higher pH$_{(ZPC)}$ resulted in negatively charged on the surface catalyst, whereas the concentration of pH lower the pH$_{(ZPC)}$ resulted in the surface of the catalyst had positively charged [24]. The result of pH$_{(ZPC)}$ would increase when increasing of calcination temperature at 700°C, which had a slightly basic pH value [14]. Phenol pollutant degradation was used in the

photocatalytic reaction, which carried out under UV light irradiation. The direct mechanism of this photocatalytic degradation of phenol to CO_2 and H_2O formation could be occurring for main by-product in form of catechol, hydroquinone and benzoquinone. The poor photocatalytic activity of phenol degradation represented in rutile phase more than anatase phase, so uncalcined TiO_2 represented higher degradation than calcined TiO_2. Moreover, results of phenol degradation was explained by anatase phase crystalline and hydroxyl groups, which could promote photocatalytic reactions [25, 26].

At lower calcination temperature resulted in the chemisorbed water directly bound to Ti^{4+}, which resulted in the intensity of surface hydroxyl groups (OH^-) or chemisorbed H_2O were decreased due to increasing of calcination temperature. Therefore, the calcination of TiO_2 led to inhibition of the photocatalytic activity [27, 28]. On the other hand, the increasing intensity of surface OH^- group led to faster photocatalytic activity. If low $pH_{(ZPC)}$ value could affect the higher activity due to the high surface-absorbed water and hydroxyl groups, so the effect of pH enhanced phenol degradation [23]. Furthermore, calcination of TiO_2 at high temperature affected the surface-absorbed, which led to partial rehydroxylation due to revealing with water [14]. The surface area influenced to convenient reaction because the large surface area may mild the density of active sites for phenol adsorption. Moreover, increasing of crystallite size was associated with decreasing of the palpate active site area between substrate and catalyst, which may result in a reduction of photocatalytic activity [14]. In addition, phenol degradation under light irradiation mechanism had light energy greater than band gap energy, which resulted in generated holes in the valence band, suddenly the electron was excited then migration of electron to the conduction band, which resulted in separation electron and hole [14, 29]. Phenol degradation was absorbed in positive holes. This effect led to the occurrence of oxidation water or hydroxyl group, which oxidized to a hydroxyl radical (OH^-) and occurred reaction with phenol. This reaction was related between a short-lived excited state of phenol and TiO_2 promoted to charge squirt into conduction band [14, 29].

Guahong Wang et al [19] studied the enhancement of photocatalytic activity of methyl orange aqueous solution suspension in P25-TiO_2 via calcination treatment. P25-TiO_2 were calcined at 400-800°C in a muffle furnace for 4h after that cool down to room temperature to obtain treated P25-TiO_2. The properties of P25-TiO_2 were already calcined after that all treated catalysts were analyzed by several characteristics, which included XRD patterns, FT-IR spectra, UV-Vis absorption spectra, band gap, SEM and TEM. P25-TiO_2 was calcined at temperature 400°C to 500°C resulted in intensities of anatase peaks was decreased. However, increasing of temperature calcination higher than 500°C resulted in anatase peaks was disappeared conversely intensities of rutile peak was gradually increased. At temperature 800°C, the content of anatase was disappeared because anatase was transformed to completely rutile. In addition, calcination of TiO_2 influenced to increasing of crystallization because it occurred from agglomerated of particle size [19].

UV – Vis spectra were reported by light absorption characteristics of P25-TiO_2 powders. Increasing calcination temperature at 500°C and 700°C for 4h led to decreasing of band gap energy, which caused by increasing of crystallite size factors and effect of transformation of anatase peaks to rutile [19, 32].

FT-IR results were attributed with hydroxylation state of titanium dioxide powders. Increasing of calcination temperature resulted in the adsorbed surface of water and hydroxyl groups, which were slightly decreased due to decreasing of specific surface area and pore volume, which are shown in Figure 4. Furthermore, the effect of the hydroxyl group on the surface of catalyst sample improved photocatalytic activity In addition, charge carriers transferred to photogenerated of holes. Therefore, they decreased recombination electron-hole pairs [30, 31].
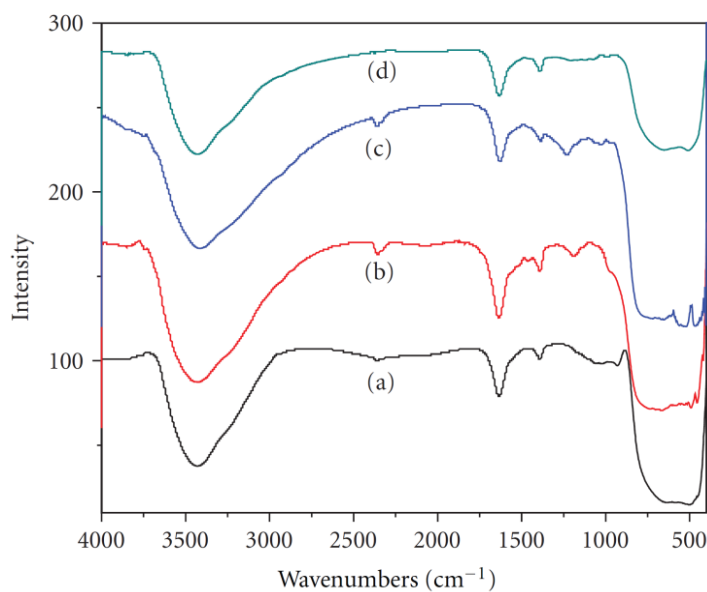
Figure 4 FT-IR spectra of the (a) P25-TiO$_2$ before and after calcination at (b) 400℃, (c) 500℃, (d) 600℃ in air for 4h [19].

BET surface area and pore distribution were represented by nitrogen adsorption-desorption isotherms of the P25-TiO$_2$ powders. Increasing of calcination temperature resulted in higher pressure rang and the decreasing of areas of the hysteresis loops. Moreover, all treated P25-TiO$_2$ powders exhibited type H3 hysteresis, which is shown in Figure 5. Effect of high calcination temperature influenced the results of average pore size were increased, but pore volume was decreased. Therefore, this effect had a relative with increasing of crystallite size of P25-TiO$_2$ [19, 33]. Figure 6 represents the pore size of treated P25-TiO$_2$ and the uncalcined P25-TiO$_2$, which had wide pore size due to increasing of calcination temperature. This effect resulted in pore size was decreased and shifted to the macropore region.
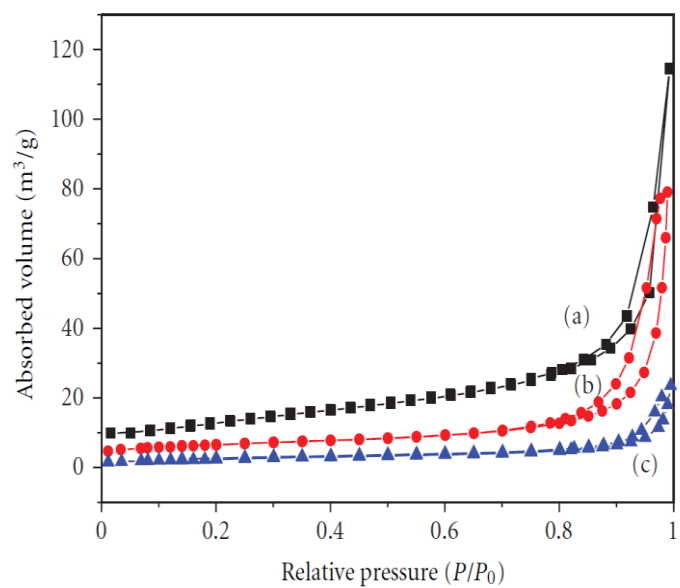
Figure 5 Nitrogen adsorption-desorption isotherm of the (a) P25-TiO$_2$ before and after calcination at (b) 500℃, (c) 700℃ in air for 4h [19].
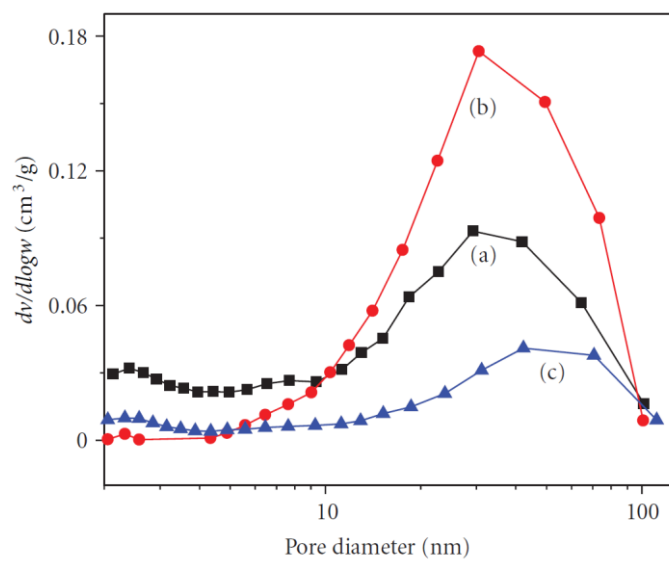
Figure 6 Pore diameter distribution curve of the (a) P25-TiO$_2$ before and after calcination at (b) 500℃, (c) 700℃ in air for 4h [19].

Morphologies of treated P25-TiO$_2$ powder exhibited in form of SEM and TEM images. Result of increasing of agglomerated particles caused by decreasing of pore volume along with phase transformation. Results of TEM images shown microstructures of treated P25-TiO$_2$ after heat treatment at 500°C for 4h, which could observe the particle size distribution about 35 nm. In addition, it represented a large number of mesopores, which caused by aggregation of primary particles size. HRTEM of treated P25-TiO$_2$ after heat treatment at 500°C for 4h exhibited interplanar distance of anatase(101) 0.35nm and rutile(110) 0.33nm, which are shown in Figure 7 [19]. Guahong Wang et al. investigated the photocatalytic activity of oxidation of methyl orange aqueous solution under UV irradiation via calcination of P25-TiO$_2$. Increasing of calcination temperature resulted in the rate constants were increased. This factor led to the enhancement of photocatalytic activity [19]. At calcination at 500°C observed higher rate constant value more than other catalysts sample. However, calcination temperature higher 500°C resulted in rate constant would decrease slightly due to the decreasing of specific surface areas and low intensities of anatase peak. Normally, photocatalytic activity on TiO$_2$ depended on properties of catalysts, which included phase component, crystallite size or surface area. Furthermore, large surface area enhanced organic reactant, which was absorbed onto the surface of the catalyst. Although, higher pore volume resulted in the rapid diffusion of different inorganic products during the photocatalytic reaction. Recombination of electron and holes influenced to photocatalytic activity when a large amount crystalline influenced to poor photocatalytic activity and increased recombination of electron and holes, but the large surface area was not an assertive factor. It well-known P25-TiO$_2$ has mixture anatase and rutile contents, which resulted in higher degradation efficiency more than pure phase (anatase, rutile), so the ratio of anatase and rutile have been an important factor for photocatalytic activity [19].
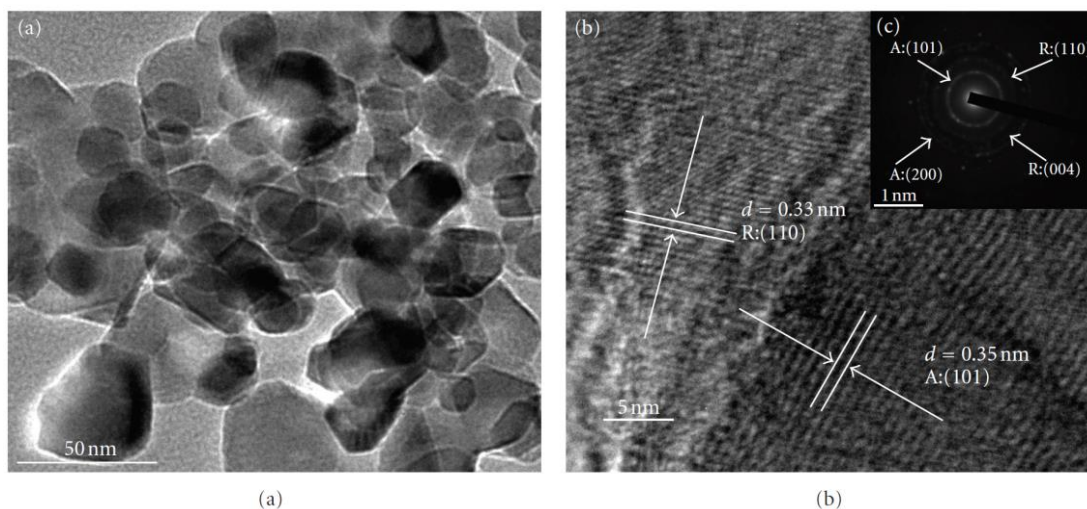
Figure 7 (a) TEM and (b) HRTEM images and SAED pattern of P25-TiO$_2$ after calcination at 500℃ in air for 4h [19].

Klaysri, R et al. [34] investigated the impact of atmospheres calcination of nanocrystalline of TiO$_2$ and Si-doped on methylene-blue degradation. Furthermore, catalysts sample were synthesized by solvothermal and sol-gel methods. Then, the catalysts sample were calcined in the atmosphere, including O$_2$, air and inert gas (N$_2$) were studied. Calcination under air resulted in surface defect site was occurred and interface species in Si-doped TiO$_2$. Moreover, calcination under inert gas (N$_2$) increased the concentration of formation Ti^{3+} site on the surface. Properties of calcination in oxygen, air, and nitrogen did not affect to gradate phase structure and crystallite size. Methylene-blue degradation both UV and visible light irradiation on TiO$_2$ calcined under N$_2$ gas along with Si-doped TiO$_2$ led to high methylene-blue degradation due to increasing of anatase phase and formation Ti^{3+} site on the surface.

Nae-Lih Wu et al. [35] studied the effect of heat treatment at 400℃ in atmosphere, which included argon, air, N$_2$, (H$_2$ 3% in N$_2$) and vacuum (~5 × 10^{-3} torr) respectively. The catalysts sample were synthesized by a sol-gel process in order to produce H$_2$ from a water/methanol (vol. ratio = 1.4/1) solution photocatalytic reaction. Heat treatment with different flow gas resulted in the anatase crystallite size of TiO$_2$. Anatase phase of treated TiO$_2$ had slightly changed, whereas heat treatment with argon flow presented higher equilibrium accumulative production and hydrogen generation rate from methanol/water mixture. Treated TiO$_2$ under vacuum

and H_2 represented the strong absorption on visible lights more than air, argon, and N_2, which associated with oxygen-deficiency in the system. In this work, argon represented highly photocatalytic activity, while calcination under H_2 and vacuum resulted in a high defect and low photocatalytic activity.

Sasithorn Kuhaudomlap et al [36] studied treatment of TiO_2 support under H_2 flow and Pt-doped on TiO_2 support catalyst by strong electrostatic adsorption (SEA) for liquid phase selective hydrogenation. The TiO_2 catalysts sample were synthesized by sol-gel process along with Pt-doped by SEA and impregnation after that they were calcined in air and H_2. The H_2 treatment exhibited high oxygen vacancy, which led to the formation of Ti^{3+} centers. The hydrogenation reaction liquid phase 3-nitrostyrene on Pt/TiO_2 combined SEA and H_2-treated exhibited high selective 3-vinylaniline and Pt dispersion along with strong interaction between Pt and surface TiO_2.

Yiqing Zeng et al [37] studied the effect of heat treatment under atmosphere along with Ce-doped on TiO_2 catalysts to obtain performance of selective catalytic reduction of NO with NH_3. The Ce-doped TiO_2 were synthesized by a sol-gel method after that the catalysts sample were calcined in air and N_2. The calcination under flow N_2 exhibited formation Ce-O-Ti, which promoted active sites for reduction NO by NH_3. The characterization confirmed Ce species incorporate into TiO_2 lattice, including XPS spectra exhibited a shift to high binding energy, when TiO_2 was calcined under N_2 and improved reduction NO by NH_3.

Xudong Jiang et al [38] studied oxygen vacancy, which associated within hydrogenation of $P25-TiO_2$. $P25-TiO_2$ was used in this reaction and it was treated by hydrogen gas flow along with temperature at 400°C for 10h, which compared as untreated $P25-TiO_2$. The characterization of annealing of $P25-TiO_2$ under hydrogen gas flow exhibited a large concentration Ti^{3+}- oxygen vacancy. The association of Ti^{3+}- oxygen vacancy sites on TiO_2 improved photocatalytic activity due to low recombination electron and hole.

Wibawa H et al. [39] studied the Ti^{3+} containing on commercial titania dioxide, which included P25, Hombikat, and rutile. The catalysts were carried out in a tube furnace with H_2 flow at different temperature (400-700°C). $P25-TiO_2$ were the hydrogenated by temperature 500°C to 700°C presented the paramagnetic from EPR

spectra, which exhibited highest concentration of Ti^{3+} and oxygen vacancy sites, which observed as compared with the catalyst sample without hydrogen treatment.

Nadia R.C. Fernandes Machado et al [14] studied the effect of thermal treatment on the phenol degradation under visible and near UV irradiation for 5h. Calcination of P25-TiO_2 various temperature at 200, 300, 400, 500, 600 and 700°C. Heat treatment above 500°C affected to reduction specific surface area, external surface area, pore diameter and the particle agglomeration due to surface diffusion. Furthermore, the results of increasing of specific acidic surface and slightly basicity, are shown in Table 4, which correlated to the ratio between acetone and propene formation due to an irreversible change in surface chemistry. Calcination temperature at 600°C resulted in anatase content, which was highly reduced due to transformed to rutile.

Table 4 Zero point charge (pH_{ZPC}) of calcination of P25-TiO_2 was reported by Nadia R.C. Fernandes Machado et al. [14].

Catalyst	pH_{ZPC}
P25	3.52
P25-200	3.61
P25-300	3.77
P25-400	5.45
P25-500	6.41
P25-600	6.61
P25-700	7.41

2.3 Hydrogenation of nitroaromatic mechanism

Functionalized aniline is produced by hydrogenation of nitroaromatic, which is organic molecules and most important processes in fine chemistry and value chemical [3]. Ciba-Geigy developed an effective catalyst for production aniline toward >99% selectivity and approach was to introduce enlarger into the formula of catalyst [3]. The network of functionalizing of aniline is 3-vinylaniline, which has

reducible vinyl-group. 3-vinylaniline is the main compound for production for fine chemicals such as polymers, pharmaceutical, and herbicide. 3-vinylaniline is produced from the hydrogenation of 3-nitrostyrene, which is proposed by Haber et al. in Figure 8.
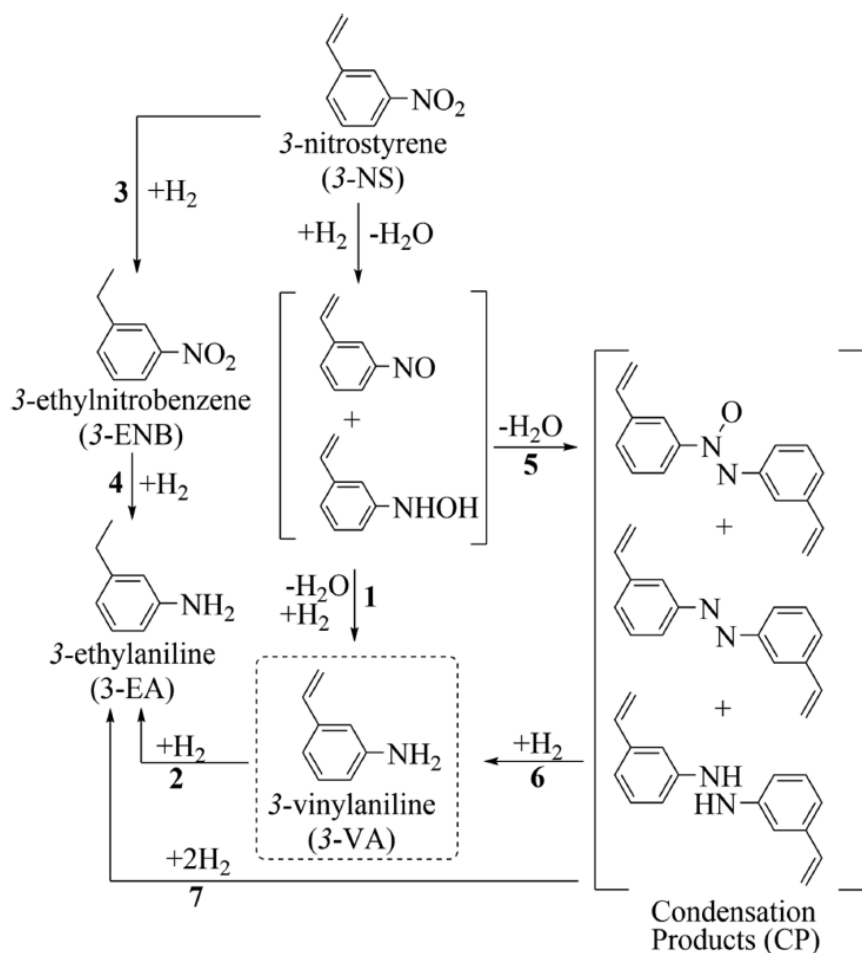
Figure 8 Mechanism of the 3-nitrostyrene hydrogenation was reported by Haber et al. [3].

Hydrogenation of 3-nitrostyrene has two pathway are suggested in this reaction. The first path is the direct pathway to 3-vinylaniline and the second path is condensation route to 3-vinylaniline. Moreover, this process normally is operated in organic solvents such as toluene and tetrahydrofuran (THF). Therefore, these solvent acute implications in term of environmental impinged [3]. Several of authors studied in liquid phase 3-NS generally operated with high temperature (T>393K) and high

hydrogen pressure (P_{H2} > 3 bar) conditions. In addition, Au/TiO$_2$ catalyst exhibited low activity, while Pt/TiO$_2$ exhibited high activity, but the ratable formation of byproduct was detected. However, semiconductor was not doped with metal resulted in not occurrence of conversion of 3-NS and selectivity to 3-VA, so doping metal on semiconductor promoted to activity and chemoselective of products [1-4, 40-43].

However, zinc metal as doped into Pt-catalyst granted to reduce C double bond (C=C) hydrogenation, which suggested the reformation of electronic properties of Zn in Pt-Zn alloy interrupted the adsorption of double bond during crotonaldehyde hydrogenation [3].

Sukanya Pisduangdaw et al. [2] studied flame-made Pt-doped on TiO$_2$ catalyst for liquid phase selective hydrogenation of 3-nitrostyrene. This reaction was operated under isothermally at 323K and H$_2$ pressure at 4MPa. Flame-made method exhibited higher Pt dispersion along with high chemical reaction activity liquid phase hydrogenation of 3-nitrostyrene. Range of temperature 500-600°C for reduction of Pt resulted in higher both Pt dispersion and interface sites between Pt and TiO$_2$ thus high activity. The reducing Pt layer atoms also decreasing of temperature enhanced selectivity to 3-vinylaniline without decreasing of activity. Moreover, flame-made method prevented an exorbitant Pt, which caused coverage active sites of TiO$_2$ species.

2.4 Photocatalytic on hydrogenation of nitroaromatic mechanism

The photocatalytic reaction is an alternative for hydrogenation of nitroaromatic reaction, which has friendly for environmental and safe. Moreover, catalysts in photocatalytic reaction discovery on TiO$_2$ based. First authors reported water splitting is Fujishima and Honda et al [44]. In 1975 Boonstra and Mutsaers who were firstly reported the hydrogenation of ethane and ethyne based on P25-TiO$_2$ and source of lights was Philip P 500w spectrum lamp [9]. The photocatalytic reduction of nitrobenzene in alcohol suspension with TiO$_2$ produced aniline and ketone groups. The commercial TiO$_2$ presented the rutile phase, which has high activity and selective of aniline, which transformed from nitroaromatic in alcohol suspension. This reaction was operated under atmospheric pressure and room temperature.

Moreover, anatase and P25-TiO$_2$ shown low activity and selective aniline [5]. Hydrogenation for nitroaromatic to aniline without using hydrogen gas, but using alcohol was hydrogen source in this reaction. TiO$_2$ semiconductor was irradiated by ultraviolet (UV) light, which led to activated to reduction and oxidation reaction. Photocatalytic hydrogenation of reduction reaction of nitroaromatic transformed to aniline via formation of nitrosobenzene and *N*-phenylhydroxylamine, which were intermediates. Figure 9 includes 5 steps in order to obtain aniline [5].

$$\text{TiO}_2 + h\nu \rightarrow \text{h}^+ + e^- \tag{1}$$

$$(\text{CH}_3)_2\text{CHOH} \xrightarrow{2\text{h}^+} (\text{CH}_3)_2\text{CO} + 2\text{H}^+ \tag{2}$$

$$\text{Ar-NO}_2 \xrightarrow{2e^-,2\text{H}^+} \text{Ar-NO} + \text{H}_2\text{O} \tag{3}$$

$$\text{Ar-NO} \xrightarrow{e^-,\text{H}^+} [\text{Ar-NOH}^\bullet] \xrightarrow{e^-,\text{H}^+} \text{Ar-NHOH} \tag{4}$$

$$\text{Ar-NHOH} \xrightarrow{e^-,\text{H}^+} [\text{Ar-NH}^\bullet] + \text{H}_2\text{O} \xrightarrow{e^-,\text{H}^+} \text{Ar-NH}_2 \tag{5}$$
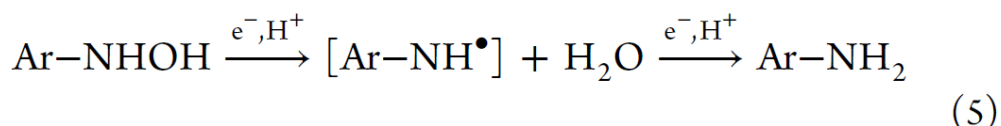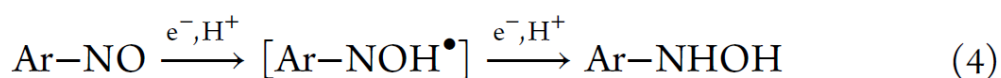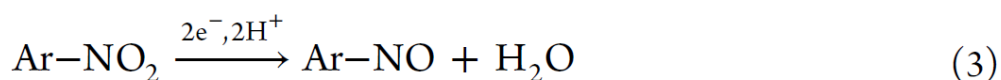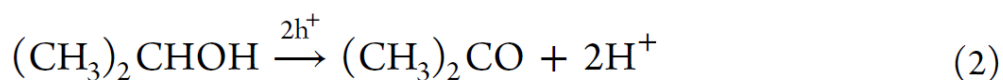
Figure 9 Mechanism of photocatalytic hydrogenation of nitroaromatic with the suspension of TiO$_2$ in 2-Propanol [5].

<u>Step 1</u>

The photonic activation of catalyst is important for photocatalytic, which substituted by thermal activation [5]. The structure of semiconductor is characterized by electronic band structure, which includes valence band and conduction band. The valence band is the highest occupied band, but conduction band is the lowest occupied energy band [8]. The photo-excited is occurred when energy equal or higher band gap (distance of conduction band to valence band) after that semiconductor is excited electron atom (e$^-$) and transferred from valence band to conduction band and positive hole (h$^+$) is simultaneously generated in valence band under irradiation, which is shown in equation (1).

$$TiO_2 + h\nu \quad \text{--->} \quad TiO_2 (e^- + h^+) \qquad (1)$$

In addition, electron and the positive hole could recombine in bulk or surface because the electron is transferred from conduction band and easily transferred back to valence band [8]. During recombination, this occurrence lead to photo-induced charge carriers a certain of energy could release in form of heat or light energy [8].

Step 2

The absorbed positive hole is called hole scavenger in this process. The alcohol served as hole scavenger and solvent in photocatalytic oxidation [5]. The photocatalytic oxidation placed onto a photo-activated semiconductor particle thus alcohol with h^+ was oxidized to ketone group and it released proton and electron. Isopropanol acted as hole-scavenger in this process and dehydrogenated to acetone, which shown in equation (2).

$$(CH_3)_2CHOH \quad \text{--->} \quad (CH_3)_2CO + 2H^+ \qquad (2)$$

Step 3-5

This step 3-5 is a photocatalytic reduction on the surface of TiO_2, which is the active and reducing species in the TiO_2. Photocatalytic reduction of nitrobenzene with isopropanol was excited electron in the conduction band. The reduction nitroaromatics and electron produced the corresponding of anilines via nitrosobenzene (Ar-NO) and N-phenylhydroxylamine (Ar-NHOH) [5].

The overall reaction of photocatalytic step can conclude and divide 4 methods following by

1. Absorption of light energy resulted in the separation of the electron-hole pair in the semiconductor.

2. Adsorption of the substrate.

3. Redox reaction (reduction and oxidation).

4. Desorption of the products.

The redox reactions involved the sort of absorbance on the semiconductor surface, which occurred just potential redox both conduction and valence potential. The reaction was accorded and occurred thermodynamically, which favored also overall process following by equation (3)

$$Ar\text{-}NO_2 + 3(CH_3)_2CHOH \quad \text{--->} \quad Ar\text{-}NH_2 + 3(CH_3)_2CO + 2H_2O \quad (3)$$

The band gap is different energy between the valence band and conduction band. When TiO_2 was stimulated by UV light, the electron was excited and transferred to an excited state.[11, 45]. Alcohol acted as a solvent for oxidation reaction and hole scavenger (D), which is an appropriate electron donor in order that generation to proton and decreasing of recombination process [6]. Electron acceptor (A) acted as grab electron and proton, which transformed into hydrogen for the hydrogenation reduction reaction. Figure 10 shows the photocatalytic reaction included reduction and oxidation reaction.
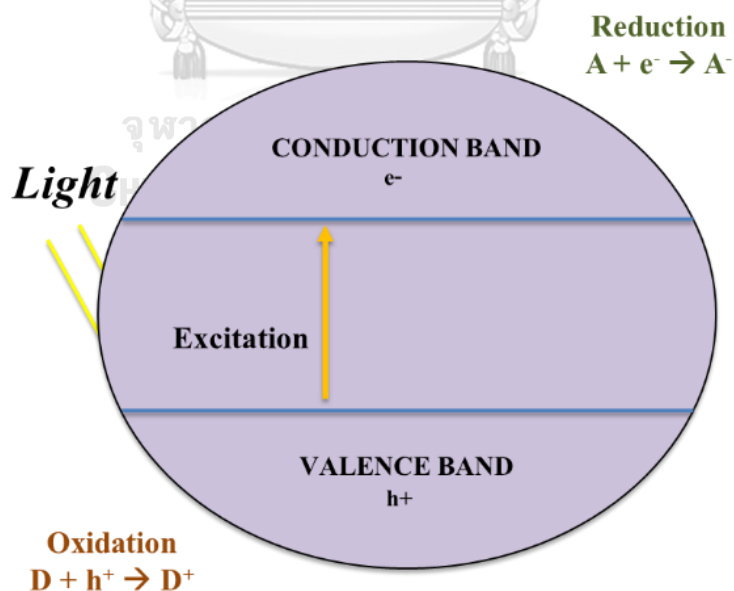
Figure 10 Mechanism of a photocatalytic reaction in semiconductor.

2.5 Recombination phenomena on photocatalytic reaction

A semiconductor is characterized by an electronic band, including conduction band and valence band, which were different occupied energy band and it is differentiated with band gap. Moreover, sub-band locate between the band gap such as a surface defect or surface state, which are shown in Figure 11.

The process I related to photo-excited. When energy is equal or higher band gap, excited electron transfer from valence band to conduction band and generates a positive hole in valance band [8].

The Process II is the band to band PL process. In this case, the photon energy verily equal to the band gap, which is described by electron migration from the bottom of conduction band to the top of valence band because excited electron could easily come back to ground state. Moreover, this occurrence has simultaneously released energy as radiation [8].

The Process III is the photoluminescence (PL) phenomenon, which is the non-radiative transitions of an excited electron from the bottom of conduction band budge thru different sub-band then radiative transitions of an excited electron to top of the valence band. This PL signal is also ascribed to a type of band–band PL occurrence. The energy of a radiative photon is different energy distance of sub-band and top of the valence band, which has lower than the band gap energy. Normally, the PL signal most affect from the surface of oxygen vacancies and surface-defects in semiconductors. Furthermore, the reasonable nanoparticle size is suggested, so the average distance is important, which the electrons could migrate freely to a very short period. This effect could occur at surface oxygen vacancies and defects, which lead to a sheaf of electrons then it results in the formation of excitons within the sub-band. This rationale is the excitonic PL phenomenon, which could occur in the nanoparticle, which includes small particle size also the larger intensity of oxygen vacancy and defect. The higher defects lead to the possibility of formed excitons phenomenon and the stronger the PL signal [8].
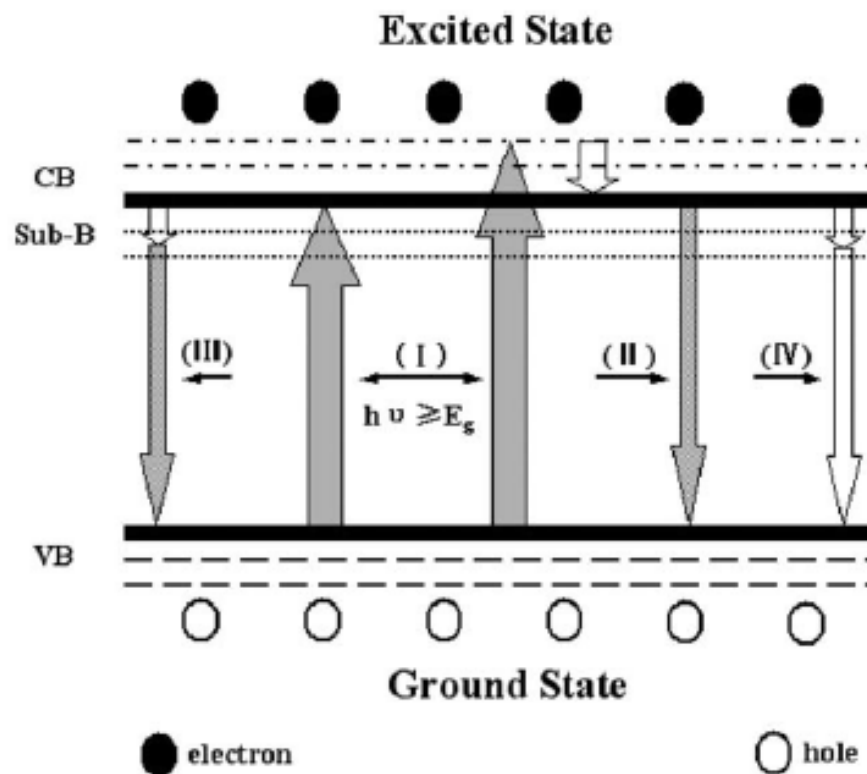
Figure 11 Photo-physical processes of a semiconductor are excited by light irradiation [8].

Fuchang Peng et al. [46] studied the synergistic effect of Sm and C Co-Doped mixed-phase crystalline of TiO_2 for visible-light photocatalytic activity. The catalysts were prepared by sol-gel method and Sm acted as anatase-rutile transformation and decreasing of favor of TiO_2 grain size and C doped, which resulted in the narrow band gap energy. Therefore, the hetero-junction structure of TiO_2 attributed to the improvement of MB degradation on photocatalytic reaction, which was observed as compared with P25-TiO_2 and pure phase of TiO_2 due to effective of separated electron and hole.

Xiuli Wang et al. [47] explained time-resolve photoluminescence spectroscopy of anatase/rutile TiO_2 phase junction. The charge separation was slowed the time scale photoluminescence, which resulted in the retarded rate for charge carriers. These results occurred in both anatase and rutile phase. However,

the slowed time-resolve of the charge carriers in anatase TiO_2 was forced, but no change in the charge carrier force of rutile TiO_2. Therefore, charge separation at the anatase and rutile phase linkage incurred favor in the separated charge carrier scale and it led to reducing electron and hole recombination.

Hiromitsu Nakajima et al. [48] studied a mixture of anatase and rutile TiO_2 nanoparticles and the effect of charge transferred between the nanoparticles on their photoluminescence excitation bands. The shapes of PL spectra of pure anatase, rutile and mixture anatase-rutile exhibited the same shapes and emission of spectra indicated to oxygen vacancy states, which had energy level ≈1eV below the conduction band. In this PL results of mixture anatase-rutile has lower intensity PL than pure anatase and rutile, so mixture anatase-rutile represented to promoted charge transfer between anatase and rutile particle. Moreover, increasing of rutile phase content resulted in narrow band gap energy.

Yang Mi & Yuxiang Weng [49] studied band alignment of anatase and rutile, in this work proposed to the prediction of electron migration. In case of large crystalline anatase and rutile in vacuum indicated the flow electron from conduction band of anatase to rutile. Nanocrystalline rutile and anatase with a diameter of 10-15nm in a vacuum, which indicated different the particle size and only the surface state and the mobility of anatase changed and mainly prediction same flow electron of large crystalline. Nanocrystalline rutile and anatase with hole scavenger, which assumed the same electron devastation rate thus electron flowed from rutile to anatase. Nanocrystalline rutile and anatase with electron scavenger such as Pt acted as received electron from the surface TiO_2 thus electron transferred from rutile to anatase.

Kenji Komaguchi et al. [50] studied photo-induced electron transferred from anatase to rutile in partially reduced TiO_2-P25 nanoparticle by ESR study. The pure anatase, rutile, and P25-TiO_2 were used for catalysts in this study. The spectra ESR of P25-TiO_2 had two different Ti^{3+} signals due to mixture anatase and rutile phases. In case of pure rutile was calcined at 673K without hydrogen treatment in vacuum, which exhibited strong Ti^{3+} signals, while pure anatase never observed Ti^{3+} as the same condition. Ti^{3+} signal of P25-TiO_2 changed slightly when P25-TiO_2 calcined in air.

In addition, Ti^{3+} of rutile were easily oxidized by air. Ti^{3+} was energy level 0.3-0.8eV, which located below conduction band and it acted as a trapped electron. In this work, the explanation was no the possibility excitation of valence band. The electron would give rise to the also Ti^{3+} of rutile. $P25-TiO_2$ certain amount electron transferred via the interface between anatase to rutile due to ESR signal because the line width of Ti^{3+} rutile smaller than anatase.

Hao Cheng et al. [51] studied the influence of phase complement, morphology and specific surface area on the photocatalytic activity of TiO_2 nanoparticle. TiO_2 was synthesized under alkaline conditions along with the different volume of HNO_3 (20, 60, 80, 120 ml) and they were compared with NaOH solution treatment. In the case of no treatment with NaOH and increasing of volume of HNO_3 led to reducing of average and crystal of rutile component. In addition, probability nanoparticle was formed. However, treatment with NaOH and increasing of volume NaOH resulted in decrease likewise no treatment with NaOH. Effect of heterogeneous phase (anatase and rutile) along with 1D of TiO_2 nanorod resulted in different conduction band energy, which acts as a driving force of electron migration and favor isoelectronic easy migrated to surface. Therefore, high efficiency for separated electron and hole led to highly MB degradation.

2.6 Oxygen vacancy and properties of photocatalytic reaction

The photocatalytic activity depends on the nature and density of surface adsorption, which shown dominant defects in TiO_2 surface are called Ti^{3+} defect and oxygen vacancy. There are two topics about the generation of Ti^{3+} surface defect from Ti^{4+} [52].

Topic 1 Ti^{4+} ion received a photoelectron. Normally, generated electron by UV-light irradiation on TiO_2. When energy is equal or higher band gap, the electron is excited and simultaneous generated hole. The generated electron could be a trap and induce to reduce Ti^{4+} and formed Ti^{3+} state. Moreover, holes oxidize with O^{2-} anions in order to form to O^-, which trap hole or even oxygen gas. The generation of the defect under UV-light irradiation shown in equations (4) to (7) [52].

$$TiO_2 + hv \quad ---> \quad e- + h^+ \qquad (4)$$

$$e^- + Ti^{4+} \quad ---> \quad Ti^{3+} \text{ trapped electron} \qquad (5)$$

$$h^+ + O^{2-} \quad ---> \quad O^- \text{ trapped hole} \qquad (6)$$

$$4h^+ + 2O^{2-} \quad ---> \quad O_2 \qquad (7)$$
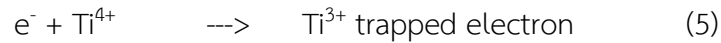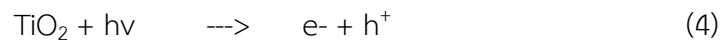
Topic 2 Ti^{4+} formed to Ti^{3+} is normally accompanied by the extinction of oxygen from surface TiO_2 due to heat treatment under H_2, CO or by fusillade by using electron beam, neutron or gamma ray. Ti^{4+} ions receive electrons from reducing gas then Ti^{3+} is formed. Likewise, lattice oxygen is removed from stoichiometric TiO_2. The location of the deformed Ti^{4+} (defect) shows in Figure 12.

O^{2-}

Deformed Ti^{4+}

Ti^{4+}
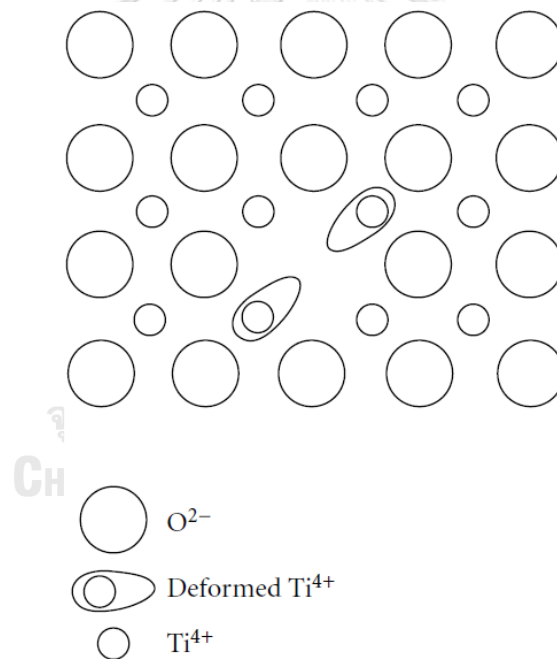
Figure 12 Model of surface defect Ti^{3+} associated with oxygen vacancy (O_V) [52].

Thermal treatment by hydrogen gas resulted in Ti^{3+} was formed, which include three kinds for the formation of Ti^{3+}. Firstly, as the temperature below 300°C, hydrogen impact physically with lattice oxygen surface incur adsorbing oxygen atom. Secondly, when the temperature was increased more than 300°C, electrons were

migrated from the H atoms to the O atoms in the lattice oxygen surface of TiO_2. Therefore, the oxygen vacancies were formed due to deficiency oxygen. In addition, the O atom was laid and contacted with the H atom then H_2O was formed. Thirdly, when the temperature was increased to 450°C, the surface of TiO_2 was impacted by H_2 then H atom was conducted more extremely, which the electrons migrated from oxygen vacancies to Ti^{4+} ions and Ti^{4+} received electrons thus Ti^{3+} ions occurred. In addition, the higher the temperature resulted in the more Ti^{3+} ions were formed. Moreover, when the temperature raised to 560°C, more energy has occurred and the electrons were saturated in the oxygen vacancies then they were disposed and migrated to Ti^{4+}. This influence was concordance with the results of EPR signal, which displayed the intensity of reduced oxygen vacancies and increased Ti^{3+} [52].

Lu et al. [52, 53] explained the structure of ideal rutile single crystal with an oxygen vacancy. The ideal model of rutile single crystal with Ti atom was located in oxygen octahedron. The symmetry of the oxygen octahedron was rhombic symmetry (D2h). The parallel (R° ‖) and vertical (R° ⊥) lattice oxygen interracial with Ti atom bonding shown in Figure 13. Ti^{3+} was formed due to reducing of Ti^{4+}. Therefore, the local electrostatic balance was cracked, so oxygen vacancy should be occurred due to charge reciprocation. Crystal field theory was used to estimate the position of the oxygen vacancy, which was relative to the local structure of the $[Ti^{3+}-O_V]$ center in the reduced rutile crystal. In this structure model, the axial O_V was positioned on the nearest position of central Ti^{3+} ion, which are shown in Figure 13.
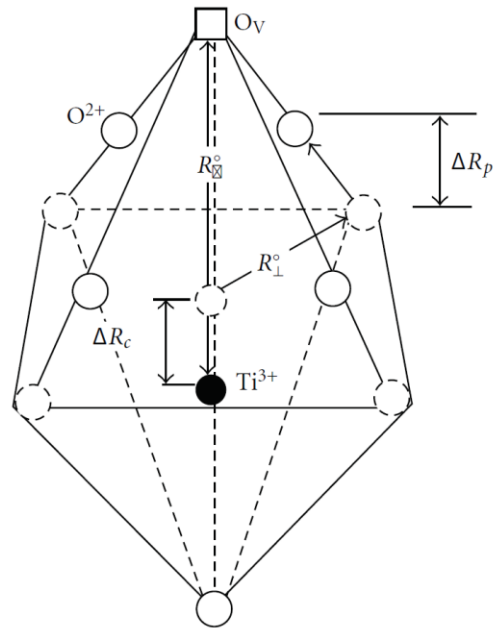
Figure 13 Model of rutile single crystal; Ti^{3+} at the centered position with oxygen vacancy (O_V), which was the nearest parallel position with Ti^{3+} [53].

The active sites of rutile TiO_2 for nitroaromatic hydrogenation is Ti^{3+} on the defect surface. O_b vacancies are two excess electrons, which migrate to the empty 3d orbital produced to two Ti^{3+}. These surface of Ti^{3+} serve as the adsorption site of nitroaromatic, which is shown in Figure 14 and 15 [5].
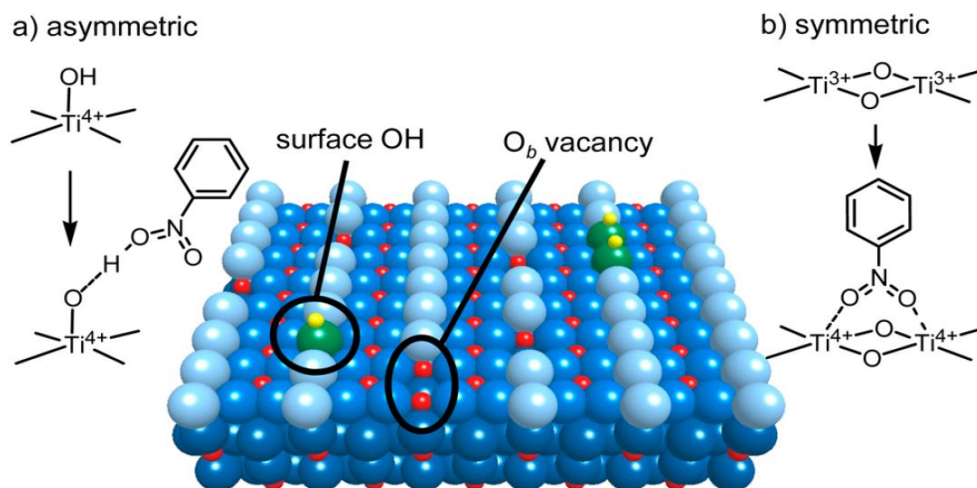
Figure 14 Surface defects on structure of rutile TiO_2 [5].
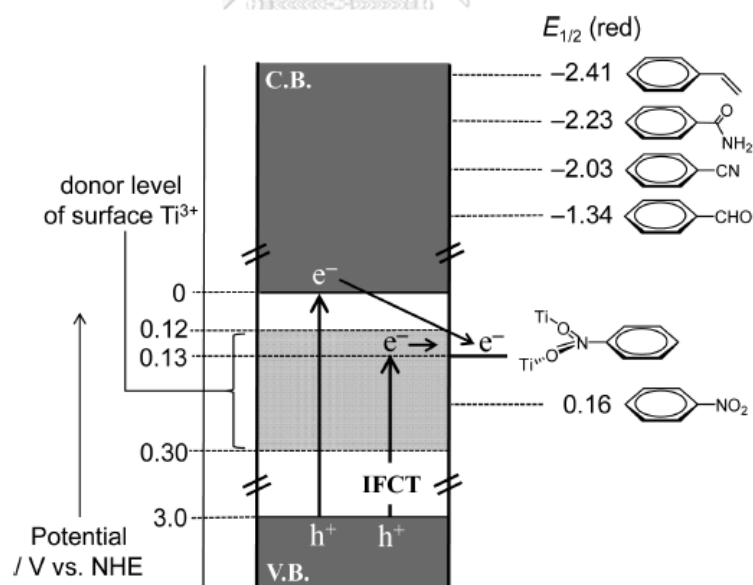
Figure 15 Energy diagram of rutile TiO_2 and surface defect [5].

2.7 Photocatalytic reaction on hydrogenation of nitroaromatics test

Yasuhiro Shiraishi et al [5] studied highly proficient and selective hydrogenation of nitroaromatics on the photocatalytic reaction by titanium dioxide. This reaction carried out in alcohol, nitroaromatics, and suspension in TiO_2 at room temperature and atmospheric pressure. TiO_2 commercials were used for catalysts, which included only anatase content, rutile content and P25 (mixture anatase and rutile). The mechanism for hydrogenation nitro group to aniline group aromatics ring occurred in this reaction because TiO_2 was irradiated by UV light, which separated electron (e^-) and holes (h^+). The electron was excited and migrated to the excited state or conduction band. The positive hole generated at valence band. Isopropanol was used for solvent in this reaction and it acted as a hole scavenger. However, some substrate may be used THF and toluene in order to dissolve substrates. Furthermore, sonication of the solution with suspension catalyst resulted in dispersed well within solution after that N_2 was bubbled through the solution in order that absence oxygen in the system. The catalysts were analyzed characteristic by using IR analysis, which shown IR spectra of the absorbed gas phase in rutile and anatase particle. IR peaks had two outstanding absorption band appear at 1522 and 1346 cm^{-1}, which assigned to surface Ti-OH and surface Ti^{3+} respectively. Rutile-TiO_2 (JRC-TIO$_6$) shown high peak 1346 cm^{-1} and high formation rate of aniline. The surface Ti^{3+} atoms of rutile TiO_2 served as adsorption site for nitroaromatics and the trapping site electron for photocatalytic. Ti^{3+} located under conduction band. Moreover, doped-metal (Pt, Pd, Ag, Au) on surface TiO_2 resulted in low photocatalytic activity. In contrast, doped metal on surface led to migrate electron from conduction band to doped metal, which resulted in separated electron and hole then it promoted high photocatalytic activity. However, in case of this study exhibited low photocatalytic activity because it retarded adsorption of nitroaromatic and coverage active site of Ti^{3+}.

Moreover, Yasushiro Shiraishi et al. [20] reported rutile crystallites isolated from Degussa P25-TiO_2 on photocatalytic hydrogenation of nitroaromatics. Isolated P25-TiO_2 could be the preparation by HF acid (Hydrofluoric acid) treatment (5%, 10%wt), which resulted in formed rutile and decreasing of band gap energy also

surface area. Photocatalytic performance for hydrogenation of nitroaromatics found HF (10%wt) treatment on P25-TiO$_2$ resulted in isolated completely rutile content and high photocatalytic activity more than JRC-TIO6 (Pure rutile content). The active site for this reaction was a number of defect on the particle. The inner defect behaved as the deactivation site, which led to recombine electron and hole, while surface defect acted as an active site for absorption for nitroaromatic.

Kazuya Imamura et al [7] studied about conditions reaction under air and absence oxygen. This reaction contained nitroaromatic, titanium dioxide (rutile, anatase, and P25-TiO$_2$) and isopropanol as hole scavenger. Photocatalytic reaction absence oxygen was removed by vacuum or under inert gas such as nitrogen or argon. After nitroaromatic were consumed and formed aniline, however small acetone was formed. The Ti^{3+} was reduced, so the color of TiO$_2$ would became blue However, TiO$_2$ was exposed with air, which led to became white color and occurred Ti^{4+}. In addition, photocatalytic reaction under air resulted in formed aniline same under absence oxygen condition, but acetone were formed more than usual. Indicating holes oxidized with 2-propanol to acetone and electrons were trapped by O$_2$ not aniline. The hydrogenation of 3-nitrostyrene after reaction 30min of light irradiation exhibited high selective to 3-vinylaniline. Moreover, nitroethlybenzene and aminoethylbenzene were not formed in this system. In addition, the other reducing group on nitrobenzene ring were studied, which exhibited similar photocatalytic activity also hydrogenation nitro compound to aniline compound. The rutile TiO$_2$ exhibited high conversion of nitrobenzene and high yield of aniline. The effect of large surface area and increasing of the active site resulted in large substrate adsorption along with high crystallinity, which retarded side-reactions between nitroaromatic and aniline.

Another work of Kazuya Imamura et al [54] studied m-nitrovinylbenzene (50µmole), which reduced to m-aminovinylbenzene in presence of hole scavenger suspension in TiO$_2$ without using metal or reducing gas. Photocatalytic chemoselective hydrogenation with a different reducing group (-CH=CH$_2$, -Cl, -Br, -COOH, -COCH$_3$) with different solvent (Acetonitrile, water content acetonitrile, methano, and ethanol). In case of using acetonitrile, which presence in oxalic acid

(200μmole) decomposition in order to eliminate oxygen in reaction because oxalic acid dissolved with the solution under deaerated condition then H_2 was formed. Furthermore, water addition in acetonitrile resulted in m-aminovinylbenzene and H_2 were decreased. However, small water addition led to be solubility substrate and oxalic acid then it promoted to increase hydrophilic TiO_2 particles. The water content 10%(v/v) addition in acetonitrile exhibited a high yield of m-aminovinylbenzene. Moreover, other reducing group resulted in the high amino compound.

Amer Hakki et al [6] studied the photocatalytic conversion of various nitroaromatic with alcohol and using four different types of TiO_2 (Sachtleben Hombikat UV100 for anatase, Crystal Global R34 for rutile, Home-made mesoporous anatase and Aeroxide P25 for mixture anatase-rutile). Furthermore, the effect of platinization had been studied in this ethanol solution. In case of without doped Pt on rutile TiO_2 found to a high selectivity primary amino compound. However, anatase TiO_2 indicated a yield imine more than amino. The platinization on TiO_2 led to condensation reaction of amine and aldehydes then it promoted to hydrogenation of NH_2 to C=N bond. Moreover, Pt nanoparticle presented the disappearance of Brønsted acid site due to the weakness of the peak at $1640cm^{-1}$. In addition, produced imine yielding was N-alkylated products, which found to occur all case. In case of investigation on different alcohol, the properties of structure alcohol resulted in polarity, which had importance for photocatalytic reduction also the high polarity. In case of isopropanol main product was aniline, while 3methyl to butanol alcohol were produced imines. The position of the methyl group in the aromatic ring did not affect the rate reaction.

CHAPTER 3

EXPERIMENTAL

These chapter referred to methods for heat treatment catalysts in different calcination atmospheres (Air, N_2 and H_2). Moreover, these chapter also included preparation method, catalyst characterization and photocatalytic reaction test.

3.1 Preparation of treated P25-TiO$_2$ by calcination at different temperatures.

Commercial TiO_2 Degussa (P25-TiO_2) was used as the main photocatalysts. Figure 16 shows the heat treatment process. P25-TiO_2 was transferred into crucible and followed by the calcination at 600, 700, 800, 900°C in a muffle furnace for 5h. After calcination, the catalysts was cooled down to the room temperature to obtain the treated P25-TiO_2 powder. In addition, heat treatment under H_2 and N_2 flow were proceeded at same condition.

Heat treatment in air at 600-900°C for 5h

Figure 16 Heat treatment process of P25-TiO_2 at different temperatures.

3.2 Preparation of solution containing substrate, solvent, and catalyst

A 200µmole of 3-nitrostyrene and 20 ml of isopropanol were transferred into 75ml pyrex glass tube and sealed with a rubber septum cap. The solution was stirred by using a magnetic bar. The catalyst 0.2g was placed into a pyrex glass tube and sonicated for 5 min. The reaction mixture was purged by bubbling N_2 gas through the solution for 5 min in order to eliminate oxygen in the system. During this process, the tube was covered by foil in order to prevent the light adsorption.

3.3 Photocatalytic test

The pyrex glass tube contained substrate, solvent and catalyst were irradiated with UV light using mercury lamp Philip 500w (λ > 300nm) for 6h with magnetic bar stirred at atmospheric pressure and room temperature. After the reaction, the catalyst was removed by filtration and all products were analyzed by using GC-FID. Substrate (3-NS) and 3-VA solution was analyzed by using Rtx5® column. Other oxidation products (isopropanol and acetone) were analyzed by using DB1-Wax column. The concentration of substrate and products were calibrated with authentic samples. Furthermore, the calculation of %conversion of 3-NS, %selectivity to 3-VA, formation rate of product and consumption rate of 3-NS show in equations (8) to (11).

$$\%\text{Conversion of 3-NS} = \frac{Mole_{3-NS,in} - Mole_{3-NS,out}}{Mole_{3-NS,in}} \tag{8}$$

Mole$_{3\text{-NS in}}$ is mole of 3-nitrostyrene inlet

Mole$_{3\text{-NS out}}$ is mole of 3-nitrostyrene outlet

$$\%\text{Selectivity to 3-VA} = \frac{Mole_{3-VA,out}}{Mole_{3-NS,in} - Mole_{3-NS,out}} \tag{9}$$

Mole$_{3\text{-NS in}}$ is mole of 3-nitrostyrene inlet

Mole$_{3\text{-NS out}}$ is mole of 3-nitrostyrene outlet

Mole$_{3\text{-VA out}}$ is mole of 3-vinylaniline outlet

$$\text{Formation rate of product} = \frac{Mole_{product,out}}{Reaction\ time \times Amount\ of\ catalysts} \tag{10}$$

Mole $_{\text{product out}}$ is mole of product outlet (μmoleg^{-1}h^{-1})

Reaction time (hours)

Amount of catalysts (gram)

$$\text{Consumption rate of 3-NS} = \frac{Mole_{3-NS,consumption}}{Reaction\ time \times Amount\ of\ catalysts} \tag{11}$$

Mole$_{3\text{-NS consumption}}$ is mole of 3-nitrostyrene is consumed (μmoleg^{-1}h^{-1})

Reaction time (hours)

Amount of catalysts (gram)

3.4 Physical and electrochemical characterization

Several techniques was applied to characterize fresh and treated P25-TiO$_2$ at different conditions.

3.4.1 X-ray diffractometry (XRD)

XRD was performed to indicate crystalline phase and crystallite size of P25 and treated P25. It was conducted using a SIEMENS D5000 X-ray diffractometer with Cu Kα radiation (λ=1.54439 A) with Ni filter. The spectra was scanned at a rate 0.04 min^{-1} in the 2Θ range of 20-80.

3.4.2 Nitrogen physisorption

BET surface areas of the catalysts was measured by Micromeritics Chemisorb 2750 Pulse Chemisorption System. 0.05g of catalysts was placed inside the tube and degassed at 200°C for one hour after that the catalysts were determined adsorption and desorption nitrogen gas. The surface area was calculated by using the single-point method.

3.4.3 X-ray photoelectron spectroscopy (XPS)

XPS was analyzed by using an AMICUS photoelectron spectrometer equipped with a Mg Kα that X-ray as a primary excitation and a KRATOS VISION2 software.

3.4.4 Thermogravimetric analysis (TGA)

TGA result was determined by using SDTQ 600 operated with flowed gas such as ambient air, inert gas and oxygen, and increasing temperature along with changing times in order to measure thermal decomposition, mass decomposition, phase transition and adsorbed reaction.

3.4.5 Scanning electron microscopy/energy dispersive X-ray spectroscopy (SEM-EDX)

SEM-EDX examined morphology on the surface of the catalyst sample. Results were obtained by using JSM-5410LV and energy dispersive using X-ray analyze component dispersion on the surface particle and quantitative of elements.

3.4.6 UV-Visible spectroscopy (UV-Vis)

Fundamental absorption edge TiO$_2$ is about 420 nm. To study the light adsorption of catalyst, the absorbance spectra of the catalyst in the wavelength

range of 200-800 nm were obtained by using Perkin Elmer Lambda 650 spectrophotometer. The band gap energy of catalyst was determined by the following equation (12).

$$Eg = \frac{1240}{\lambda} \qquad (12)$$

Where Eg is band gap (eV) of catalyst, λ is the wavelength of the onset of the spectrum (nm).

3.4.7 Photoluminescence spectroscopy (PL)

It was light emission from light excited source impinged object after that the absorption of photons. Luminescence light energy (light emission) was released during absorption and emission of a photon may different rage from short femtosecond-regime for emission and associated free-carrier plasma in inorganic semiconductors. During the recombination procedure of photo-induced charge carriers, a definite quantity of chemical energy could be released energy, which would further convert probably to form heat or light energy. The light energy could be differentiated as radiation, which resulted in a luminescence emission of semiconductor particle, defined the PL phenomenon of the semiconductor. The instrument was Fluromax® by Horiba and using Xenon lamp used to source of excitation at 320 nm.

CHAPTER 4

RESULTS AND DISCUSSION

In this chapter, the investigation of the physiochemical and catalytic properties of fresh and treated P25-TiO$_2$ were reported. The effects of various calcination temperatures and atmospheres, including air nitrogen and hydrogen are also studied. All catalysts were tested in photocatalytic selective hydrogenation of 3-nitrostyrene. The catalysts particles were analyzed by using XRD, BET surface area, XPS, UV-Vis, photoluminescence spectroscopy, TGA, SEM-EDX.

Table 5 The symbol of catalysts in this work

Symbol	Detail of symbol
A-700-air	Commercial of TiO$_2$ (JRC-TIO1) was calcined at 700°C in air for 5 h
P25	Commercial of TiO$_2$ (Degussa)
P25-600-air	P25 was calcined at 600°C in air for 5h
P25-700-air	P25 was calcined at 700°C in air for 5h
P25-800-air	P25 was calcined at 800°C in air for 5h
P25-900-air	P25 was calcined at 900°C in air for 5h
P25-700-H$_2$	P25 was calcined at 700°C in hydrogen flow for 5h
P25-700-N$_2$	P25 was calcined at 700°C in nitrogen flow for 5h

4.1 Characterization of all treated TiO$_2$ catalysts

4.1.1 X-ray diffraction (XRD)

Figure 17, shows the XRD patterns of P25-TiO$_2$ before and after calcination at difference temperatures for 5h in muffle furnace. Untreated P25-TiO$_2$ had the mixture phase components of both anatase (101) and rutile (110) phases along with constituted component of both anatase ≈ (20%) and rutile ≈ (80%) contents, in which exhibited peak at 2θ = 25.3° and 27.4 respectively [15]. After that calcination at 600°C, the XRD peaks corresponding to anatase phase was slightly decreased. However, further increasing of calcination temperature resulted in rapid increased rutile phase content and the crystallite size. For the catalyst sample calcined at temperature higher than 800°C, peaks of anatase phase was completely disappeared and transformed to rutile phase.
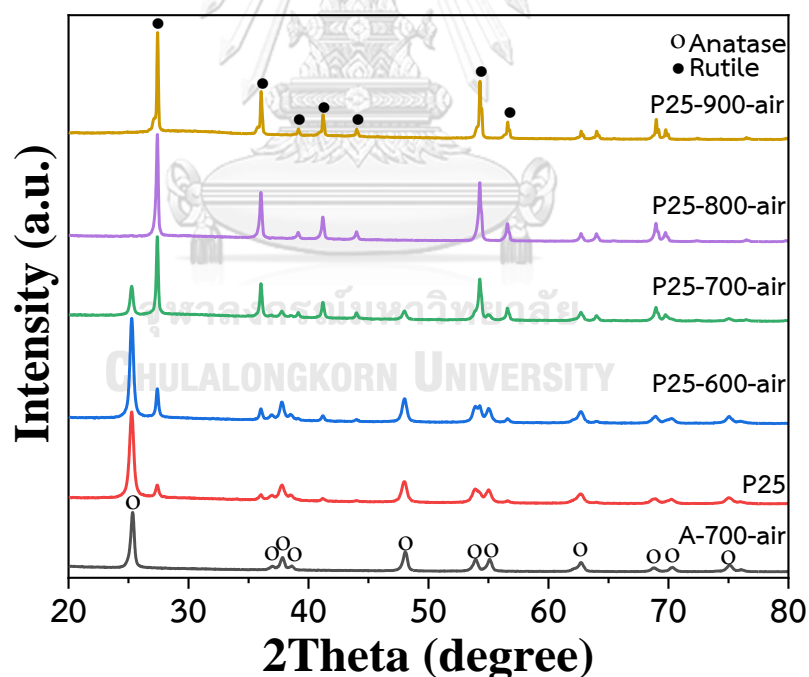
Figure 17 XRD patterns of A-700-air and P25-TiO$_2$ before and after heat treatment at 600-900°C in air for 5h.

At the same temperature condition, P25-TiO$_2$ were treated under nitrogen gas and hydrogen gas flow. XRD results are shown in Figure 18. Anatase phase was decreased likewise with calcination in air except the hydrogen treated catalyst, which represented lower anatase peak. The higher rutile phase content was probably due to the higher formation oxygen vacancy. Moreover, heat treatment with hydrogen gas affected to high reduction on lattice surface TiO$_2$, which resulted in an increasing of rutile content [55].
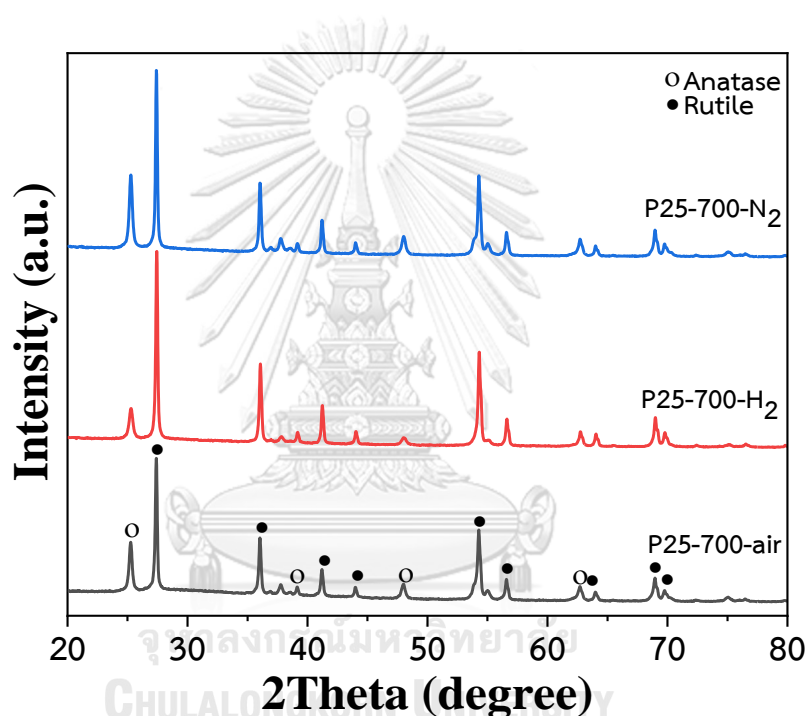
Figure 18 XRD patterns of P25-TiO$_2$ after heat treatment at 700°C in air, H$_2$ and N$_2$ flow for 5h.

Furthermore, the calcination temperature influenced the phase composition and crystallization. It was reasonable to suggest that high temperature calcination led to phase transformation from anatase to rutile [56, 57]. Therefore, phase transformation was associated with crystal growth. In Table 6 shows the phase composition and crystallite size of anatase and rutile of all treated P25-TiO$_2$ and A-700-air. The crystallization of P25-TiO$_2$ before and after calcination were estimated

from the full-width at half maximum (FHWM) of the anatase peak (101) and rutile peak (110), which indicated from results of XRD pattern and it could calculate by Scherrer's formula. At calcination temperature higher 800°C in air presented only crystallite size of rutile due to disappeared anatase peak. In addition, heat treatment under H_2 flow, which exhibited wide FHWM of the anatase peak (101). Therefore, the anatase crystallite size had smaller than calcination in air and N_2 due to the higher formation of oxygen vacancy, which acted as reduce crystallinity [57]. In other hand, heat treatment under inert gas (H_2) could be anticipated to increase the number of oxygen vacancies in the anatase lattice. Therefore, it advocated the transformation to rutile. Moreover, structure c-axis of anatase had more atoms per unit cell than rutile because rutile phase had stable lattice than anatase phase. This non-stoichiometry may be presented in anatase as well. The oxygen vacancies in anatase could be anticipated to advocate the transformation to rutile belated to the facilitated rearrangement of ions [56, 58].

Table 6 Phase composition and crystallize size both anatase and rutile of A-700-air and P25-TiO$_2$ before and after heat treatment.

Catalysts	%Anatase	%Rutile	Crystallize size anatase 101 (nm)	Crystallize size rutile 110 (nm)
A-700-air	100	-	30	-
P25	83	17	23	33
P25-600-air	73	27	29	59
P25-700-air	23	77	43	76
P25-800-air	-	100	-	92
P25-900-air	-	100	-	>100
P25-700-H$_2$	11	89	27	81
P25-700-N$_2$	24	76	40	85

5.1.2 N$_2$ physisorption

N$_2$ physisorption include nitrogen adsorption and desorption isotherms. The measurement fundamental of these properties is the external surface area available for adsorption of gas molecules, which substituted by N$_2$ liquid at 77K on solid-porosity. This technique is the most widely for determined surface area characterization [59]. This equation used single-point determination, which relative pressure drop (P/P$_0$) range of 0.2 to 0.3 and derived by assuming the BET intercept (1/c$_{BET}$) equals zero, then it established BET plot [59-61].

In Table 7 exhibits properties of the surface area of all treated P25-TiO$_2$ and A-700-air. The surface area of P25-TiO$_2$ exhibited 40m^2/g. The observation of the trend of increasing of calcination temperature led to be decreasing of surface area due to higher relative pressure, which had corresponding with significant pore size and particle agglomeration [19]. Moreover, the influence of calcination temperature affected to be a decreasing of pore volume and porosity of the catalyst samples [14, 62, 63]. However, heat treatment under air, H$_2$, and N$_2$ flow at same temperature resulted in not changing of surface area.

Table 7 BET surface area of A-700-air and P25-TiO$_2$ before and after heat treatment.

Catalysts	BET surface area (m^2/g)
A-700	14
P25	40
P25-600-air	31
P25-700-air	9
P25-800-air	6
P25-900-air	5
P25-700-H$_2$	9
P25-700-N$_2$	10

However, the influence of heat treatment led to be decreasing of BET surface area and increasing of rutile component, which are shown in Figure 19. These correlation caused by the effect of surface diffusion and changing of the phase structure of catalyst.
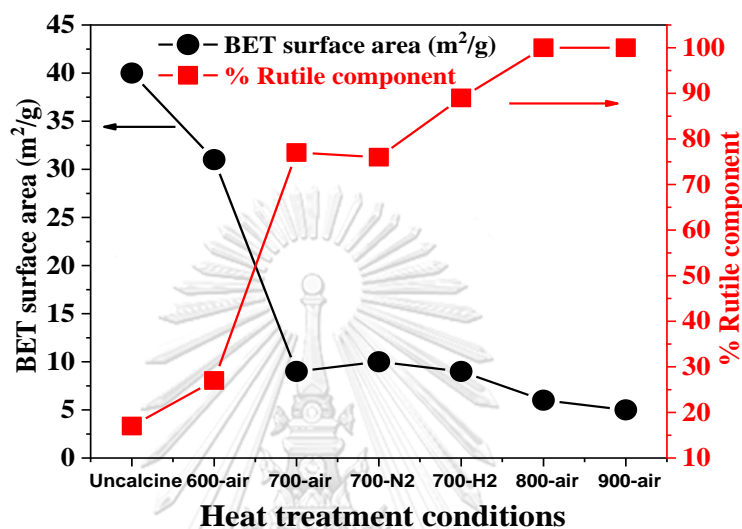
Figure 19 Correlation between heat treatment conditions of P25-TiO$_2$ versus BET surface area and formation of rutile component.

4.1.3 X-ray photoelectron spectroscopy (XPS)

XPS technique is most widely for using in physical chemistry, which evaluate and analyze the characterization of the surface chemistry elemental composition, chemical state of the sample. Principle of XPS is considered by X-ray electron beam irradiation on the surface then photoelectron was released from the surface sample after that the released photoelectron is analyzed and used to measure the kinetic energy of the released photoelectron in forms of binding energy and intensity of photoelectron peaks, which present by trace amount of carbon and high solution Ti2p and O1s state [64]. The high resolution XPS spectrum of Ti 2p core levels of pure TiO$_2$ is also fitted by Gaussian fitted curve, which found four peaks. The main peaks of titanium dioxide (Ti^{4+}) and two shoulder peaks of titanium sub oxide (Ti^{3+}), which are shown in Figure 20 [65].

Figure 20 X-ray photoelectron spectra Ti2p of A-700-air and P25-TiO$_2$ before and after heat treatment; at (a) 600-900°C in air for 5h, (b) at 700°C in air, H$_2$ and N$_2$ flow for 5h.

In case of, Ti elemental of TiO$_2$ has Ti 2p$_{3/2}$ and Ti 2p$_{1/2}$, which associated with the binding energy at centered peaks 458.5 eV and 464.5 eV respectively, which indicated with the lattice of Ti^{4+} valence state [38, 66, 67]. Furthermore, titanium sub

oxide had two shoulder peaks at 457.3 and 463, which indicated Ti^{3+} valence state of $2p_{3/2}$ and $2p_{1/2}$ respectively. In addition, Ti^{3+} valence state associated with oxygen vacancies (Ov) defect in the system [38, 66, 67]. Figure 21 and 22, represent deconvolution peaks of Ti2p core levels with Gaussian fitting curve.

Figure 21 exhibits concentration Ti^{3+} of P25-TiO_2 before and after calcination in air, which exhibited slightly increased Ti^{3+} due to filling oxygen on lattice surface. However, the concentration of Ti^{4+} was reduced because an extinction of oxygen atom from the surface TiO_2 resulted in Ti-O-Ti was broken. In addition, the lattice of Ti^{4+} was reduced also atom of Ti received the electrons from lattice oxygen, which removed from stoichiometric TiO_2.

Figure 21 X-ray photoelectron spectra Ti2p of A-700-air and P25-TiO$_2$ before and after heat treatment at 600-900°C in air for 5h, which were deconvoluted by Gaussian fitting curve.

Moreover, calcination with H$_2$ and N$_2$ gas flow resulted in the concentration of Ti^{3+} higher than calcination in air at the same temperature condition, which are shown in Figure 22. In case of, calcination with H$_2$ flow led to broken Ti-O-Ti network along with it was generally accompanied by loss oxygen from deficient oxygen, which affected to the surface of TiO$_2$ then more electrons transferred to the lattice of Ti^{4+} then Ti^{3+} was formed [68]. In addition, the ratio both Ti2p 3/2 and Ti2p 1/2 (Ti^{3+}/Ti^{4+}) were changed, which are shown in Table 8.

Figure 22 X-ray photoelectron spectra Ti2p of P25-TiO$_2$ after heat treatment at 700°C in air, H$_2$ and N$_2$ flow for 5h, which were deconvoluted by Gaussian fitting curve.

Table 8 Ratio of Ti^{3+}/Ti^{4+} of A-700-air and P25-TiO$_2$ before and after heat treatment.

Catalysts	Ratio Ti2p 3/2 Ti^{3+}/Ti^{4+}	Ratio Ti2p 1/2 Ti^{3+}/Ti^{4+}
A-700-air	0.04	0.04
P25	0.03	0.04
P25-600-air	0.04	0.05
P25-700-air	0.03	0.05
P25-800-air	0.04	0.05
P25-900-air	0.03	0.04
P25-700-H$_2$	0.12	0.13
P25-700-N$_2$	0.08	0.08

In case of, XPS spectra peaks of O1s core levels, which associated with lattice oxygen and oxygen vacancies. Using Gaussian fitting curve of O1s core presented two peaks centered binding energy at 529.80 and 531.30 eV, which assigned to Ti-O-Ti bond and interaction Ti^{3+}- oxygen vacancies on the surface and subsurface regions for TiO$_2$ respectively, [28, 66, 67], which are shown in Figure 23.

Figure 23(a) shows calcination in air, peak at 529.80eV was reduced because high calcination temperature reduced lattice oxygen due to thermal stress, these effect caused by the rapid change in Ti-O-Ti network, whereas calcination under H$_2$ flow in the system, which could create more oxygen vacancies then observation area of peak centered at 531.3eV was raised, which is shown in Figure 23(b) Moreover, an electron from hydrogen through surface lattice oxygen then electron was released and transferred to Ti^{4+} and then Ti^{4+} received electron, so Ti^{3+} was formed [28, 52, 68, 69].
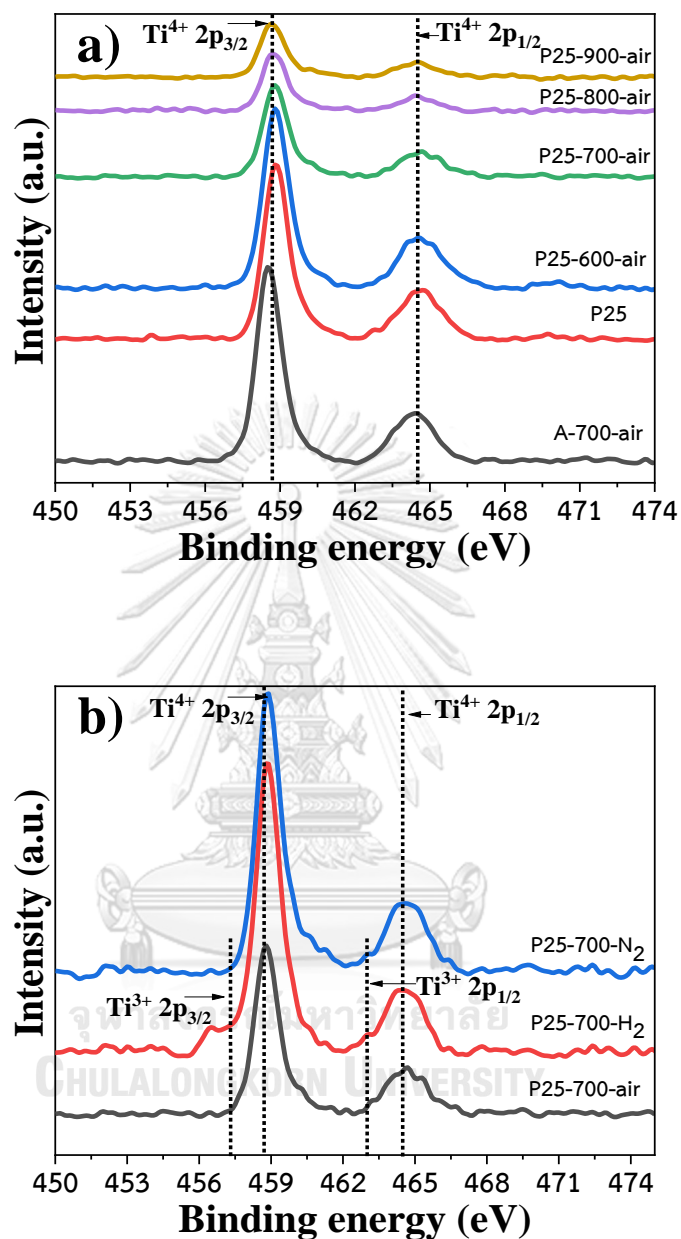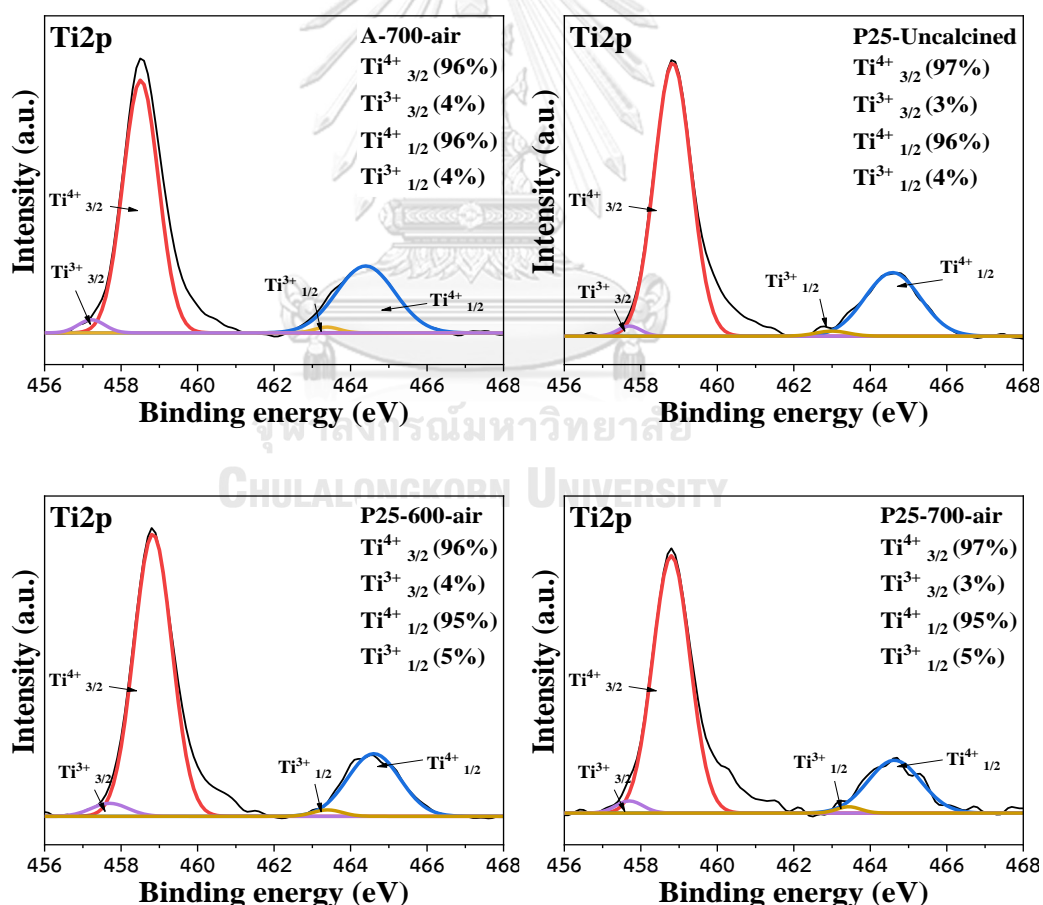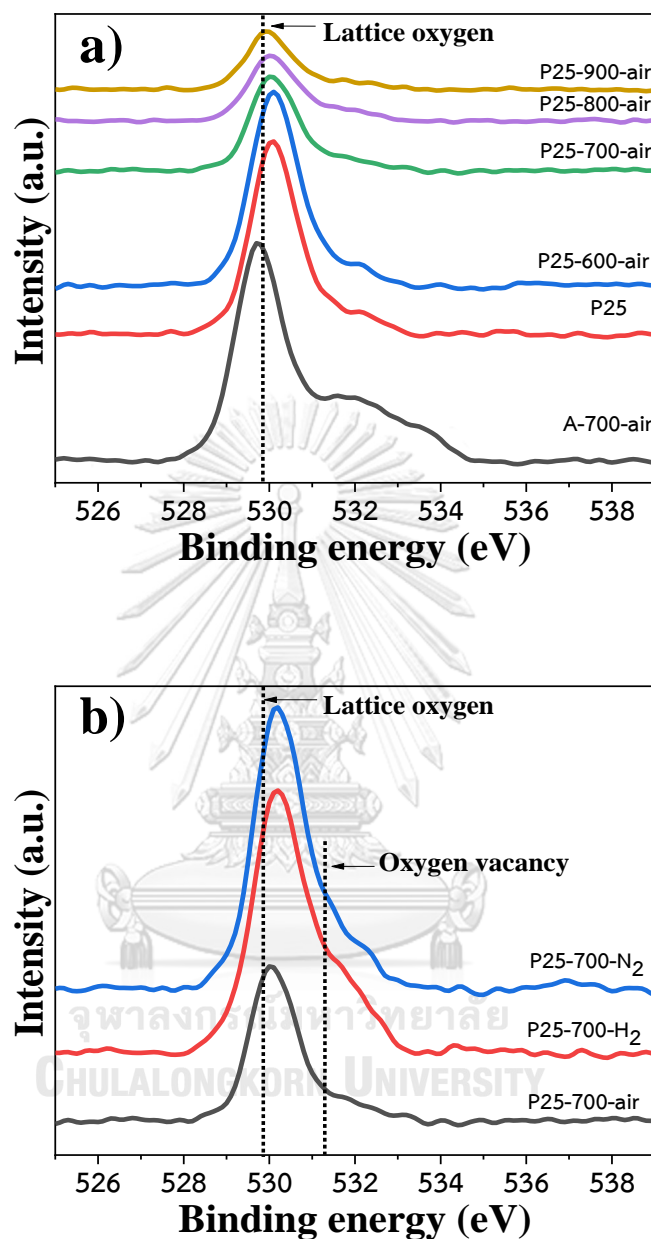
Figure 23 X-ray photoelectron spectra O1s of A-700-air and P25-TiO_2 before and after heat treatment; (a) at 600-900°C in air for 5h, (b) at 700°C in air, H_2 and N_2 flow for 5h.

However, P25-TiO_2 was calcined in air with different temperature, which found the concentration of oxygen vacancies slightly changed because of additional oxygen in the system, which are shown in Figure 24. In addition, oxygen acted as oxidation on lattice oxygen.
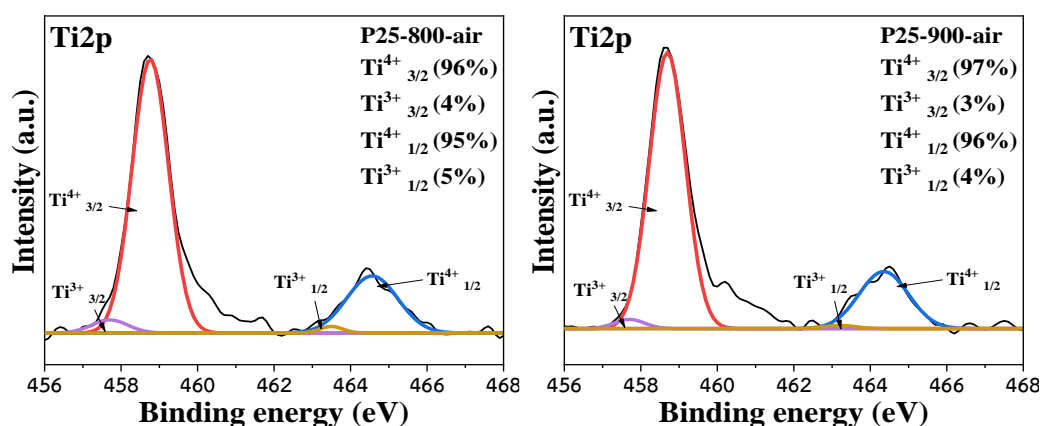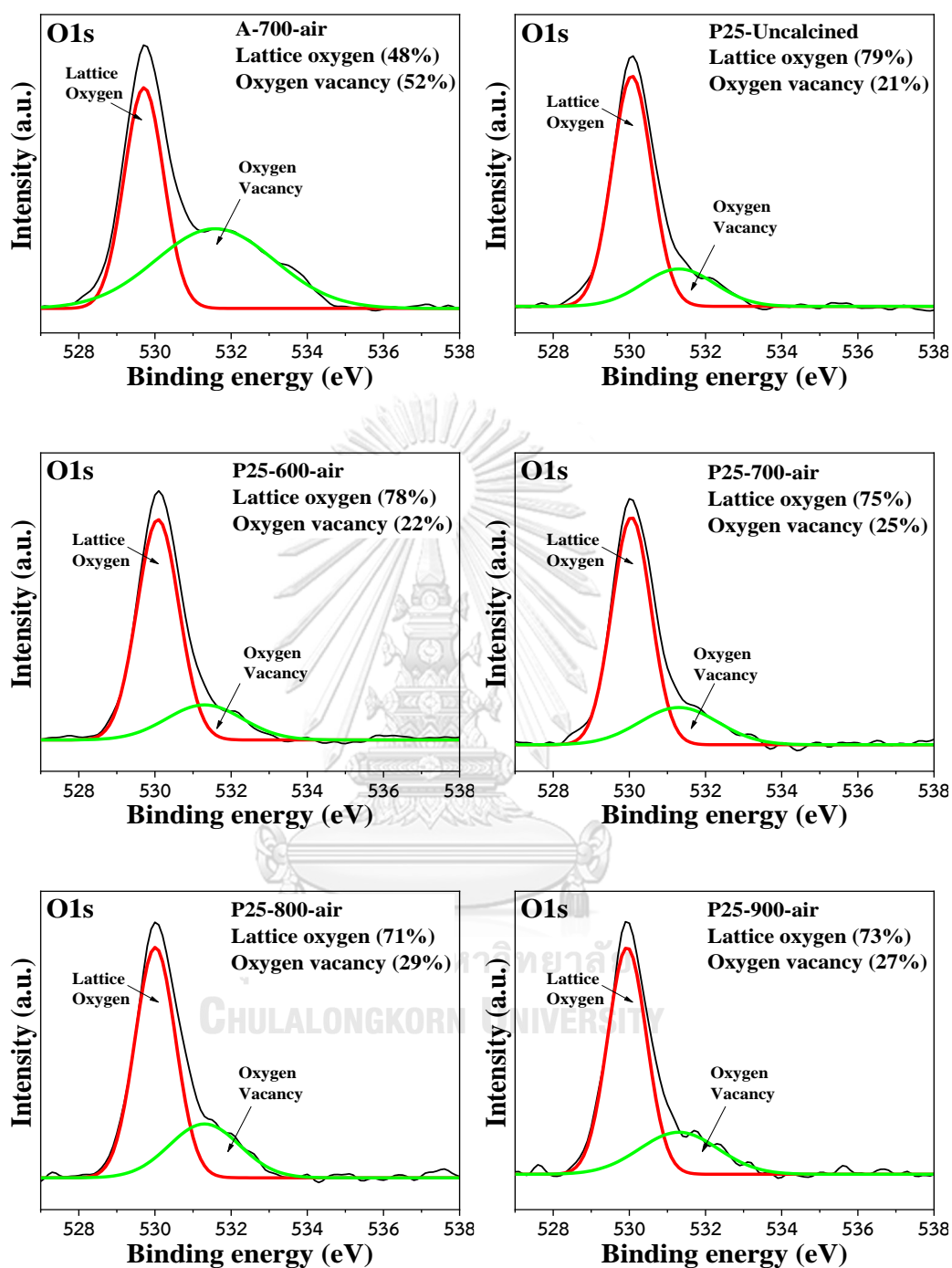
Figure 24 X-ray photoelectron spectra O1s of A-700-air and P25-TiO$_2$ before and after heat treatment at 600-900℃ in air for 5h, which were deconvoluted by Gaussian fitting curve.

In case of O1s, calcination under H_2 and N_2 gas flow resulted in peak at 531.3 was raised, which are shown in Figure 25. Furthermore, calcination under H_2 gas flow had the maximum formation of oxygen vacancy and Ti^{3+} because of more deficient oxygen in the system. Therefore, loss of oxygen lattice on the surface from H_2 heat treatment proposed the interaction between H_2 and surface of TiO_2, which proceeded more tremendously because more energy was supplied from H atom then the electron transferred from oxygen vacancies to Ti^{4+} ion then Ti^{3+} were formed [68, 70, 71].
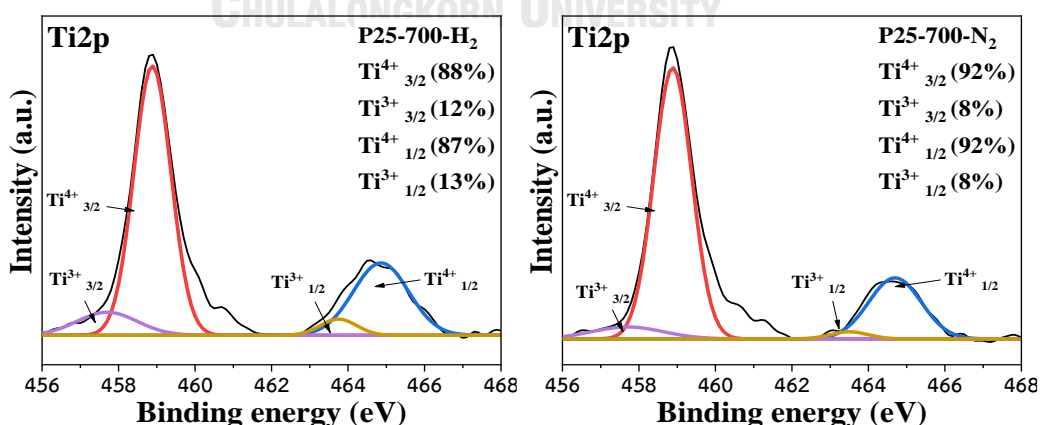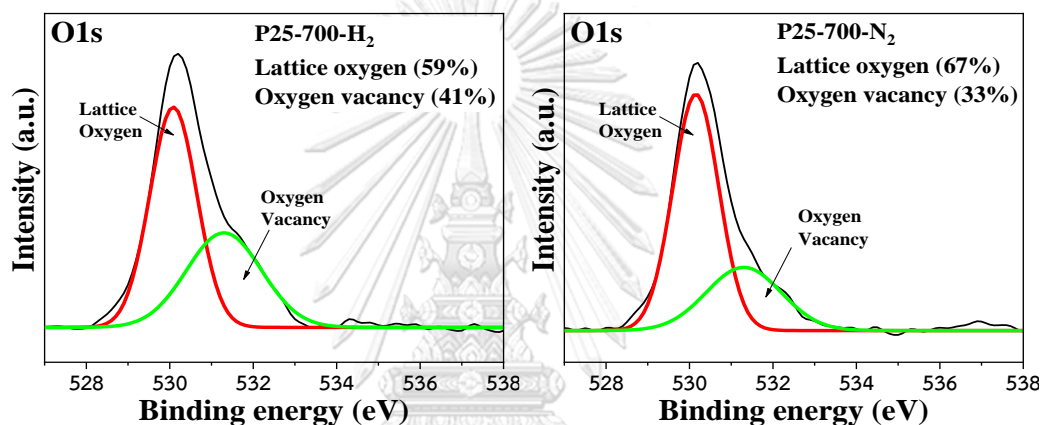

Figure 25 X-ray photoelectron spectra O1s of P25-TiO_2 after heat treatment at 700℃ in air, H_2, and N_2 flow for 5h, which were deconvoluted by Gaussian fitting curve.

The conclusion of the XPS signal, both Ti 2p and O1s of calcination in air may not affect to surface defect, while calcination under N_2 and H_2 clearly affected to reduce from Ti^{4+} to Ti^{3+} and more created oxygen vacancy due to deficiency oxygen atmosphere. Changing of ratio oxygen on the surface of A-700-air and all treated P25-TiO_2 show in Table 9.

Table 9 Ratio of Oxygen vacancy/Lattice oxygen of A-700-air and P25-TiO$_2$ before and after heat treatment.

Catalysts	Ratio Oxygen vacancy/Lattice oxygen
A-700-air	0.52
P25	0.21
P25-600-air	0.22
P25-700-air	0.25
P25-800-air	0.29
P25-900-air	0.27
P25-700-H$_2$	0.41
P25-700-N$_2$	0.33

4.1.4 UV-Visible spectroscopy (UV-Vis)

These technique used to analyze light absorption on the solid or liquid sample, so the effect of calcination temperature on P25-TiO$_2$ resulted in increasing of the absorption edges, which shifted toward red shift. In addition, high calcination temperature increased longer wavelengths absorbance, which could be referred to absorption of light when light energy equal or higher absorption, light initiated excitation of photoelectron from valence band to conduction band. The effect of calcination temperature of all treated P25-TiO$_2$ on light absorption show in Figure 26 and 27. Figure 27 exhibit high calcination temperature under H$_2$ flow led to trends of wavelength along with increasing of absorption visible light range. The change of adsorption wavelength because the influence of increasing both of crystallite size and phase structure transformation anatase to rutile [19, 72].
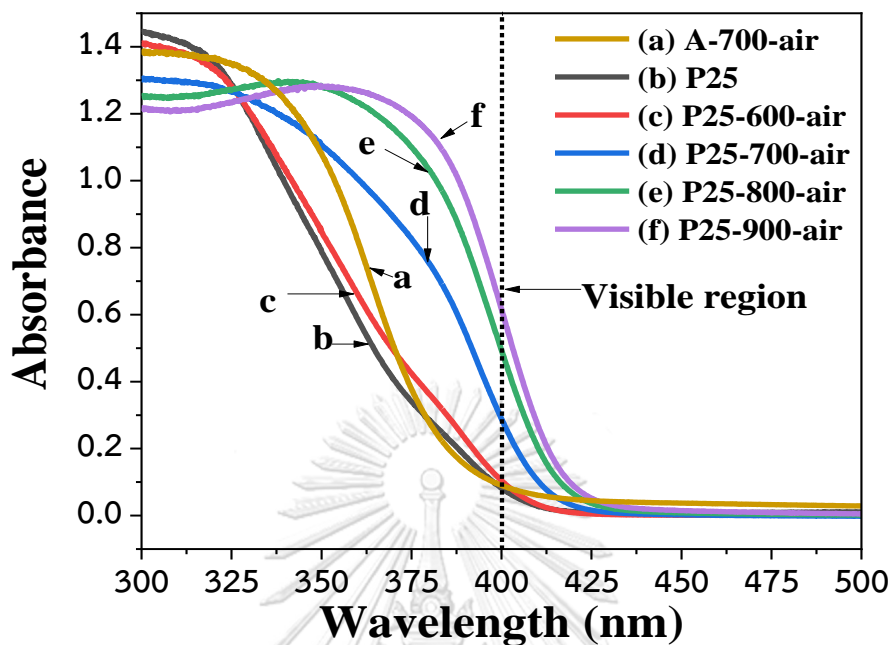
Figure 26 UV-Vis absorption spectra of A-700-air and P25-TiO$_2$ before and after heat treatment at 600-900°C in air for 5h.
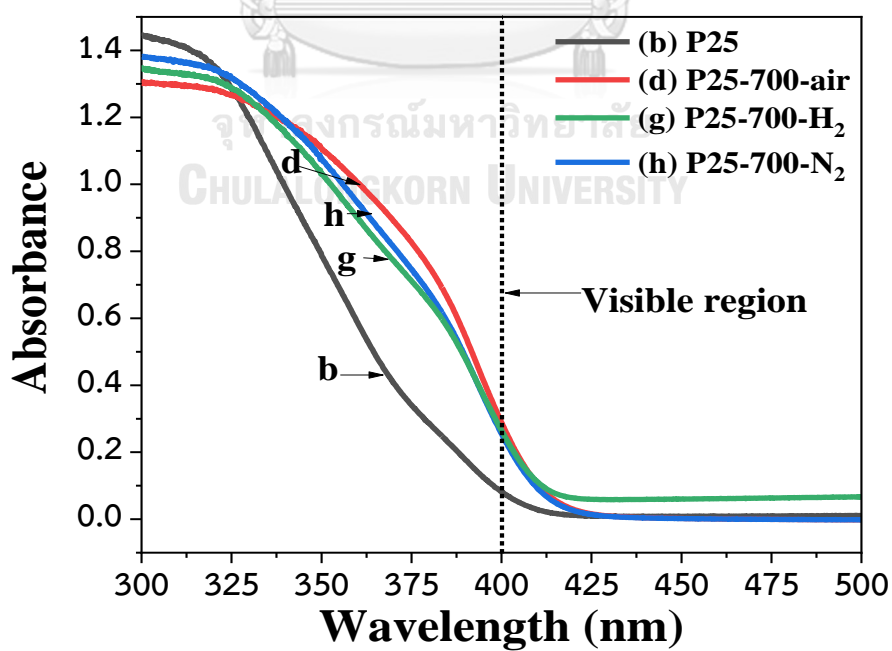
Figure 27 UV-Vis absorption spectra of P25-TiO$_2$ before and after heat treatment at 700°C in air, H$_2$ and N$_2$ flow for 5h.

The adsorption edges wavelength after calcination at 600°C indicated a decreasing of band gap energy as compared with uncalcined P25-TiO$_2$, which are shown in Figure 28. Furthermore, estimation band gap from a plot of $(hv\alpha)^{1/2}$ versus photon energy (hv), which the relation between the absorption coefficient (α) and incident photon energy (eV) [19]. Since absorbance was relative to absorption coefficients, so calcination of P25-TiO$_2$ led to decreasing of band gap due to increased crystallite size. These results led to a red shift in the adsorption spectra. On the other hand, after calcination at 600°C may be a result of phase transformation from anatase to rutile and particle agglomeration [19, 72].
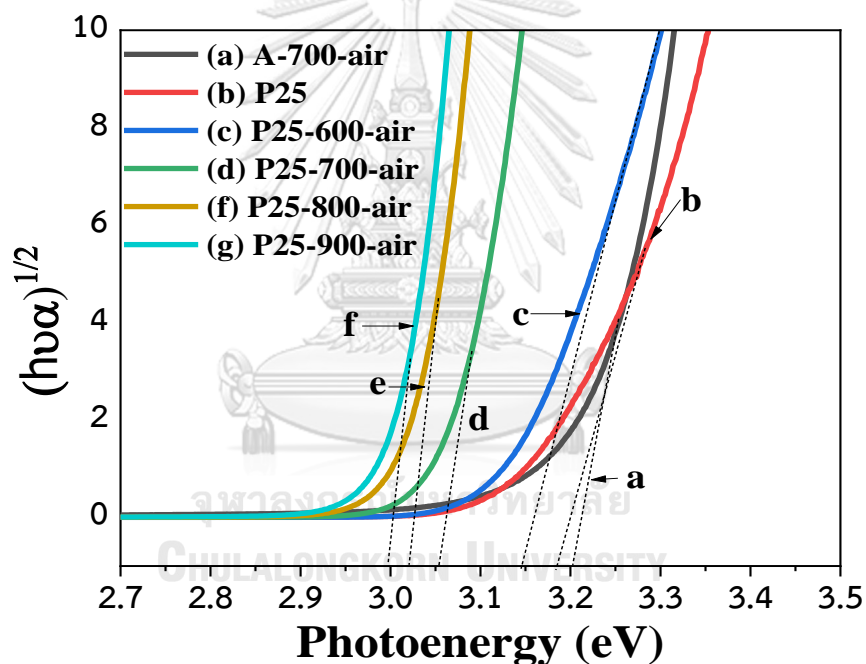
Figure 28 Photoenergy of A-700-air and P25-TiO$_2$ before and after heat treatment at 600-900°C in air for 5h.

Calcination temperature over 800°C resulted in completely rutile component, which has band gap nearly 3.00. Furthermore, atmosphere (air, H_2, and N_2) not influenced by wavelength and band gap due to nearby rutile component. In addition, the effect of particle agglomeration has more influence, which are shown in Figure 28-29. Table 10 exhibits a summary of wavelength and band gap energy of all treated P25-TiO_2 and A-700-air. The band gap was decreased by these reasonable to suggest that temperature calcination and may be phase component [62].

However, P25-700-H_2 exhibited addition adsorption spectra in the visible light region. Similar results were reported by Naldoni et al. [55, 73]. The black TiO_2 obtained from thermal treatment of amorphous commercial TiO_2 in H_2 flow exhibited the adsorption spectra at the visible light region. They suggest that the increasing of concentration of vacancy site could create a free oxygen vacancy band below the conduction band, which is responsible for visible light absorption.
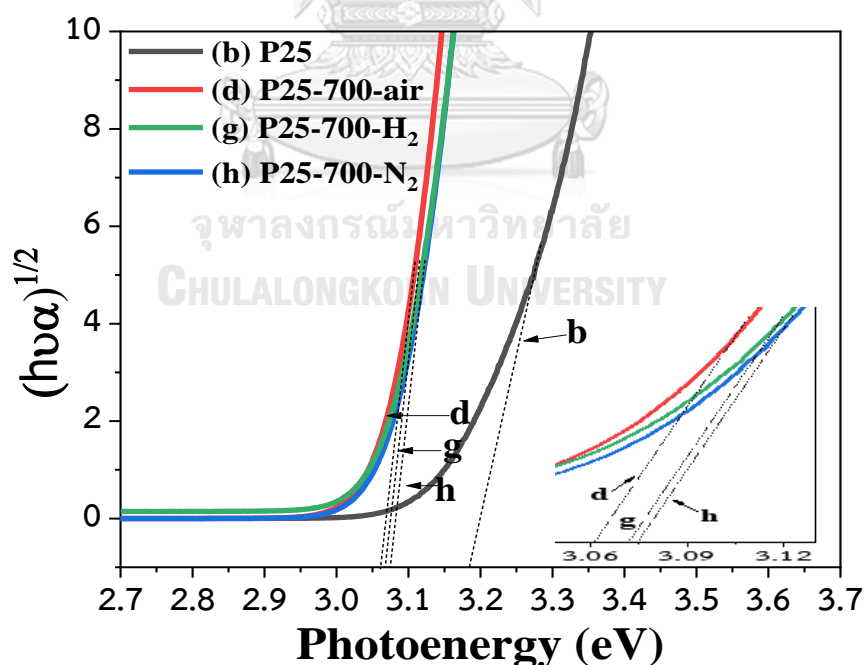
Figure 29 Photoenergy of P25-TiO_2 before and after heat treatment at 700°C in air, H_2 and N_2 flow for 5h.

Table 10 The wavelength and band gap of A-700-air and P25-TiO$_2$ before and after heat treatment.

Catalysts	Wavelength (nm)	Band gap (eV)
A-700-air	387	3.20
P25	390	3.18
P25-600-air	395	3.14
P25-700-air	407	3.05
P25-800-air	412	3.01
P25-900-air	416	2.98
P25-700-H$_2$	406	3.06
P25-700-N$_2$	404	3.07

4.1.5 Photoluminescence spectroscopy (PL)

The PL emission spectra are used to examine the performance of charge carrier trapping of photo-induced and transferred photoelectron. PL measurement estimates the surface structure and excited states, which associate with the electron and hole lifetime of semiconductor material. Normally, peak PL emissions on semiconductor material occurred from the radiative recombination of photo-generated electron and hole. Furthermore, PL signals could be excited by using two major photo-physical procedures in a semiconductor. The first was a direct band to band transition photoluminescence, which was the release of luminescence light or heat side by side that of the photo-generated electron, which could transfer back from the conduction band to valence band after the irradiation by light higher than band gap energy. The second was the photo-physical relative band to sub-band, which in the form of oxygen vacancy or defects. In general, the defect was formed at below conduction band. The photoelectron was excited by light energy then electron transferred from bottom of conduction band via non-radiative to sub-band and then excited photoelectron transferred from sub-band to the valence band via a radiative transition with the release luminescence emission called PL signals [8, 74].

Figure 30 and 31 exhibit the various peak emission at 451,469,484 and 492 nm, which attributed to the formed oxygen vacancies at nearly surface, which related to shallow trap level below conduction band [75, 76]. The peak at 436 nm was attributed to self-trapped photo-excitons localized on TiO_6 octahedra [77]. The long wavelength range of 451-484nm were purported to the oxygen vacancy with two trapped electrons to the valence band of semiconductor TiO_2 [75, 78]. The peak at 492nm corresponding with oxygen vacancy with one electron [79].
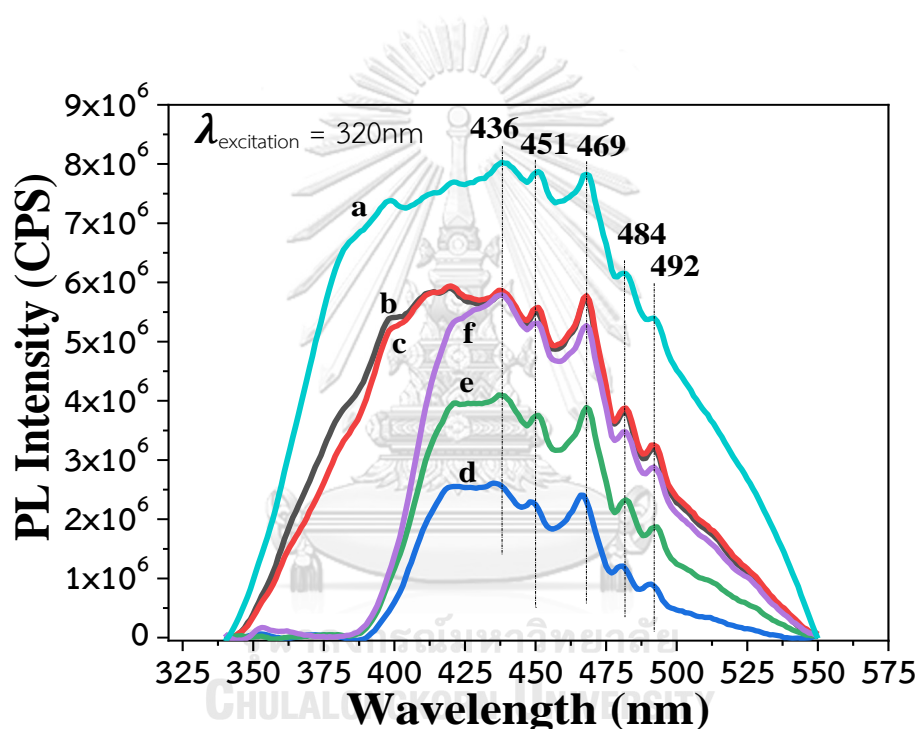
Figure 30 Photoluminescence spectra of A-700-air and P25-TiO_2 before and after heat treatment at 600-900℃ in air for 5h.

(a) A-700-air, (b) P25, (c) P25-600-air, (d) P25-700-air, (e) P25-800-air, (f) P25-900-air.
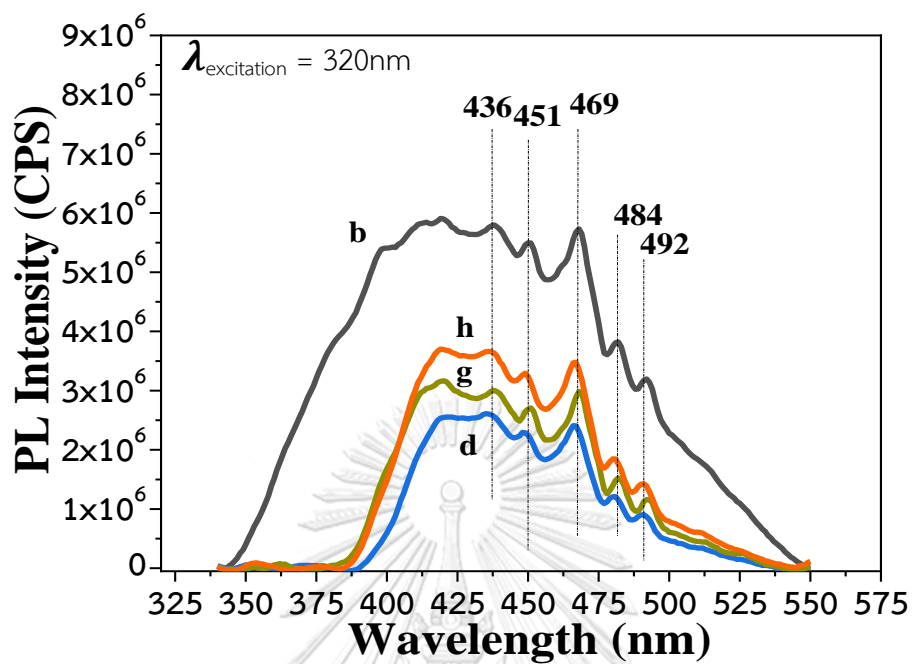
Figure 31 Photoluminescence spectra of P25-TiO$_2$ before and after heat treatment at 700°C in air, H$_2$ and N$_2$ flow for 5h.

(b) P25, (d) P25-700-air, (g) P25-700-H$_2$, (h) P25-700-N$_2$.

4.2 Photocatalytic activity test liquid hydrogenation selective of 3-NS

      4.2.1 Photocatalytic activity test under UV-light irradiation

      In this process had a reduction and oxidation reaction. In Table 11 exhibits photocatalytic activity under UV-light irradiation. Calcination temperature at 700°C in air exhibited a maximum of %conversion of 3-nitrostyrene (3-NS) and %selectivity to 3-vinylaniline (3-VA). Moreover, the photocatalytic activity with all treated P25-TiO$_2$ not affected to selectivity to 3-VA. Furthermore, the formation rate of acetone was proportional with the formation rate of 3-VA because this reaction generated H$^+$ from isopropanol then 3-NS received H$^+$, which resulted in the formation of 3-VA and acetone respectively. Scheme 1 shows the mechanism of photocatalytic hydrogenation of this reaction. Moreover, photocatalytic hydrogenation of 3-NS versus with time exhibited consumption rate of 3-NS, which was proportional to the formation rate of acetone, which are shown in Figure 32.

Table 11 Results of photocatalytic hydrogenation selective of 3-nitrostyrene to 3-vinylaniline performance for A-700-air and P25-TiO$_2$ before and after heat treatment.

Catalysts	%Conversion 3-NS	%Selectivity 3-VA	Rate 3-VA formed (μmole g^{-1}h^{-1})	Rate Acetone formed (μmole g^{-1}h^{-1})
A-700-air	21.9	100.0	37.0	106.9
P25	45.4	96.7	74.2	208.3
P25-600-air	43.1	100.0	71.7	210.0
P25-700-air	70.9	100.0	120.0	340.0
P25-800-air	57.8	100.0	99.2	287.4
P25-900-air	51.5	100.0	87.0	240.6
P25-700-H$_2$	61.4	100.0	103.3	290.0
P25-700-N$_2$	57.6	100.0	96.9	288.6

$$TiO_2 + hv \qquad\qquad \rightarrow \qquad TiO_2\ (e^- + h^+) \qquad\qquad (1)$$

$$TiO_2\ \{h^+\} + (CH_3)_2CHOH \qquad \rightarrow \qquad TiO_2\ \{e^-\} + (CH_3)_2CO + 2H^+ \qquad (2)$$

$$2TiO_2\ \{e^-\} + (C_8H_7NO_2) + 2H^+ \qquad \rightarrow \qquad 2TiO_2 + (C_8H_7NO) + H_2O \qquad (3)$$

$$2TiO_2\ \{e^-\} + (C_8H_7NO) + 2H^+ \qquad \rightarrow \qquad 2TiO_2 + (C_8H_9NO) \qquad (4)$$

$$2TiO_2\ \{e^-\} + (C_8H_9NO) + 2H^+ \qquad \rightarrow \qquad 2TiO_2 + (C_8H_7NH_2) + H_2O \qquad (5)$$
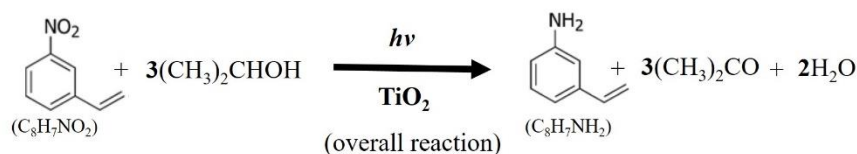
Scheme 1 Mechanism of photocatalytic hydrogenation of 3-NS.
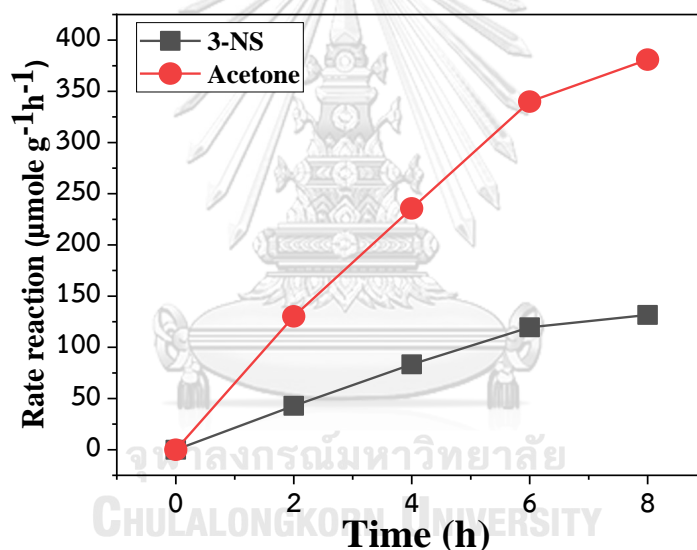
Figure 32 Consumption rate of 3-NS and Formation rate of acetone versus reaction time (h) of P25-700-air.

In this work exhibited the effect of heat treatment of P25-TiO$_2$. Influence of high calcination temperature resulted in increased crystallite size both anatase and rutile, which are shown in Figure 33 (a) and (b) respectively. Calcination at 700°C in air had mixture anatase and rutile contents, which exhibited a low PL intensity because it promoted enhancement of interface between anatase and rutile, which led to well-separated electron and hole [46, 47, 51, 80]. However, calcination above 800°C

exhibited completely formed rutile and disappeared anatase. Therefore, this resultant led to return of increased PL intensity. It well-known important factor of heat treatment resulted in high crystallization, which reduced PL intensity, so this resultant favored to prevent the occurrence of recombined electron and hole, so it led to high photocatalytic activity. However, high calcination temperature along with the formation of oxygen vacancy led to weak crystallization [19]. Influence of increased particle size led to increased PL intensity, which favored low photo-activity due to a distance of migration electron-hole. Furthermore, small particle had a short distance of electron and hole, which had to migrate to the reaction site on the surface then it resulted in decreasing of recombination of electron and hole [81]. Increasing of crystallization caused by heat treatment, so this effect had to mindful for increased particle size too. Moreover, increasing of crystallinity along with crystallite size of anatase and rutile were decisive of decreased PL intensity, which led to suppression surface defects then it trapped from increased crystallinity, so this effect led to decreasing of defects in the crystal.

A surface defect such as Ti^{3+} and oxygen vacancy sites led to reducing the radiative recombination process, which are exhibited in Figure 33(d) and (e). Oxygen vacancies sites were important for inhibitor recombination rate of electron and hole pairs and higher separation efficiency, which indicated a lower PL intensity, so it affected higher photocatalytic activity [75]. Moreover, oxygen vacancies were formed nearly surface, which were relative with the non-radiative process originated by defects. Therefore, oxygen vacancies indicated on the surface and on the grain boundary, which promoted reduction PL intensity. In addition, oxygen vacancies were formed at the interface of the anatase and rutile crystallites, these oxygen vacancies acted as non-radiative centers only. Therefore, surface defects at the interface between anatase and rutile in the mixed phase component acted as charge carrier trapping sites and charge transfusion of an electron from anatase to rutile. The explanation of these defects at the interface may act as non-radiative centers and decrease of emission intensity. In addition, the various band alignment at the interface between anatase and rutile may also retard the consolidation of electron and holes from the recombination process. Therefore, the various band alignment

resulted in reduction the PL emission intensity [49, 82]. High calcination temperature at 700°C in air removed many of the radiative oxygen vacancy centers along with non-radiative centers, so these resultant reduced the PL emission intensity. These explanations that why mixed phase decreased PL intensity.

Meanwhile, excessive oxygen vacancies could occur. In case of heat treatment with H_2 and N_2 flow due to heat treatment under deficiency oxygen system. The excessive oxygen vacancies led to the formation of many oxygen vacancies in absent lattice oxygen, which led to un-localized molecular orbital exists below the bottom of the conduction band, so it led to low efficiency in the excitation of the ambulant of electrons at conduction band. Furthermore, excessive oxygen vacancies may be trapping electron, which acted as recombination center because it served to block electron thus it led to not separate electron and hole. Calcination at 700°C under H_2 and N_2 flow led to the trend of reduction of photocatalytic activity [83-85]. In other hand, defects were formed inside bulk semiconductor affected to fast recombination due to the wide distance of electron migration to active site and defect.

Band edge was changed because the influence of microstructure such as crystallite size, phase structure, oxygen vacancy, which cohere with the energy of photo-excited. It well-known reduction of band gap energy affected to enhancement red shift in visible adsorption spectra. Therefore, adsorption in a visible led to a decrease of the amount of energy required for photo-excited from valence band to the conduction band within semiconductor [86, 87]. Figure 33 (c) exhibit the effect of heat treatment to band gap, whereas intolerable decrease band gap due to the completely rutile phase transition, it led to fast recombination.

The consumption rate of 3-NS in this reaction versus intensity of PL spectroscopy exhibited all peak at 436, 451, 469, 484 and 492nm, which are shown in Figure 33 (f). Normally, the lower PL intensity indicated a high charge to separate of photo-induced electron and hole pairs then it resulted in high photocatalytic activity. Changes in the calcination atmosphere also affected the PL signal and the signal decreased in order of Air < H_2 < N_2.

The microstructure of P25-700-air associated with two difference crystallite size anatase and rutile. It is well-known that the mixture of anatase and rutile component has a high photo-activity than pure phase [48, 58, 88]. Therefore, the explanation for presence mixed phase both anatase and rutile phase, which promoted the synergistic antenna effect and activation effect by anatase phase, so the effect of antenna led to separate electron and hole and enhancement for photocatalytic activity [49, 50, 80, 89]. The Ti^{3+} and oxygen vacancy site on the surface of TiO_2 were an active site for trapping nitroaromatic at conduction band [5, 7]. In addition, the formation of oxygen vacancies site, which located at the interface of anatase and rutile, enhancement for charge separated electron and hole. [82, 90]. However, increasing of crystallite size after calcination resulted in a decrease of surface area, which affected to reduce absorption site. The band edge of anatase and rutile have 3.2eV and 3.0eV respectively, which depended on morphology and component phase [12, 13]. However, calcination at a higher temperature resulted in the complete transformation of anatase to rutile phase and large crystallite of the TiO_2, which led to the loss of synergistic effect of the mixed phases and the loss of active surface area of the photocatalysts. Moreover, the excessive Ti^{3+} and oxygen vacancy site led to the formation of the un-localized band at the conduction band, leading to faster recombination.

Furthermore, Figure 33 (a) to (g) exhibit relation of properties all treated P25-TiO_2 then the recombination had a more effective to the consumption of rate 3-NS than other properties. However, PL results were in order of Air<H_2<N_2, which were similar in trend to the photocatalytic activity. The heat treatment affected to properties of crystallite size, phase ratio, Ti^{3+}- oxygen vacancy sites and band gap, which were importance role play for recombination process, which enhanced to photocatalytic activity.

a)

700°C air

700°C H$_2$

700°C N$_2$

Uncalcined

600°C air

A-700°C air

Rate 3-NS consumed (μmole g^{-1}h^{-1})

Crystallite size of anatase (nm)

b)

700°C air

700°C H$_2$

800°C air

700°C N$_2$

Uncalcined

600°C air

Rate 3-NS consumed (μmole g^{-1}h^{-1})

Crystallite size of rutile (nm)

c)

d)
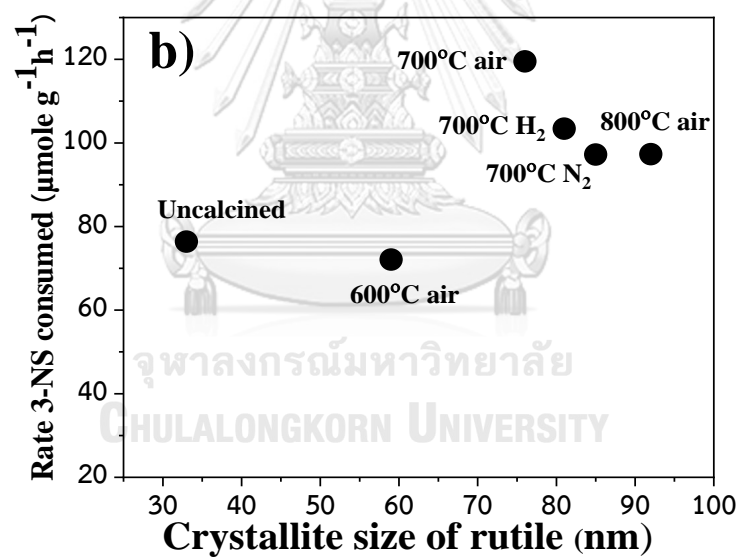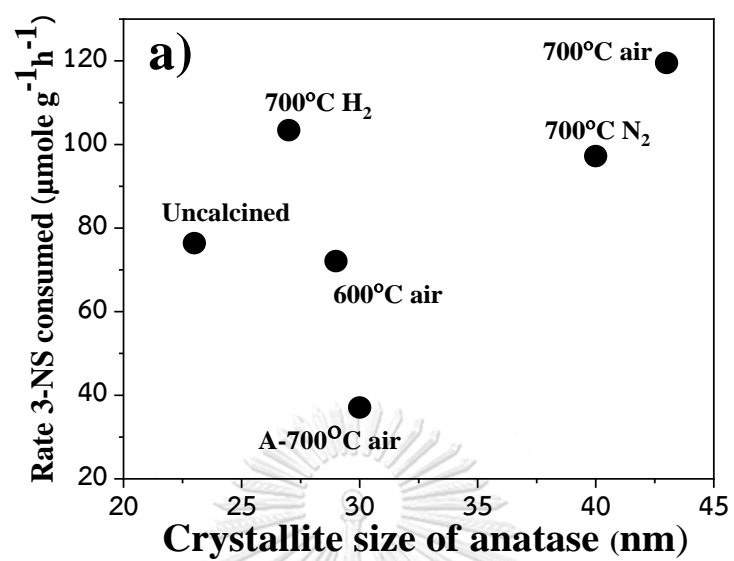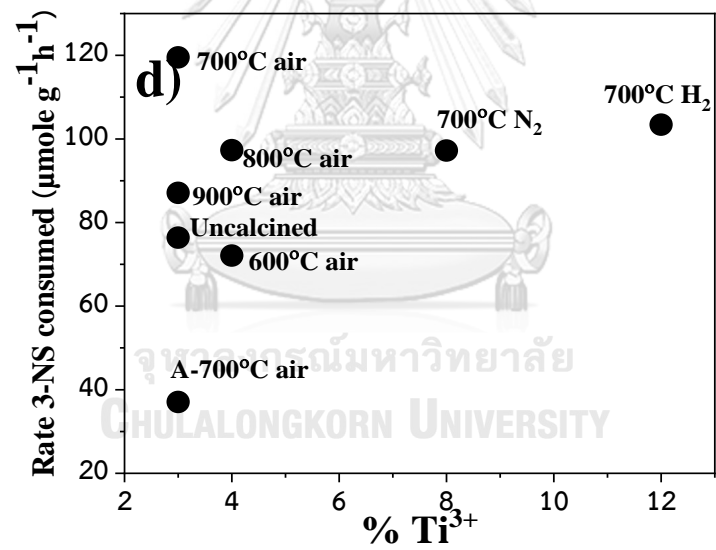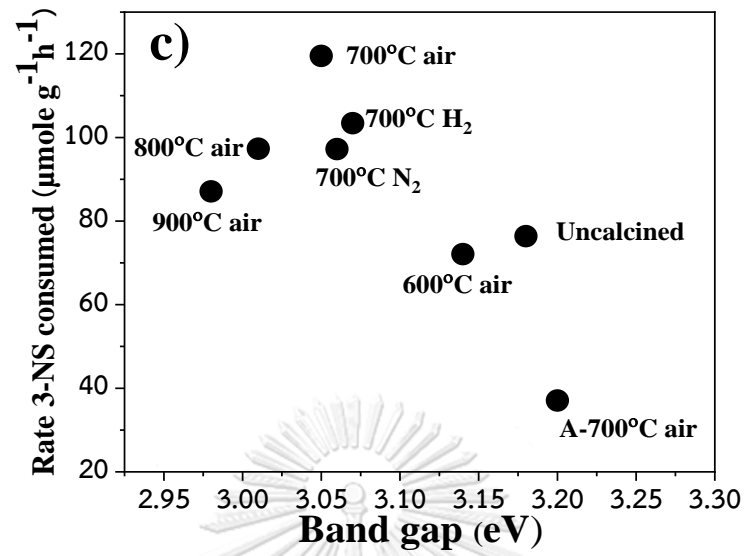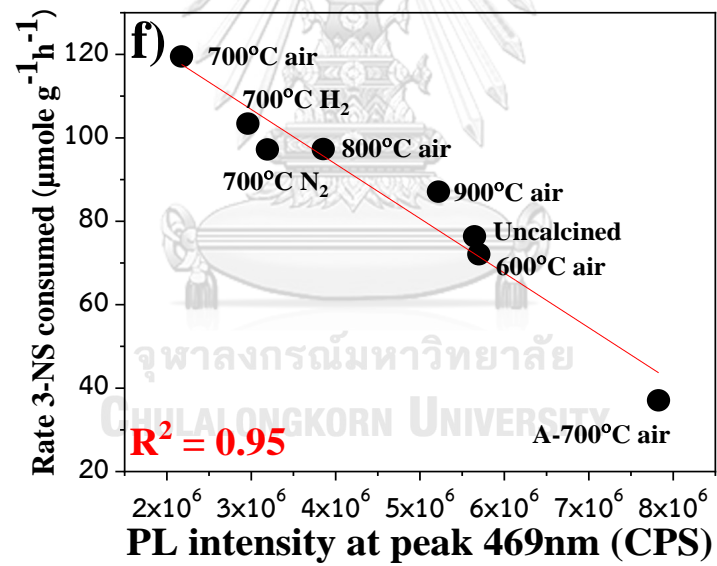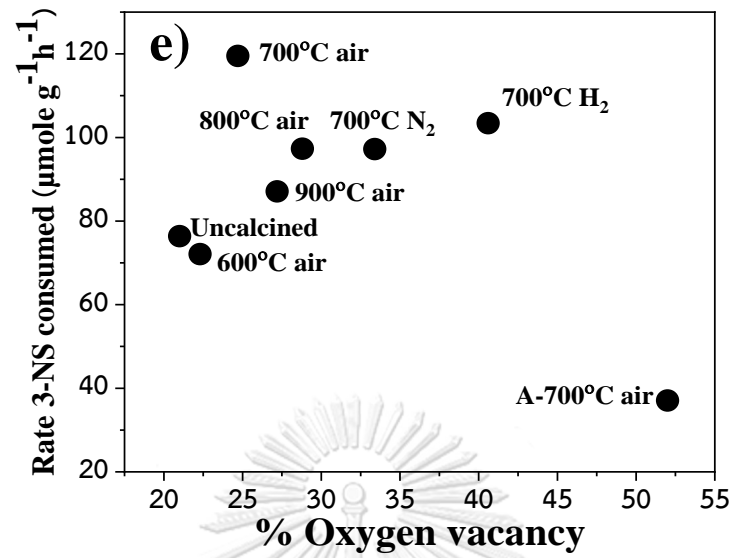
Figure 33 Rate consumption of 3-NS versus (a) crystallite size anatase, (b) crystallite size rutile, (c) band gap, (d) %Ti^{3+}, (e) %oxygen vacancy, (f) PL intensity at peak 469nm, (g) PL intensity at peak 436, 451, 469, 482 and 492 nm.

4.2.2 Recyclability and properties of spent catalysts

Moreover, investigation stability and recyclability of the catalysts in order that, determination performance of catalysts in photocatalytic selective hydrogenation of 3-nitrostyrene. The catalyst was recovered by using centrifugation from suspension mixture then the recovered catalyst was repeated for five cycles for the photocatalytic test. Figure 34 exhibit the %conversion of 3-NS was observed that insignificant loss activity. Moreover, the selectivity to 3-VA has remained. Therefore, the preparation for this active site could be used for the long term in this reaction.
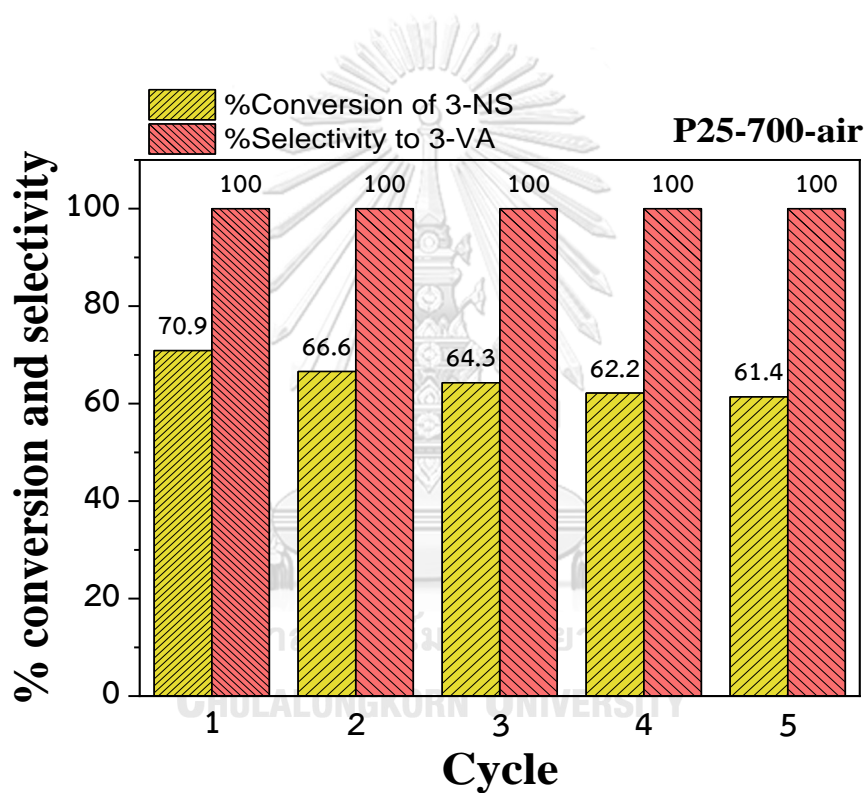
Figure 34 The 5 Cycles of recyclability performance of P25-700-air.

4.2.3 TGA analysis of spent catalysts

The physiochemical properties included decomposition or volatilization, which were estimated using by TGA analysis. Figure 35 shows the TGA analysis of all spent catalysts. The spent catalysts were analyzed and represented %weight loss (0.8-5%) in range temperature (100-500°C). The weight loss could possibly be because catalyst was thermally treated along with flowed gas, which exhibited thermal decomposition or volatilization of chemical substance [91, 92]. In addition, increasing of temperature treatment led to the weight loss within the particle and formation of Ti-O-Ti bond due to condensation between Ti-OH groups. Moreover, treated P25-TiO$_2$ resulted in the loss molecule of water. The process of crystal growth and increasing rutile phase transformation, which associated with these effects. The increasing calcination temperature resulted in %weight loss decreased due to thermal treatment process caused by chemical substance and loss of water had already.
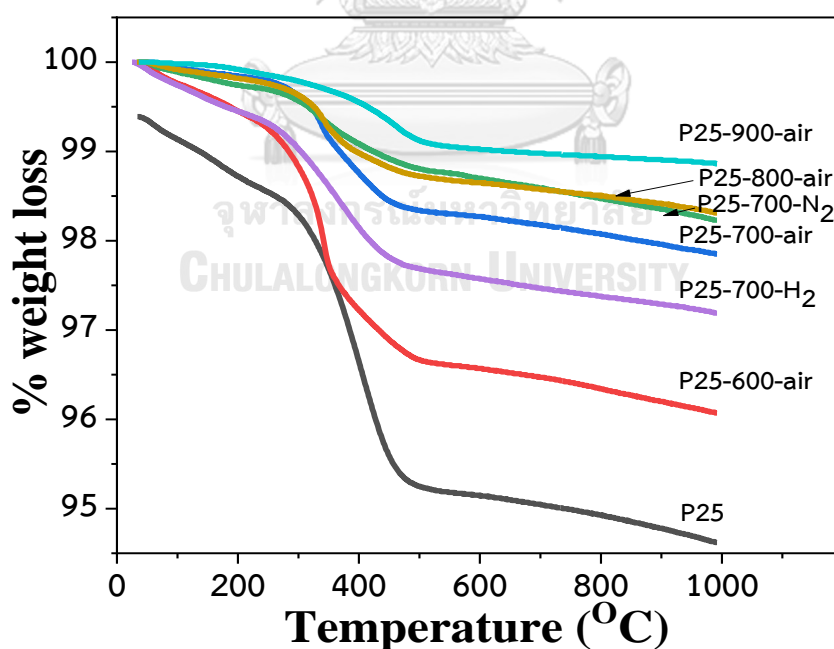
Figure 35 TGA analysis of spent catalysts.

CHAPTER 5

CONCLUSION AND RECOMMENATION

5.1 Conclusion

1) Effect calcination temperature of $P25$-TiO_2 led to phase transformation, crystallite size, light absorption, BET surface area. $P25$-TiO_2 were heat treatment in air resulted in an increase of rutile component, large crystallite size, and particle, adsorption edge toward red shift, whereas it led to decrease of band gap energy and surface area due to agglomeration particle and decreasing of pore volume and porosity. In case of, $P25$-TiO_2 were heat treatment under H_2 and N_2 flow resulted in a similar trend of microstructure as calcination in air except for a concentration oxygen vacancy and Ti^{3+} had higher than calcination in air and it presented higher rutile content.

2) At calcination at 700°C in air exhibited mixed phases both anatase and rutile. The well-known presence mix phases of anatase and rutile also contributed photocatalytic activity due to the effect of the antenna. In this work, calcination at 700°C in air exhibited the highest photocatalytic activity due to its high crystallinity and optimum amount of mixed phase content, leading to the reduction of the electron-hole recombination process by a synergistic effect, which motivated by anatase crystallite size. However, calcination at above 800°C resulted in extinction synergistic effect of mix phase due to complete transformation to rutile and large crystallite size, which incurred and returned to recombination of electron and hole. The Ti^{3+} and oxygen vacancy site on the surface TiO_2 were an active site for trapping electron and adsorption nitroaromatic in this reaction. Moreover, changing of H_2 and N_2 flow led to excessive oxygen vacancy site, which resulted in the formation un-localized state at conduction band then it favored fast recombination.

3) Photocatalytic selective hydrogenation of 3-NS to 3VA was operated under UV-light irradiation and suspension of TiO_2 in isopropanol. Investigation various calcination temperature exhibited a linear correlation between PL intensity versus consumption rate of 3-NS, so the recombination process was the main factor in this reaction. In addition, properties of crystallite size, phase ratio, Ti^{3+}- oxygen vacancy

sites and band gap, which were importance role play for the recombination process, which enhanced to photocatalytic activity.
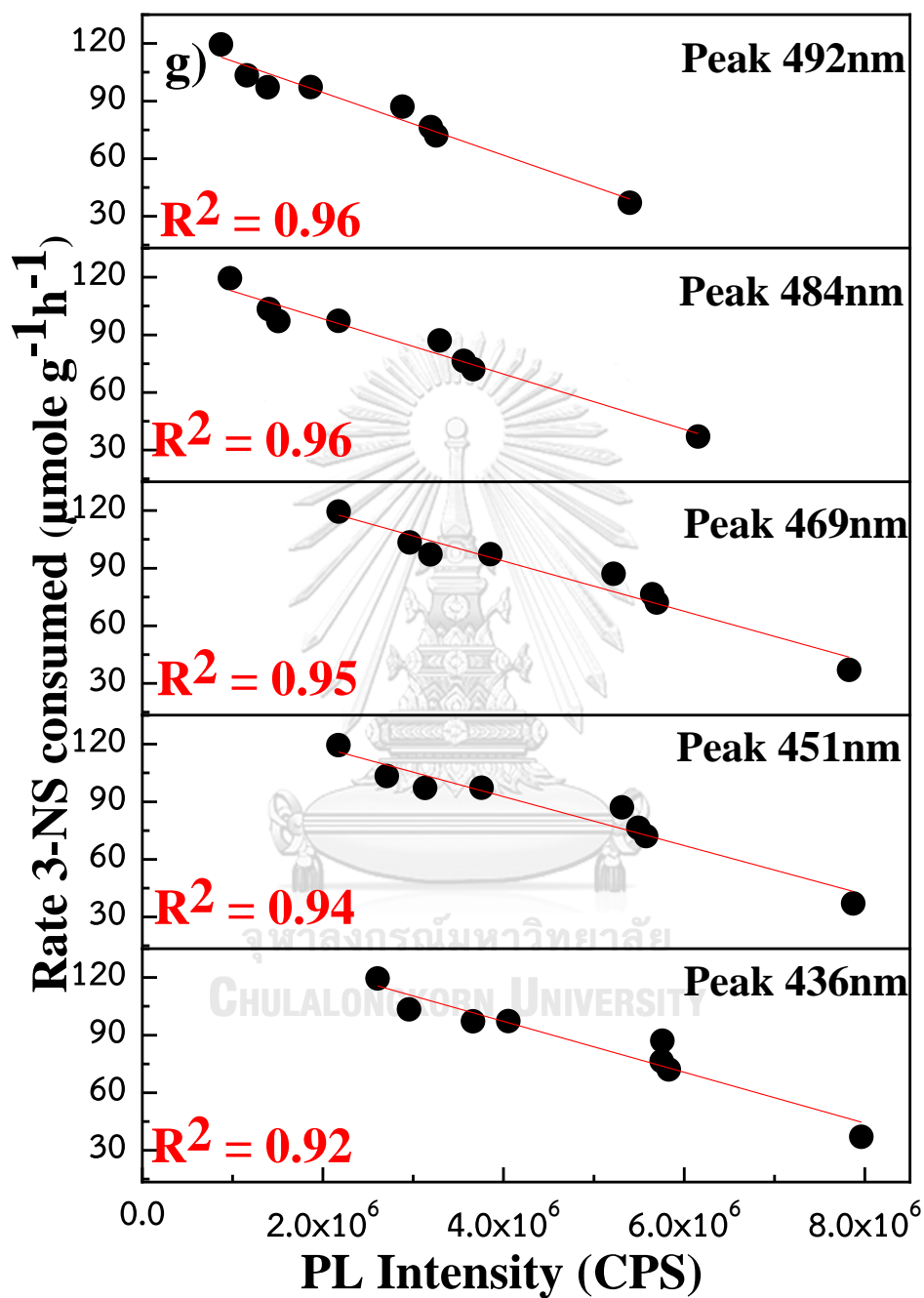
5.2 Recommendation

1) The effect of calcination on TiO_2 in the other alcohol or substrates should be investigated.

2) The effect of doping such as metal or non-metal on TiO_2 in photocatalytic hydrogenation reactions should be investigated.

จุฬาลงกรณ์มหาวิทยาลัย

CHULALONGKORN UNIVERSITY

REFERENCES

1.   Serna, P., Concepción, P. and Corma, A., Design of highly active and chemoselective bimetallic gold–platinum hydrogenation catalysts through kinetic and isotopic studies. *Journal of Catalysis* **2009,** *265* (1), 19-25.

2.   Pisduangdaw, S., Mekasuwandumrong, O., Yoshida, H., Fujita, S.-I., Arai, M. and Panpranot, J., Flame-made Pt/TiO$_2$ catalysts for the liquid-phase selective hydrogenation of 3-nitrostyrene. *Applied Catalysis A: General* **2015,** *490,* 193-200.

3.   Berguerand, C., Yarulin, A., Cárdenas-Lizana, F., Wärnå, J., Sulman, E., Murzin, D. Y. and Kiwi-Minsker, L., Chemoselective Liquid Phase Hydrogenation of 3-Nitrostyrene over Pt Nanoparticles: Synergy with ZnO Support. *Industrial & Engineering Chemistry Research* **2015,** *54* (35), 8659-8669.

4.   Pisduangdaw, S., Mekasuwandumrong, O., Fujita, S.-I., Arai, M., Yoshida, H. and Panpranot, J., One step synthesis of Pt–Co/TiO$_2$ catalysts by flame spray pyrolysis for the hydrogenation of 3-nitrostyrene. *Catalysis Communications* **2015,** *61,* 11-15.

5.   Shiraishi, Y., Togawa, Y., Tsukamoto, D., Tanaka, S. and Hirai, T., Highly Efficient and Selective Hydrogenation of Nitroaromatics on Photoactivated Rutile Titanium Dioxide. *ACS Catalysis* **2012,** *2* (12), 2475-2481.

6.   Hakki, A., Dillert, R. and Bahnemann, D. W., Factors affecting the selectivity of the photocatalytic conversion of nitroaromatic compounds over TiO$_2$ to valuable nitrogen-containing organic compounds. *Physical Chemistry Chemical Physics* **2013,** *15* (8), 2992-3002.

7.   Imamura, K., Yoshikawa, T., Hashimoto, K. and Kominami, H., Stoichiometric production of aminobenzenes and ketones by photocatalytic reduction of nitrobenzenes in secondary alcoholic suspension of titanium(IV) oxide under metal-free conditions. *Applied Catalysis B: Environmental* **2013,** *134-135,* 193-197.

8.   Liqiang, J., Yichun, Q., Baiqi, W., Shudan, L., Baojiang, J., Libin, Y., Wei, F., Honggang, F. and Jiazhong, S., Review of photoluminescence performance of nano-sized semiconductor materials and its relationships with photocatalytic activity. *Solar Energy Materials and Solar Cells* **2006,** *90* (12), 1773-1787.

9.   Munir, S., Dionysiou, D. D., Khan, S. B., Shah, S. M., Adhikari, B. and Shah, A., Development of photocatalysts for selective and efficient organic transformations. *Journal of Photochemistry and Photobiology B: Biology* **2015,** *148*, 209-222.

10.   Paz, Y., Application of TiO_2 photocatalysis for air treatment: Patents' overview. *Applied Catalysis B: Environmental* **2010,** *99* (3-4), 448-460.

11.   Kohtani, S., Yoshioka, E. and Miyabe, H., Photocatalytic Hydrogenation on Semiconductor Particles. In *Hydrogenation*, 2012.

12.   Leal, J. H., Cantu, Y., Gonzalez, D. F. and Parsons, J. G., Brookite and anatase nanomaterial polymorphs of TiO_2 synthesized from $TiCl_3$. *Inorganic Chemistry Communications* **2017,** *84*, 28-32.

13.   Reyes-Coronado, D., Rodriguez-Gattorno, G., Espinosa-Pesqueira, M. E., Cab, C., de Coss, R. and Oskam, G., Phase-pure $TiO_{(2)}$ nanoparticles: anatase, brookite and rutile. *Nanotechnology* **2008,** *19* (14), 145605.

14.   Fernandes Machado, N. R. C. and Santana, V. S., Influence of thermal treatment on the structure and photocatalytic activity of TiO_2 P25. *Catalysis Today* **2005,** *107-108*, 595-601.

15.   Ohtani, B., Prieto-Mahaney, O. O., Li, D. and Abe, R., What is Degussa (Evonik) P25? Crystalline composition analysis, reconstruction from isolated pure particles and photocatalytic activity test. *Journal of Photochemistry and Photobiology A: Chemistry* **2010,** *216* (2-3), 179-182.

16.   Bokhimi, X., Morales, A., Aguilar, M., Toledo-Antonio, J. and Pedraza, F. J. I. j. o. h. e., Local order in titania polymorphs. *International journal of hydrogen energy* **2001,** *26* (12), 1279-1287.

17.   Regonini, D., Bowen, C. R., Jaroenworaluck, A. and Stevens, R., A review of growth mechanism, structure and crystallinity of anodized TiO_2 nanotubes. *Materials Science and Engineering: R: Reports* **2013,** *74* (12), 377-406.

18.   Ohno, T., Sarukawa, K., Tokieda, K. and Matsumura, M., Morphology of a TiO_2 Photocatalyst (Degussa, P-25) Consisting of Anatase and Rutile Crystalline Phases. *Journal of Catalysis* **2001,** *203* (1), 82-86.

19.   Wang, G., Xu, L., Zhang, J., Yin, T. and Han, D., Enhanced Photocatalytic Activity of Powders (P25) via Calcination Treatment. *International Journal of*

Photoenergy **2012,** *2012,* 1-9.

20.   Shiraishi, Y.,   Hirakawa, H.,   Togawa, Y.,   Sugano, Y.,   Ichikawa, S. and Hirai, T., Rutile Crystallites Isolated from Degussa (Evonik) P25 TiO$_2$: Highly Efficient Photocatalyst for Chemoselective Hydrogenation of Nitroaromatics. *ACS Catalysis* **2013,** *3* (10), 2318-2326.

21.   Ohno, T.,   Sarukawa, K. and Matsumura, M. J. T. J. o. P. C. B., Photocatalytic activities of pure rutile particles isolated from TiO$_2$ powder by dissolving the anatase component in HF solution. *The Journal of Physical Chemistry B* **2001,** *105* (12), 2417-2420.

22.   Ohtani, B.,   Okugawa, Y.,   Nishimoto, S. and Kagiya, T. J. J. o. P. C., Photocatalytic activity of titania powders suspended in aqueous silver nitrate solution: correlation with pH-dependent surface structures. *Journal of Physical Chemistry* **1987,** *91* (13), 3550-3555.

23.   Gervasini, A.,   Fenyvesi, J. and Auroux, A. J. C. L., Study of the acidic character of modified metal oxide surfaces using the test of isopropanol decomposition. *Catalysis Letters* **1997,** *43* (3-4), 219-228.

24.   Xiong, C.,   Wang, S.,   Sun, W. and Li, Y., Selective adsorption of Pb(II) from aqueous solution using nanosilica functionalized with diethanolamine: Equilibrium, kinetic and thermodynamic. *Microchemical Journal* **2019,** *146,* 270-278.

25.   Yaghoubi, H.,   Dayerizadeh, A.,   Han, S.,   Mulaj, M.,   Gao, W.,   Li, X.,   Muschol, M.,   Ma, S. and Takshi, A., The effect of surfactant-free TiO$_2$ surface hydroxyl groups on physicochemical, optical and self-cleaning properties of developed coatings on polycarbonate. *Journal of Physics D: Applied Physics* **2013,** *46* (50).

26.   Wu, C. Y.,   Tu, K. J.,   Deng, J. P.,   Lo, Y. S. and Wu, C. H., Markedly Enhanced Surface Hydroxyl Groups of TiO$_{(2)}$ Nanoparticles with Superior Water-Dispersibility for Photocatalysis. *Materials (Basel)* **2017,** *10* (5).

27.   Atiqullah, M.,   Akhtar, M. N.,   Moman, A. A.,   Abu-Raqabah, A. H.,   Palackal, S. J.,   Al-Muallem, H. A. and Hamed, O. M., Influence of silica calcination temperature on the performance of supported catalyst SiO$_2$–nBuSnCl$_3$/MAO/(nBuCp)$_2$ZrCl$_2$ polymerizing ethylene without separately feeding the MAO cocatalyst. *Applied Catalysis A: General* **2007,** *320,* 134-143.

28.   Paul, K. K., Jana, S. and Giri, P. K., Tunable and High Photoluminescence Quantum Yield from Self-Decorated TiO_2 Quantum Dots on Fluorine Doped Mesoporous TiO_2 Flowers by Rapid Thermal Annealing. *Particle & Particle Systems Characterization* **2018,** *35* (9).

29.   Dang, T. T. T., Le, S. T. T., Channei, D., Khanitchaidecha, W. and Nakaruk, A., Photodegradation mechanisms of phenol in the photocatalytic process. *Research on Chemical Intermediates* **2016,** *42* (6), 5961-5974.

30.   Yu, J., Wang, G., Cheng, B. and Zhou, M., Effects of hydrothermal temperature and time on the photocatalytic activity and microstructures of bimodal mesoporous TiO_2 powders. *Applied Catalysis B: Environmental* **2007,** *69* (3-4), 171-180.

31.   Du, P., Bueno-López, A., Verbaas, M., Almeida, A. R., Makkee, M., Moulijn, J. A. and Mul, G., The effect of surface OH^- population on the photocatalytic activity of rare earth-doped P25-TiO_2 in methylene blue degradation. *Journal of Catalysis* **2008,** *260* (1), 75-80.

32.   Xiao, Q. and Ouyang, L., Photocatalytic activity and hydroxyl radical formation of carbon-doped TiO_2 nanocrystalline: Effect of calcination temperature. *Chemical Engineering Journal* **2009,** *148* (2-3), 248-253.

33.   Liu, S., Yu, J. and Jaroniec, M. J. J. o. t. A. C. S., Tunable photocatalytic selectivity of hollow TiO_2 microspheres composed of anatase polyhedra with exposed {001} facets. *Journal of the American Chemical Society* **2010,** *132* (34), 11914-11916.

34.   Klaysri, R., Wichaidit, S., Tubchareon, T., Nokjan, S., Piticharoenphun, S., Mekasuwandumrong, O. and Praserthdam, P., Impact of calcination atmospheres on the physiochemical and photocatalytic properties of nanocrystalline TiO_2 and Si-doped TiO_2. *Ceramics International* **2015,** *41* (9), 11409-11417.

35.   Wu, N.-L., Lee, M.-S., Pon, Z.-J. and Hsu, J.-Z., Effect of calcination atmosphere on TiO_2 photocatalysis in hydrogen production from methanol/water solution. *Journal of Photochemistry and Photobiology A: Chemistry* **2004,** *163* (1-2), 277-280.

36.   Kuhaudomlap, S., Mekasuwandumrong, O., Praserthdam, P., Fujita, S.-I., Arai, M. and Panpranot, J., The H_2-Treated TiO_2 Supported Pt Catalysts Prepared by Strong Electrostatic Adsorption for Liquid-Phase Selective Hydrogenation. *Catalysts* **2018,** *8* (2).

37.   Zeng, Y., Zhang, S., Wang, Y., Liu, G. and Zhong, Q., The effects of calcination

atmosphere on the catalytic performance of Ce-doped TiO_2 catalysts for selective catalytic reduction of NO with NH_3. *RSC Advances* **2017,** *7* (38), 23348-23354.

38.   Jiang, X., Zhang, Y., Jiang, J., Rong, Y., Wang, Y., Wu, Y. and Pan, C., Characterization of Oxygen Vacancy Associates within Hydrogenated TiO_2: A Positron Annihilation Study. *The Journal of Physical Chemistry C* **2012,** *116* (42), 22619-22624.

39.   Saputera, W. H., Mul, G. and Hamdy, M. S., Ti^{3+}-containing titania: Synthesis tactics and photocatalytic performance. *Catalysis Today* **2015,** *246*, 60-66.

40.   Wei, H., Liu, X., Wang, A., Zhang, L., Qiao, B., Yang, X., Huang, Y., Miao, S., Liu, J. and Zhang, T., FeO_x-supported platinum single-atom and pseudo-single-atom catalysts for chemoselective hydrogenation of functionalized nitroarenes. *Nature communications* **2014,** *5*, 5634.

41.   Yoshida, H., Igarashi, N., Fujita, S.-i., Panpranot, J. and Arai, M., Influence of Crystallite Size of TiO_2 Supports on the Activity of Dispersed Pt Catalysts in Liquid-Phase Selective Hydrogenation of 3-Nitrostyrene, Nitrobenzene, and Styrene. *Catalysis Letters* **2014,** *145* (2), 606-611.

42.   Xu, G., Wei, H., Ren, Y., Yin, J., Wang, A. and Zhang, T., Chemoselective hydrogenation of 3-nitrostyrene over a Pt/FeO_x pseudo-single-atom-catalyst in CO_2-expanded liquids. *Green Chemistry* **2016,** *18* (5), 1332-1338.

43.   Camacho-Bunquin, J., Ferrandon, M., Sohn, H., Yang, D., Liu, C., Ignacio-de Leon, P. A., Perras, F. A., Pruski, M., Stair, P. C. and Delferro, M., Chemoselective Hydrogenation with Supported Organoplatinum(IV) Catalyst on Zn(II)-Modified Silica. *Journal of the American Chemical Society* **2018,** *140* (11), 3940-3951.

44.   Fujishima, A. and Honda, K. J. n., Electrochemical photolysis of water at a semiconductor electrode. *nature* **1972,** *238* (5358), 37.

45.   Aditya, T., Pal, A. and Pal, T., Nitroarene reduction: a trusted model reaction to test nanoparticle catalysts. *Chemical Communications* **2015,** *51* (46), 9410-9431.

46.   Peng, F., Gao, H., Zhang, G., Zhu, Z., Zhang, J. and Liu, Q., Synergistic Effects of Sm and C Co-Doped Mixed Phase Crystalline $TiO_{(2)}$ for Visible Light Photocatalytic Activity. *Materials (Basel)* **2017,** *10* (2).

47.   Wang, X., Shen, S., Feng, Z. and Li, C., Time-resolved photoluminescence of anatase/rutile TiO_2 phase junction revealing charge separation dynamics. *Chinese*

Journal of Catalysis **2016,** *37* (12), 2059-2068.

48.   Nakajima, H., Mori, T., Shen, Q. and Toyoda, T., Photoluminescence study of mixtures of anatase and rutile TiO_2 nanoparticles: Influence of charge transfer between the nanoparticles on their photoluminescence excitation bands. *Chemical Physics Letters* **2005,** *409* (1-3), 81-84.

49.   Mi, Y. and Weng, Y., Band Alignment and Controllable Electron Migration between Rutile and Anatase TiO_2. *Scientific reports* **2015,** *5*, 11482.

50.   Komaguchi, K., Nakano, H., Araki, A. and Harima, Y., Photoinduced electron transfer from anatase to rutile in partially reduced TiO_2 (P-25) nanoparticles: An ESR study. *Chemical Physics Letters* **2006,** *428* (4-6), 338-342.

51.   Cheng, H., Wang, J., Zhao, Y. and Han, X., Effect of phase composition, morphology, and specific surface area on the photocatalytic activity of TiO_2 nanomaterials. *RSC Advances* **2014,** *4* (87), 47031-47038.

52.   Xiong, L.-B., Li, J.-L., Yang, B. and Yu, Y., Ti^{3+}in the Surface of Titanium Dioxide: Generation, Properties and Photocatalytic Application. *Journal of Nanomaterials* **2012,** *2012*, 1-13.

53.   Lu, T.-C., Wu, S.-Y., Lin, L.-B. and Zheng, W.-C. J. P. B. C. M., Defects in the reduced rutile single crystal. *Physica B: Condensed Matter* **2001,** *304* (1-4), 147-151.

54.   Imamura, K., Hashimoto, K. and Kominami, H., Chemoselective reduction of nitrobenzenes to aminobenzenes having reducible groups by a titanium(IV) oxide photocatalyst under gas- and metal-free conditions. *Chemical Communications* **2012,** *48* (36), 4356-4358.

55.   Naldoni, A., Allieta, M., Santangelo, S., Marelli, M., Fabbri, F., Cappelli, S., Bianchi, C. L., Psaro, R. and Dal Santo, V. J. J. o. t. A. C. S., Effect of nature and location of defects on bandgap narrowing in black TiO_2 nanoparticles. *Journal of the American Chemical Society* **2012,** *134* (18), 7600-7603.

56.   Hanaor, D. A. H. and Sorrell, C. C., Review of the anatase to rutile phase transformation. *Journal of Materials Science* **2010,** *46* (4), 855-874.

57.   Tauseef, A., Wang, L., Naveed, H., Wang, C., Rizwan Ur Rehman, S. and Liang, T., Effect of Annealing Atmosphere Induced Crystallite Size Changes on the Electrochemical Properties of TiO_2 Nanotubes Arrays. *Journal of Electrical Engineering*

2016, *4* (2), 43-51.

58. Wang, W. K., Chen, J. J., Zhang, X., Huang, Y. X., Li, W. W. and Yu, H. Q., Self-induced synthesis of phase-junction TiO_2 with a tailored rutile to anatase ratio below phase transition temperature. *Scientific reports* **2016,** *6*, 20491.

59. Naderi, M., Surface Area. In *Progress in Filtration and Separation*, 2015; pp 585-608.

60. Liu, B., Liu, L.-M., Lang, X.-F., Wang, H.-Y., Lou, X. W. and Aydil, E. S., Doping high-surface-area mesoporous TiO_2 microspheres with carbonate for visible light hydrogen production. *Energy & Environmental Science* **2014,** *7* (8), 2592-2597.

61. Chen, M., Ma, Y., Zhou, Y., Liu, C., Qin, Y., Fang, Y., Guan, G., Li, X., Zhang, Z. and Wang, T., Influence of Transition Metal on the Hydrogen Evolution Reaction over Nano-Molybdenum-Carbide Catalyst. *Catalysts* **2018,** *8* (7).

62. Yuangpho, N., Le, S. T. T., Treerujiraphapong, T., Khanitchaidecha, W. and Nakaruk, A., Enhanced photocatalytic performance of TiO_2 particles via effect of anatase–rutile ratio. *Physica E: Low-dimensional Systems and Nanostructures* **2015,** *67*, 18-22.

63. Park, G. C., Seo, T. Y., Park, C. H., Lim, J. H. and Joo, J., Effects of Calcination Temperature on Morphology, Microstructure, and Photocatalytic Performance of TiO_2 Mesocrystals. *Industrial & Engineering Chemistry Research* **2017,** *56* (29), 8235-8240.

64. Jun, J., Dhayal, M., Shin, J.-H., Kim, J.-C. and Getoff, N., Surface properties and photoactivity of TiO_2 treated with electron beam. *Radiation Physics and Chemistry* **2006,** *75* (5), 583-589.

65. Bharti, B., Kumar, S., Lee, H. N. and Kumar, R., Formation of oxygen vacancies and $Ti^{(3+)}$ state in TiO_2 thin film and enhanced optical properties by air plasma treatment. *Scientific reports* **2016,** *6*, 32355.

66. Wang, X., Li, Y., Liu, X., Gao, S., Huang, B. and Dai, Y., Preparation of Ti^{3+} self-doped TiO_2 nanoparticles and their visible light photocatalytic activity. *Chinese Journal of Catalysis* **2015,** *36* (3), 389-399.

67. Tshabalala, Z. P., Motaung, D. E., Mhlongo, G. H. and Ntwaeaborwa, O. M., Facile synthesis of improved room temperature gas sensing properties of TiO_2 nanostructures: Effect of acid treatment. *Sensors and Actuators B: Chemical* **2016,** *224*,

841-856.

68.   Liu, H., Ma, H., Li, X., Li, W., Wu, M. and Bao, X. J. C., The enhancement of TiO$_2$ photocatalytic activity by hydrogen thermal treatment. *Chemosphere* **2003,** *50* (1), 39-46.

69.   Amano, F., Hydrogen Reduced Rutile Titanium Dioxide Photocatalyst. In *Titanium Dioxide*, 2017.

70.   Amano, F., Nakata, M., Yamamoto, A. and Tanaka, T., Effect of Ti^{3+} Ions and Conduction Band Electrons on Photocatalytic and Photoelectrochemical Activity of Rutile Titania for Water Oxidation. *The Journal of Physical Chemistry C* **2016,** *120* (12), 6467-6474.

71.   Mehta, M., Kodan, N., Kumar, S., Kaushal, A., Mayrhofer, L., Walter, M., Moseler, M., Dey, A., Krishnamurthy, S., Basu, S. and Singh, A. P., Hydrogen treated anatase TiO$_2$: a new experimental approach and further insights from theory. *Journal of Materials Chemistry A* **2016,** *4* (7), 2670-2681.

72.   Natarajan, T. S., Bajaj, H. C. and Tayade, R. J., Enhanced direct sunlight photocatalytic oxidation of methanol using nanocrystalline TiO$_2$ calcined at different temperature. *Journal of Nanoparticle Research* **2014,** *16* (11).

73.   Naldoni, A., Riboni, F., Marelli, M., Bossola, F., Ulisse, G., Di Carlo, A., Píš, I., Nappini, S., Malvestuto, M., Dozzi, M. V., Psaro, R., Selli, E. and Dal Santo, V., Influence of TiO$_2$ electronic structure and strong metal–support interaction on plasmonic Au photocatalytic oxidations. *Catalysis Science & Technology* **2016,** *6* (9), 3220-3229.

74.   Yan, J., Wu, G., Guan, N., Li, L., Li, Z. and Cao, X., Understanding the effect of surface/bulk defects on the photocatalytic activity of TiO$_2$: anatase versus rutile. *Physical Chemistry Chemical Physics* **2013,** *15* (26), 10978-10988.

75.   Hou, C. and Liu, W., One-step synthesis of OH$^-$TiO$_2$/TiOF$_2$ nanohybrids and their enhanced solar light photocatalytic performance. *Royal Society open science* **2018,** *5* (6), 172005.

76.   Jiang, Y., Yang, Z., Zhang, P., Jin, H. and Ding, Y., Natural assembly of a ternary Ag–SnS–TiO$_2$ photocatalyst and its photocatalytic performance under simulated sunlight. *RSC Advances* **2018,** *8* (24), 13408-13416.

77. Khan, H. and Berk, D., Effect of a Chelating Agent on the Physicochemical Properties of TiO_2: Characterization and Photocatalytic Activity. *Catalysis Letters* **2014,** *144* (5), 890-904.

78. Tahir, M. and Amin, N. S., Indium-doped TiO_2 nanoparticles for photocatalytic CO_2 reduction with H_2O vapors to CH_4. *Applied Catalysis B: Environmental* **2015,** *162*, 98-109.

79. Kamerman, G., Steinvall, O., Lewis, K. L., Gonglewski, J. D., Fedorenko, V., Iatsunskyi, I., Pavlenko, M., Jancelewicz, M., Coy, E. and Viter, R., Structural and optical properties of TiO_2–Al_2O_3 nanolaminates produced by atomic layer deposition. In *Electro-Optical Remote Sensing, Photonic Technologies, and Applications IX*, 2015; Vol. 9649, pp 96490X1-96490X6.

80. Lei, S. H. I. and Duan, W. E. N. G., Highly active mixed-phase TiO_2 photocatalysts fabricated at low temperatureand the correlation between phase compositionand photocatalytic activity. *Journal of Environmental Sciences* **2008,** *20* (10), 1263-1267.

81. Jafari, T., Moharreri, E., Amin, A. S., Miao, R., Song, W. and Suib, S. L., Photocatalytic Water Splitting-The Untamed Dream: A Review of Recent Advances. *Molecules* **2016,** *21* (7).

82. Choudhury, B. and Choudhury, A., Oxygen defect dependent variation of band gap, Urbach energy and luminescence property of anatase, anatase–rutile mixed phase and of rutile phases of TiO_2 nanoparticles. *Physica E: Low-dimensional Systems and Nanostructures* **2014,** *56*, 364-371.

83. Gan, J., Lu, X., Wu, J., Xie, S., Zhai, T., Yu, M., Zhang, Z., Mao, Y., Wang, S. C., Shen, Y. and Tong, Y., Oxygen vacancies promoting photoelectrochemical performance of $In_{(2)}O_{(3)}$ nanocubes. *Scientific reports* **2013,** *3*, 1021.

84. Zhang, F., Ma, W., Guo, H., Zhao, Y., Shan, X., Jin, K., Tian, H., Zhao, Q., Yu, D., Lu, X., Lu, G. and Meng, S., Interfacial Oxygen Vacancies as a Potential Cause of Hysteresis in Perovskite Solar Cells. *Chemistry of Materials* **2016,** *28* (3), 802-812.

85. Samsudin, E. M., Hamid, S. B. A., Juan, J. C., Basirun, W. J. and Kandjani, A. E., Surface modification of mixed-phase hydrogenated TiO_2 and corresponding photocatalytic response. *Applied Surface Science* **2015,** *359*, 883-896.

86. Johar, M. A., Afzal, R. A., Alazba, A. A. and Manzoor, U., Photocatalysis and

Bandgap Engineering Using ZnO Nanocomposites. *Advances in Materials Science and Engineering* **2015,** *2015*, 1-22.

87.　Sharma, R., Khanuja, M., Sharma, S. N. and Sinha, O. P., Reduced band gap & charge recombination rate in Se doped α-Bi_2O_3 leads to enhanced photoelectrochemical and photocatalytic performance: Theoretical & experimental insight. *International Journal of Hydrogen Energy* **2017,** *42* (32), 20638-20648.

88.　Paul, S. and Choudhury, A., Investigation of the optical property and photocatalytic activity of mixed phase nanocrystalline titania. *Applied Nanoscience* **2013,** *4* (7), 839-847.

89.　Yeniyol, S., Mutlu, I., He, Z., Yuksel, B., Boylan, R. J., Urgen, M., Karabuda, Z. C., Basegmez, C. and Ricci, J. L., Photocatalytical Antibacterial Activity of Mixed-Phase TiO_2 Nanocomposite Thin Films against Aggregatibacter actinomycetemcomitans. *BioMed research international* **2015,** *2015*, 705871.

90.　Fu, W., Li, G., Wang, Y., Zeng, S., Yan, Z., Wang, J., Xin, S., Zhang, L., Wu, S. and Zhang, Z., Facile formation of mesoporous structured mixed-phase (anatase/rutile) TiO_2 with enhanced visible light photocatalytic activity. *Chemical Communications* **2017,** *54* (1), 58-61.

91.　Li, D., Chen, S., Wang, D., Li, Y., Shao, W., Long, Y., Liu, Z. and Ringer, S. P., Thermo-analysis of nanocrystalline TiO_2 ceramics during the whole sintering process using differential scanning calorimetry. *Ceramics International* **2010,** *36* (2), 827-829.

92.　Souza, I. P. A. F., Pezoti, O., Bedin, K. C., Cazetta, A. L., Melo, S. A. R., Souza, L. S., Silva, M. C. and Almeida, V. C., Chemometric study of thermal treatment effect on the P25 photoactivity for degradation of tartrazine yellow dye. *Ceramics International* **2018,** *44* (11), 12292-12300.

APPENDIX

APPENDIX A

CALCULTION OF CRYTALLITE SIZE

- **Calculation of the crystallite size by Debye-Scherrer equation**

The crystallite size can be calculated from 2θ profile analysis, FWHM, by Debye-Scherrer equation shows in equation (13) that was suitable for particle size below 100 nm.

From Scherrer equation

$$D = \frac{k\lambda}{\beta cos\theta} \qquad (13)$$

Where **D** = Crystallite size, Å

K = Crystalline-shape factor = 0.9

λ = X-ray wavelength, 1.5418 Å for CuKα

θ = Observed peak angle, degree

β = X-ray diffraction broadening, radian

The X-ray diffraction broadening (β) is the pure width of the powder diffraction, free of all broadening due to the experimental equipment. Standard α-alumina is used to observe the instrumental broadening since its crystallite size is larger than 2000 Å. The X-ray diffraction broadening (β) can be obtained by using Warren's formula shows in equation (14).

From Warren's formula

$$\beta^2 = B^2_m - B^2_s$$

$$\beta = \sqrt{B_m^2 - B_s^2} \qquad (14)$$

Where B_M = Measured peak width in radians at half peak height

B_S = Corresponding width of a standard material

Example: calculation of the crystallite site of P25-TiO2

The half-weight width of (101) diffraction peak $\quad\quad$ = 1.0602°

$\quad\quad\quad\quad\quad\quad\quad\quad\quad\quad\quad\quad\quad\quad\quad\quad\quad\quad\quad\quad\quad$ = 0.018504 radian

The corresponding half-height width of peak of TiO_2 (P25) = 0.003836 radian

The pure width $\quad\quad$ $\beta = \sqrt{B_m^2 - B_s^2}$

$\quad\quad\quad\quad\quad\quad\quad\quad\quad\quad$ = $\sqrt{0.00717^2 - 0.003836^2}$

$\beta \quad\quad = \quad\quad$ 0.0061 radian

$2\theta \quad\quad = \quad\quad$ 25.3

$\theta \quad\quad = \quad\quad$ 12.65

$\lambda \quad\quad = \quad\quad$ 1.5418 Å

The crystallite size = $\dfrac{0.9 \times 1.5418}{0.0061 cos 12.65}$ = 229.58 Å = 22.96 nm
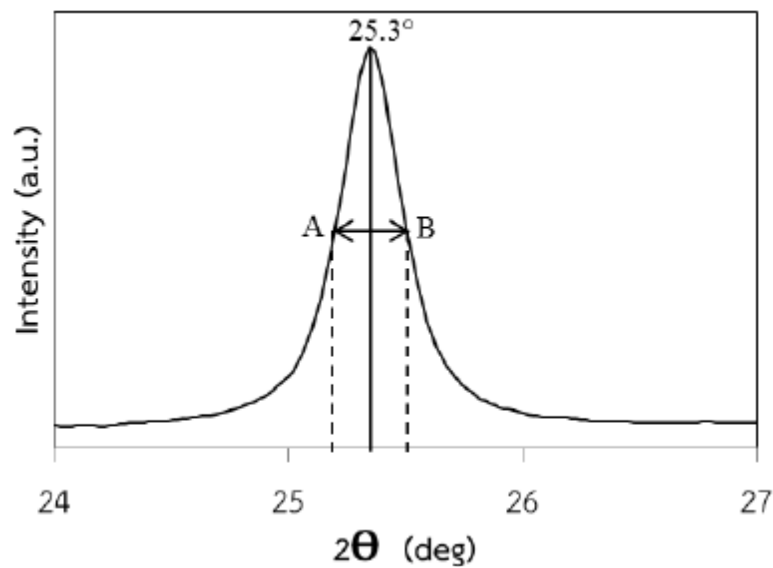
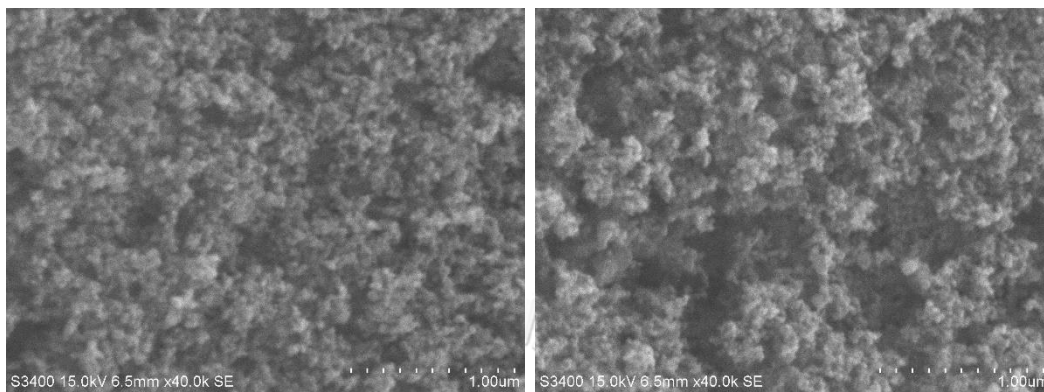**Figure 36** The FHWM of 2θ at 25.3 degree.

APPENDIX B

SEM IMAGES OF P25-TiO$_2$ BEFORE AND AFTER HEAT TREATMENT
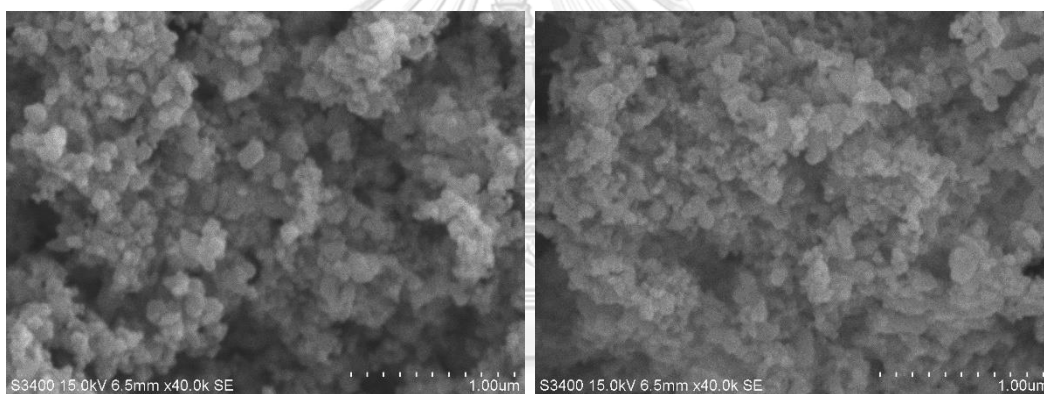

Figure 37 SEM images of P25.

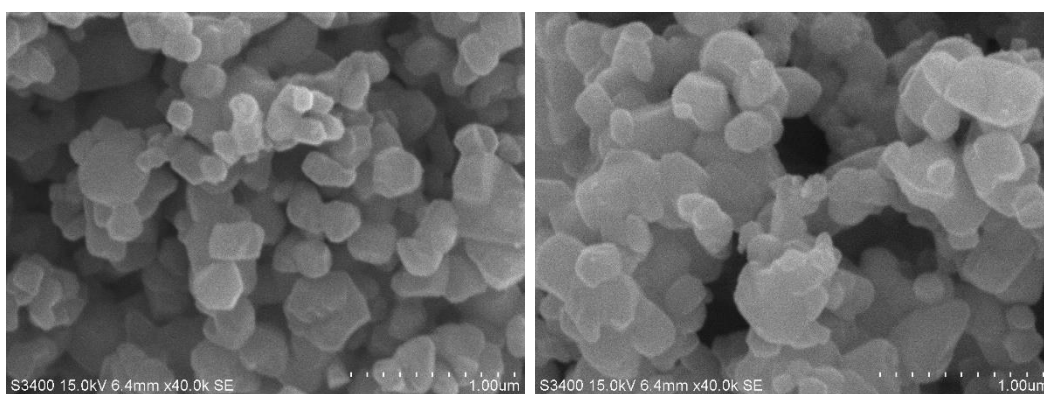**Figure 38** SEM images of P25-700-air.

Figure 39 SEM images of P25-900-air.

APPENDIX C

CALIBRATION CURVE

Photocatalytic activity for 3-Nitrostyrene and 3-Vinylaniline were evaluated by moles from the calibration curve versus area from GC-FID analysis

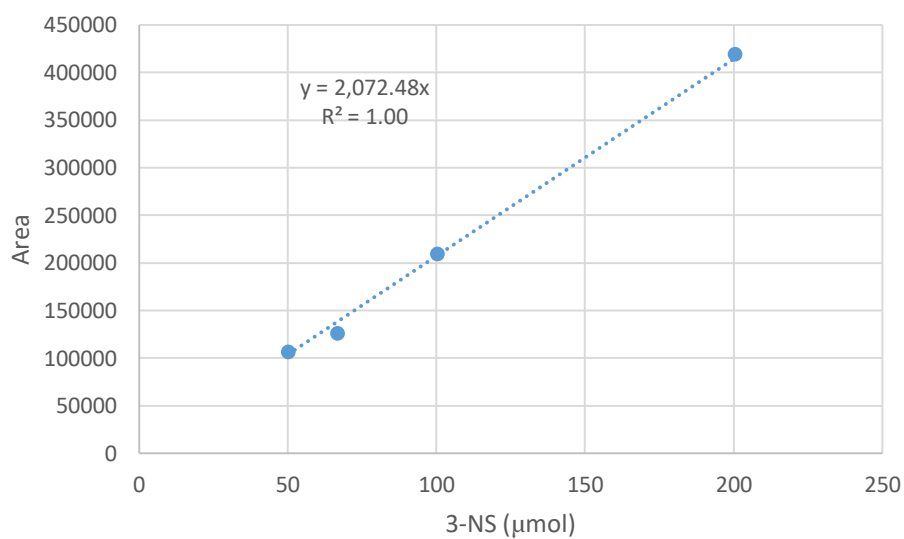- Calibration curve of 3-Nitrostyrene

$y = 2{,}072.48x$
$R^2 = 1.00$

Figure 40 Calibration curve of 3-nitrostyrene.

- Calibration curve of 3-Vinylaniline

จุฬาลงกรณ์มหาวิทยาลัย
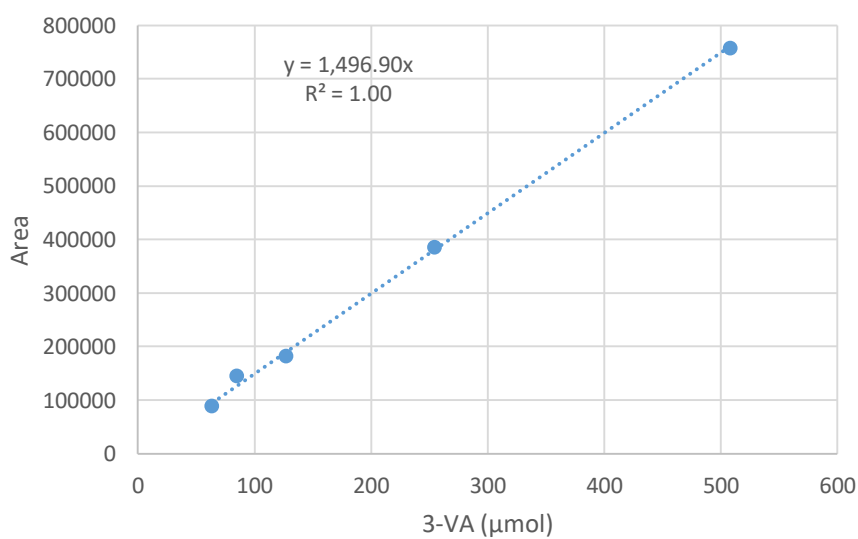

$y = 1{,}496.90x$
$R^2 = 1.00$

Figure 41 Calibration curve of 3-vinylaniline.
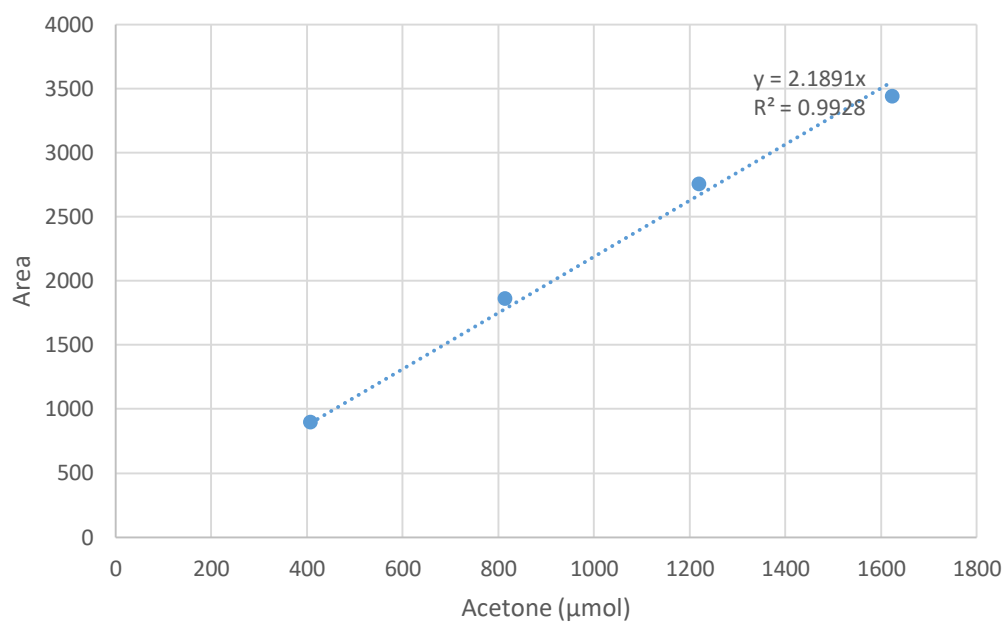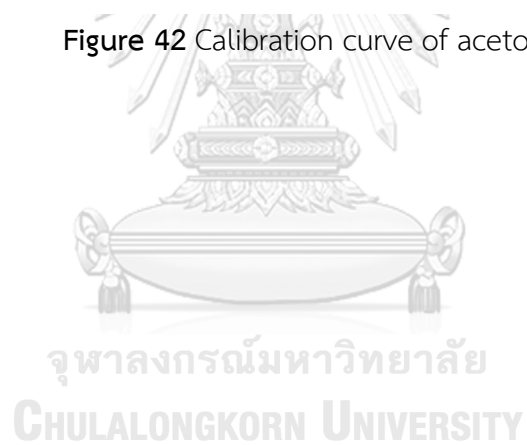
- Calibration curve of Acetone

Figure 42 Calibration curve of acetone.

APPENDIX D

# PROPERTIES OF CHEMICALS AND DETECTOR METHOD OF GC-FID IN THIS REACTION

Table 12 Properties of substrate, product and solvent in this reaction.

Chemical	Suppliers	Density	Molecular weight
3-nitrostyrene ($C_8H_7NO_2$), 96%	Aldrich Chem. CO. Ltd	1.07g/ml At 25°C (lit.)	149.15 g/mol
3-vinylaniline ($C_8H_7NH_2$), 97%	Aldrich Chem. CO. Ltd	1.05g/ml At 25°C (lit.)	119.16 g/mol
Isopropanol ($(CH_3)_2CHOH$), 99.95%	Fisher Chem. CO. Ltd	2.1g/ml At 20°C	60.1 g/mol
Acetone (CH_3COCH_3)	Merck CO. Ltd	0.79g/ml At 20°C	58.08 g/mol

Table 13 Properties and detector method of GC-FID in this reaction.

Gas chromatography	Shimadzu GC -2014	Shimadzu GC -2014
Detector	FID	FID
Packed column	Rtx5®	DB1-Wax
Carrier gas	Helium (99.99 vol. %)	Helium (99.99 vol. %)
Make-up gas	Air (99.9 vol. %)	Air (99.9 vol. %)
Column temperature	140°C	45°C
Injector temperature	270°C	230°C
Detector temperature	310°C	250°C
Time analysis	20 min	6 min

APPENDIX E

SCHEMATIC DIAGRAM OF PHOTOCALYTIC TEST
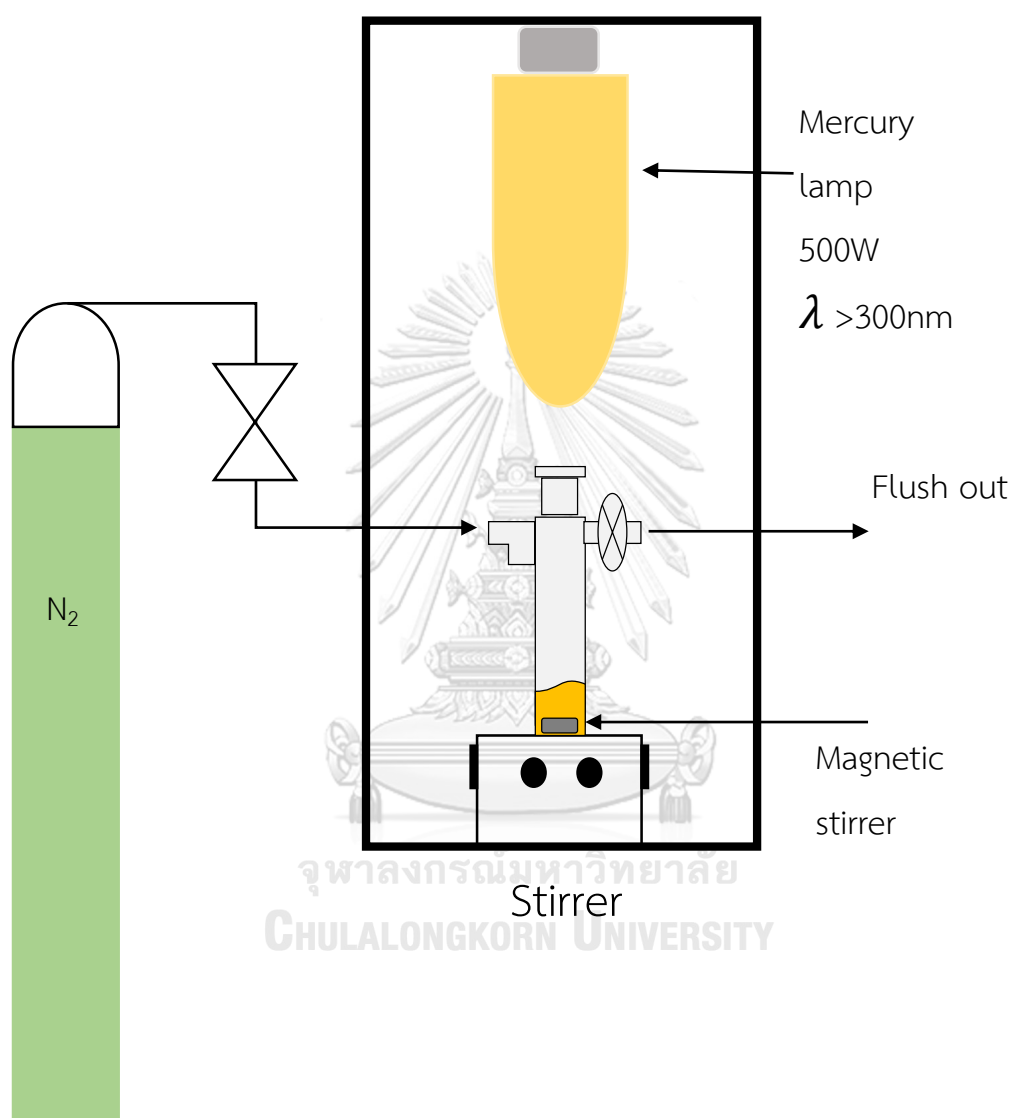
Scheme 2 The schematic of photocatalytic test.

VITA

NAME	Mr. Saknarin Chaitaworn
DATE OF BIRTH	24 January 1994
PLACE OF BIRTH	Songkhla Thailand
INSTITUTIONS ATTENDED	Bachelor's Degree of Chemical Engineering from the Department of Chemical Engineering Faculty of Engineering, Prince of Songkhla University in 2016.
HOME ADDRESS	Hatyai District, Songhkla Province, 90110, Thailand
PUBLICATION	Photocatalytic Liquid-Phase Selective Hydrogenation of 3-Nitrostyrene to 3-vinylaniline of Various Treated-TiO2 Without Use of Reducing Gas. Published in Catalysts Journal in MDPI Volume 9, Issue 4